APPROACHES TO QUANTIFYING EEG FEATURES FOR DESIGN PROTOCOL ANALYSIS

Philon Nguyen

A Ph.D. Thesis

in

The Department

of

Concordia Institute for Information Systems Engineering

Presented in Partial Fulfillment of the Requirements

For the Degree of Doctor of Philosophy

Concordia University

Montréal, Québec, Canada

March 2017

© Philon Nguyen, 2017

Concordia University

School of Graduate Studies

This is to certify that the research proposal prepared

By: **Mr. Philon Nguyen**

Entitled: **Approaches to Quantifying EEG Features for Design Protocol Analysis**

and submitted in partial fulfillment of the requirements for the degree of

Doctor of Philosophy (Ph.D. of Information & Systems Engineering)

complies with the regulations of this University and meets the accepted standards with respect to originality and quality.

Signed by the final examining commitee:

_____ Chair
Dr. Abdessamad Ben Hamza

_____ External Examiner
Dr. Gaetano Cascini

_____ External to Program
Dr. Ali Akgunduz

_____ Examiner
Dr. Anjali Awasthi

_____ Supervisor
Dr. Yong Zeng

Approved by: _____
Chair of Department or Graduate Program Director

Abstract

Approaches to Quantifying EEG Features for Design Protocol Analysis

Philon Nguyen, Ph.D.

Concordia University, 2017

Recently, physiological signals such as eye-tracking and gesture analysis, galvanic skin response (GSR), electrocardiograms (ECG) and electroencephalograms (EEG) have been used by design researchers to extract significant information to describe the conceptual design process. We study a set of video-based design protocols recorded on subjects performing design tasks on a sketchpad while having their EEG monitored. The conceptual design process is rich with information on how designer's do design. Many methods exist to analyze the conceptual design process, the most popular one being concurrent verbal protocols. A recurring problem in design protocol analysis is to segment and code protocol data into logical and semantic units. This is usually a manual step and little work has been done on fully automated segmentation techniques. Also, verbal protocols are known to fail in some circumstances such as when dealing with creativity, insight (e.g. Aha! experience, gestalt), concurrent, nonverbalizable (e.g. facial recognition) and nonconscious processes. We propose different approaches to study the conceptual design process using electroencephalograms (EEG). More specifically, we use spatio-temporal and frequency domain features. Our research is based on machine learning techniques used on EEG signals (functional microstate analysis), source localization (LORETA) and on a novel method of segmentation for design protocols based on EEG features. Using these techniques, we measure mental effort, fatigue and concentration in the conceptual design process, in addition to creativity and insight/nonverbalizable processing. We discuss the strengths and

weaknesses of such approaches.

Acknowledgments

I wish to thank NSERC for the Discovery Grant that has supported this research. I also wish to thank the volunteers at the Design Lab for their contributions. I would also like to thank my thesis advisor, Professor Yong Zeng, for his continuing support and insight and the doctoral examining committee for the time and effort they have put to understand and support my research. I would also like to thank Dr Thanh An Nguyen and the Concordia Design Lab for their contributions. Finally, I would like to thank my father, my mother and my sister, as they has always been a source of inspiration.

Contents

List of Figures **x**

List of Tables **xvi**

List of Algorithms **xviii**

List of Code Listings **xix**

1 Introduction **1**

1.1 Previous Work at the Concordia Design Lab 6

1.2 New Contributions 8

2 Background **9**

2.1 Design Theories 9

2.1.1 Early Theories: Prescriptive Models 11

2.1.2 Formal Approaches 12

2.1.3 Contemporary Theories: Generative Models 14

2.2 Physiological Studies of Design: Effort, Fatigue and Concentration 18

2.2.1 Cognitive Aspects of Mental Effort 18

2.2.2 Cognitive Aspects of Fatigue 21

2.2.3 Cognitive Aspects of Concentration 22

2.3 Neurological Aspects of Creativity 23

2.4 Design Protocol Analysis and Automated Methods 25
2.4.1 Content Based Analysis Methods for Textual Protocols: Ontologies . 29
2.4.2 Content Based Analysis Methods for Non-Textual Protocols: Image Processing and Pattern Recognition 31
2.4.3 Non-Content Based Analysis Methods for Non-Textual Protocols: Physiological Methods 32
2.5 Weaknesses of Verbal Protocols 33

3 EEG Analysis **36**
3.1 Fundamentals of EEG 38
3.1.1 Stochasticity and Fractality 39
3.1.2 Analyticity and Interpolation 41
3.1.3 Gradient Fields 42
3.2 Spatio-Temporal Features: Microstates 47
3.2.1 Unsupervised Clustering of Scalp Field Maps: Comparisons 47
3.2.2 The P2ML Algorithm: An Outline 50
3.3 Frequency-Domain Features 55
3.4 Source-Localization 56
3.5 Mathematical Validity of Machine Learning Algorithms on EEG Data . . . 58
3.5.1 Concentration of Measure 61
3.5.2 Experimental Validation 61

4 Approaches to Quantifying EEG Features **63**
4.1 Experimental Protocol 63
4.2 Problem Hardness and Transient Microstate Percentages 65
4.2.1 Experiments 67
4.2.2 Discussion 68
4.3 Segmentation of Design Protocols Using EEG 71

4.3.1 Physiologically Based Segmentation 71
4.3.2 Experiment and Analyses 73
4.3.3 Discussion 74
4.4 Validation of EEG Based Segmentation of Design Protocols 75
4.4.1 Physiologically Based Segmentation Using Transient Microstates . . 75
4.4.2 Experiments and Analysis 76
4.4.2.1 Experimental Protocol 76
4.4.2.2 Domain Expert Vs Domain Expert 81
4.4.2.3 Algorithm Vs Domain Expert 82
4.4.2.4 Algorithm Vs Algorithm 83
4.5 Fatigue as a Multidimensional Concept in EEG Analysis 85
4.5.1 Multistate Analysis of EEG Signal 86
4.5.2 Experimental Results and Analysis 88
4.6 Effort, Fatigue and Concentration In the Conceptual Design Process 92
4.6.1 Quantitative Analysis of EEG signals of Design Protocols 94
4.6.1.1 Quantifying Effort 95
4.6.1.2 Quantifying Fatigue 96
4.6.1.3 Quantifying Concentration 97
4.6.2 Analysis 99
4.7 Modal Shifts in Concentration Indicate Creativity 102
4.8 A Real-Time Algorithm for Transient Microstate Percentages 109
4.8.1 Real-Time Approximation of Transient Microstates 109
4.8.2 Experiments and Validation 111
4.8.3 Discussion 111

5 Conclusion **113**

Bibliography **116**

Appendix A: A Mathematica Implementation of P2ML **141**

Appendix B: A Mathematica Implementation of LORETA **144**

Index **146**

List of Figures

1.1 Illustration of our 7 research hypotheses. 4

2.1 Different design of the clothing iron. Early models (a) were heated on charcoal before incorporating the charcoal in the design (b). The modern iron (c) is multi-functional, safe and easy to use. 10

2.2 Kahneman's capacity model theory [Kah73]: A mental state is an activator that regulates the capacity of another mental state. 19

2.3 (left) Regions of the brain. (right) Functions of the left/right hemispheres. . 23

2.4 Ontology generated using FRED for the first conversation line of the Samantha-Theodore dialogue. 30

2.5 (a) displays a typical answer question segment, (b) a read question segment, (c) a design object segment and (d) a rate problem segment. 31

3.1 Both plots show the channel labels $(1, 2, \ldots, n)$ on the x) axis and time on the y axis for convenience. The gradient field of an EEG epoch is computed using the directional derivative in the time direction. Smaller arrows or blanks denote small changes in potential or no changes in potential while larger arrows show larger changes in potential. Here the subject was asked to close his eyes for 1 minute and clear his mind. The EEG signals show an sequence of 0.2 seconds taken at the beginning of the epoch of 1 minute. 43

3.2 Scalp field maps associated to points on the global field power curve of an EEG. The subject was asked to perform an acitvity. 45
3.3 Microstates obtained from different algorithmic implementations. 46
3.4 Fuzzy membership functions of the first 250 samples of an EEG clustered using fuzzy c-means. The strongest component is clearly the second centroid. The first and the fourth centroid follow whereas the third centroid has a low average membership. 49
3.5 Global field power curve with non-regularized (a) and regularized (b) microstate segmentation of an epoch of length 200. The subject was asked to keep his eyes closed. 54
3.6 (left) 2-D scalp field map. (center) Interpolated 3D scalp field map using 107 points. (right) Voxels representing the brain using 452 voxels. 57
3.7 Computed probability density functions on different Hurst indices with sythetic data simulating n electrodes and an epoch-length of N. Lower Hurst indices tend to aggregate around low correlation scores ($\rho < 0.5$). 59
3.7 (continued) Higher Hurst indices tend to aggregate around higher absolute value correlation scores ($\rho \approx (-1, 1)$). 60

4.1 Screenshots of various stages in our experimental protocol: (a) multiple choice question, (b) read question, (c) sketch a solution and (d) rate the hardness of the question 63
4.2 Feeback loops in a typical BCI subsystem. 66

4.3 The number of transient microstates is computed using segment regularization and is defined as the difference between the number of segments in the non-regularized microstate segmentation (yellow) and the number of segments in the regularized segmentation (blue). The number of transient microstates (yellow) is significantly higher for EEG signals during an activity (right) than an EEG signal recorded eyes closed (left). 66

4.4 The plots show the time-varying transient microstate percentage of EEG signals of subjects asked to perform tasks of varying difficulty. In the leftmost and center-left figures, a subject was asked to close his eyes (gray) and the perform an activity (black) and then close his eyes (light gray). In the center-right and rightmost figure, a subject was asked to perform tasks of varying difficulty: he rated the tasks as easy with a score of 5 (lightgray), average with a score of 10 (gray) and hard with a score of 15 (black). The window size used was 1,000. 68

4.5 (a) shows the time-varying transient microstate percentage of EEG signals of a subject who was asked to perform a set of tasks over 30 minutes. In (b), the transient microstate percentage curve was classified into low segment (lighter gray) medium segments (light gray), high segments (gray) and very high segments (black). A trending curve was added. In (c), histograms were computed. Lower microstate percentages correlated with easier tasks while higher microstate percentages correlated with harder tasks. In (d), the transient microstate percentage was computed on a subject with eyes closed using different window sizes. The percentage shows stability with respect to window size. 72

4.6 Coarse-grained segmentation of design protocol video based on the transient microstate percentage. A window size of 5 (25 seconds) was chosen. Values in the window were averaged. The resulting values were clustered into 4 clusters. 74

4.7 Figure 7: Distance matrix between various segmentation strategies averaged across the 8 datasets. Distances are measured in minutes (e.g. 0.01 is equivalent to 1 second). The first 3 rows show the distance between Domain Expert segmentation (R1, R2, R3) and algorithm segmentation (TM1%, A1, B1, . . . ,H2). Our nearest neighbor metric was used to compute deviations in seconds between different segmentations using different segmentation algorithms. See Table 4.6 for label descriptions. 80

4.8 Standard error matrix associated to the distance matrix. See Table 4.6 for label descriptions. 80

4.9 Distance matrix of each of the 8 datasets (from top to bottom: FEB28, FEB18, AUG5, APR18, APR16, APR8, APR23, APR21) with respects to the distance between the domain expert segmentation (R1,R2,R3). 81

4.10 Sequence of screenshots from experimental protocol comparing manual segmentation and automated segmentations: (top) lists segments found by a domain expert; (bottom) shows segments found by the transient microstate algorithm with window size 1. Major segments (screenshot 1, 2, 5 and 6) are roughly aligned when comparing domain expert segmentation and automated segmentation. Automated segmentation is however much more fine-grained than manual segmentation. Unlabelled segments show segments that are observed to be a continuation of the previous segment label and for which not obvious observation can be made. 82

4.11 Sequence of screenshots from experimental protocol comparing two automated segmentations: (top) lists segments found by the transient microstate algorithm with window size 1; (bottom) shows segments found by the beta algorithm with window size 1. The beta algorithm misses a few segments and shows a slight deviation from the transient microstate algorithm. However, in screenshot 6, the beta algorithm showed a high level of granularity for the "Stops and thinks" segment. This can be explained by the fact that the beta range measures concentration. 84

4.12 Features are analyzed as an ensemble of interrelated concepts (left) rather than isolated facts (right). 87

4.13 Multistate analysis provides a grid of interrelations between features of a set of physiological signals and are aggregate across different experiment datasets. The strength of the relationship is aggregated in a distance matrix. 88

4.14 Figure (a) shows the number of transient microstates (y-axis) vs the segment label (x-axis). Figure (b) shows feature (theta+alpha)/beta (y-axis) vs the segment label (x-axis). A trended curve is given in red and shows a negative correlation between both Figure (a) and (b) curves. 88

4.15 Correlations matrix between different EEG features: (A) transient microstate percentage, (B) alpha range - TYPE-1 Fatigue, (C) beta range, (D) theta range, (E) delta range, (F) (theta+alpha)/beta - TYPE-2 Fatigue, (G) alpha/beta - TYPE-3 Fatigue, (H) (theta+alpha)/(alpha+beta) - TYPE-4 Fatigue and (I) theta/beta - TYPE-5 Fatigue. 89

4.16 Excerpt from the design protocol data of a subject solving Problem 4. Below are timestamps generated by the segmentation algorithm. At screenshot 6, a large quantity of timestamps are generated. This indicates a modal shift in concentration. In this case, the modal shift occurs while the subject is erasing his previous design and redrawing from scratch a new one (tabula rasa event). 98

4.17 Plot of computed concentration levels for a given protocol: a sliding window of length 1 second and offset 5 seconds was used on the time segmentation of the Beta range curves. The number of segments that occurred within the range of the sliding window was counted (y-axis). 99

4.18 Screenshot from a video protocol (the question was to design an escalator for people in wheelchairs) where the subject is entering a *tabula rasa* sequence and erasing partially his design to replace it with a new design. Such sequences were found to have heightened measured concentration levels. 100

4.19 Excerpt from the design protocol data of a subject solving Problem 4. Below are timestamps generated by the segmentation algorithm. At screenshot 6, a large quantity of timestamps are generated. This indicates a modal shift in concentration. In this case, the modal shift occurs while the subject is erasing his previous design and redrawing from scratch a new one (tabula rasa event). 105

4.20 Slices of the spherical 3D model of the brain we used at different z values (-0.79, -0.58, - 0.37, -0.16, 0.05, 0.26, 0.47, 0.68, 0.89) which also corresponded to the location of the voxel slices. White denotes high density magnitudes while black denotes low density magnitudes. 107

4.21 Computation of the transient microstate percentages using P2ML and our method comparisons. F_1 and F_2 parameters were $\epsilon = 15$, $\kappa = 1$ and $\omega = 2$. The average number of transient microstates found using P2Ml was 513.116 and 537.858 using our method, or less than half a percent difference. 110

List of Tables

2.1 Chronology of a few remarkable design theories 13

2.2 Some publications on the use of EEG analysis in design protocol analysis and the study of the conceptual design process 16

3.1 EEG scalp field map pre-processing techniques 40

3.2 Radial Basis Functions 44

3.3 EEG frequency-domain features 56

4.1 Experimental Design Protocol Problem List 64

4.2 Performance benchmarks of the P2ML Algorithm 70

4.3 Performance benchmarks of the regularized P2ML Algorithm 70

4.4 Segmentation of the design protocol video into design moves. Underlined rows were detected by means of the automated physiological method. Non-underlined rows were expected design moves in the segmentation that were not detected by the method. 77

4.5 EEG Features 78

4.6 Segment Labels and Methods 79

4.7 Approximate regions of the brain activated related to creativity. Timestamps are relative to the beginning of the sequence (with high levels of concentration) excerpted from a design episode. The sequence occurs while a subject is solving Problem 4 and is in a tabula rasa event. 108

4.8 Performance benchmarks 111

List of Algorithms

3.1 K-Means Algorithm 51
3.2 Fuzzy C-Means Algorithm 51
3.3 P2ML Algorithm 52
3.4 Regularized P2ML Algorithm 53

4.1 General Segmentation Algorithm 96
4.2 Levels of Concentration Algorithm Using Binning 97

Listings

1 P2ML Algorithm Implementation 141
2 Regularized P2ML Algorithm Implementation 142
3 Transient Microstate Computation 143
4 Computation of the Brain Model 144
5 Computation of the LORETA Resolution Matrix 144
6 Computation of the LORETA Densities 145

Chapter 1

Introduction

Can the mechanics of the human mind performing easy to complex design tasks be measured in various ways like an engineering system can be monitored and understood from its sensors? [Sea92] argues that all mental phenomena (from pain to creativity) can be understood by lower (e.g. pain) or higher (e.g. creativity) neurological and biological processes and are, by extension, physically measurable. According to [Nag74], the reason why the mind remains mysterious to the scientific method is ultimately due to a lack of knowledge. Well-known criticisms to these two views [Wit54, Hac03] argue that the mind-body duality is an illusion of language and that mental and biological states should be treated using different sets of vocabulary to avoid confusion. The end-result, the scope and applicability of current physiological methods and the complexity of such an endeavour is effectively on a completely other scale than a regular engineering system and a lot of research in design sciences and cognition, physiology and neurosciences has been done on the subject [Ara12, Ber37, Cho59, KB04, Kah73, Sta04]. While not falling into the traps of a La Mettrie world view, it can be argued that the availability of such physiological methods, within the scope of their applicability, to support the design process and offer insight on or validation of design theories and methodologies can be invaluable [NZ16b, GEGS15, JFR+15, Goe14, NZ10a].

In our previous work, we proposed a transient microstate (i.e. a spatio-temporal feature of

EEGs) measure of mental effort and frequency domain measures of fatigue and concentration in the context of design protocol analysis [NNZ15a, NNZ17a]. We analyzed various metrics of fatigue measured during the conceptual design process [NNZ16]. We also proposed a technique to segment design protocols using transient microstates [NNZ15b, NNZ17c]. These works follow from [NZ10a]. Furthermore, we analyzed creativity using source localization on segments we quantified as having high concentration values [NNZ17b]. Questions we ask ourselves are as follows:

- What are effort, fatigue and concentration?
- How are they relevant to the conceptual design process?
- How can EEG quantify effort, fatigue and concentration?
- How can EEG measures of effort, fatigue and concentration be interpreted in the conceptual design process?
- How can quantified measures of effort, fatigue and concentration relate to design research?
- How can EEG be used to segment the design protocols?
- Can creativity be detected using EEG?

The pros of such an EEG-based approach can be seen as follows: EEG analysis of design cognition features form fully automated methods that can be readily integrated into engineering systems and real-time environments. As commercial EEG headsets become more available, less intrusive, more user friendly and comfortable to wear, a real push towards EEG applications can be seen in the market [BLC+04]. Measures of fatigue have been incorporated in vehicular security systems [SB15]. While it is objective and does not suffer from intra or post-hoc imprecisions like traditional expert-driven analysis, it may suffer from false positives (as most pattern recognition methods do).

The cons of such an approach would then be as follows: EEG analysis does not replace

traditional design protocol analysis or expert-driven analysis, but rather serves as a complement. The algorithmics required to solve a specific problem pertaining to design (e.g. can a design protocol be significantly segmented using EEG) may take time to be developed if they can be developed at all in the current state of research. When applicable, physiological methods and EEG allow us to glimpse at and see cognitive structures that would remain unseen using traditional methods while some evidence shows that some EEG based methods can emulate simple design protocol analysis [NNZ15b].

While EEG excels at measuring states of mind (e.g. effort, fatigue, concentration), the question of the applicability of EEG analysis to higher complex cognitive tasks remains an open question. An early critic [GZD+79] argues that complex cognitive tasks could not be distinguished using EEG patterns in their three sets of experiments (serial addition, letter substitution, block rotation). [PRCS00] argues that complex cognitive tasks can be distinguished using pattern recognition in the context of Brain-Computer Interfaces (BCI) modulo false positives.

In this thesis, we address the following 7 hypotheses using quantitative EEG analysis on design protocol data:

Hypothesis 1. *Design protocol segmentation using EEG is a feasible method.*

A common technical point in our research is the conversion of EEG feature curves (which are too high frequency to be analyzed in the context of design research) into time points using clustering that can be synced to a video protocol. Effectively, our data consisted of EEGs monitored on subjects who were asked to solve easy to complex design tasks on a sketchpad. The sketchpad recordings provided the video protocols.

Hypothesis 2. *Mental effort can be measured using transient microstates.*

In our previous research [NNZ15a], we find that transient microstate percentages correlate with mental effort measured using subjective ratings. This can be understood by seeing that, as scalp field maps change their configuration in a more transient manner (short lasting

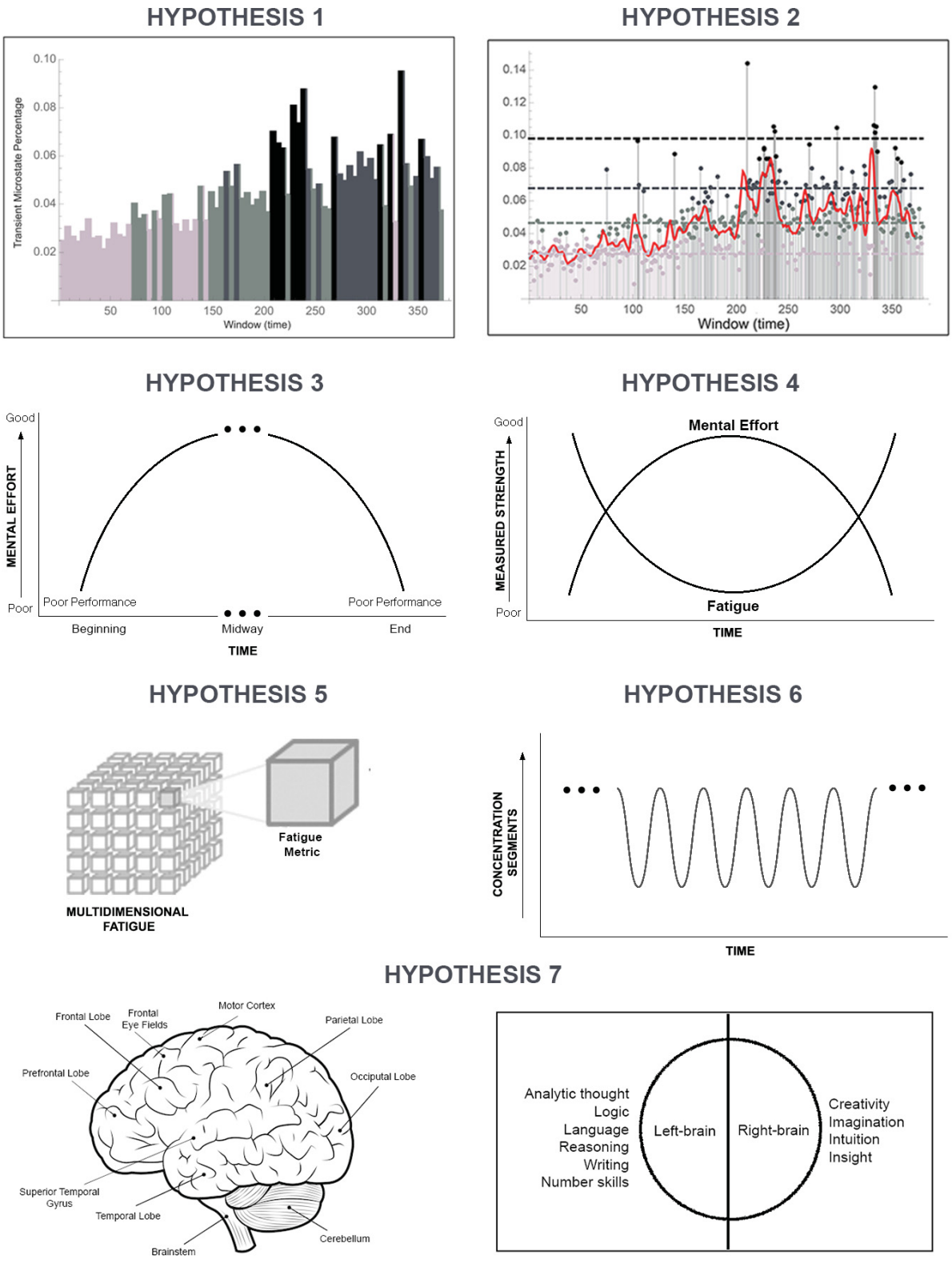

Figure 1.1: Illustration of our 7 research hypotheses.

.

configuration changes), the brain is using more energy and this is more likely to correlate with mental effort.

Hypothesis 3. *Effort (and by extension fatigue) is subject to an ice-breaking and end of task phenomena during the conceptual design process.*

In our design protocol, although tasks were easy at first fatigue was high and effort low, which could be interpreted through phenomena such as *ice-breaking* or boredom [Cha13]). At the end of the design protocol. although tasks were hard, effort was also low and fatigue high. Spikes of fatigue at the end of the design protocols can be due to prolonged and sustained effort during the experiments [Ara12]. Spikes at the beginning of the design protocol reiterate sound design methodologies which advocate the usefulness of warm-up problems in design problem solving [WSJ13].

Hypothesis 4. *Fatigue and effort follow a capacity model.*

The capacity theory of mental states [Kah73] states that 'a capacity theory is a theory of how one pays attention to objects and to acts."

Hypothesis 5. *Fatigue is multidimensional.*

[De 05, Hoc13] argue that different types of fatigue (physical, mental, drowsniness) are routinely confused with each other in research, being multidimensional in nature.

Hypothesis 6. *Concentration follows a modal shift model during the conceptual design process.*

In [Cro01], a modal shift theory of creativity is discussed. Following this theory, our research shows that concentration occurs in highly transient beta band segmentations of design protocols and would be related to creativity. Furthermore, [NZ12c] describes creativity as a sequence of iterates that can fall into a chaotic pattern.

Hypothesis 7. *Modal shifts in concentration indicate creativity.*

After having identified segments where modal shifts in concentration were occurring, we used the LORETA source localization algorithm [PMML94b] to identify the regions of the brain that were active during such modal shifts. Cross-checking with the physiology and neurology literature, we found that the prefrontal cortex, the basal ganglia and the superior temporal gyrus were active. These are regions associated with creativity [dGT$^+$14, GYdL$^+$13, Die04, HNB03]. Furthermore, it is an open debate in the design literature whether nonconscious processing (nonverbalizable processing) is significant. Using source localization, we determine what hemispheres of the brain are active during modal shifts in concentration. It is known that the left hemisphere indicates processing related to logic, analytical thinking and language while the right hemisphere indicates creativity, insight and intuition [Orn77, Gaz67].

1.1 Previous Work at the Concordia Design Lab

The Concordia Design Lab has pioneered research in Design Engineering from the perspective of Environment-Based Design [Zen11] which extends Axiomatic Theory of Design Modeling (ATDM) [Zen02]. The approach is formal, focusing on the recursive nature of design thinking. ADTM explored, using abstract algebra, the very fluid notion of design logic while the environment-based formulation of design problems focused on the notion of automation of the design process by recursively iterating the environment/solution space using, notably, natural language processing techniques such as the ROM diagram [Zen08]. In [NZ12c], it is found that creativity follows a nonlinear model where Problem-Knowledge-Solution triplets evolve iteratively from one state to the other. In the context of this foundational research, the Design Lab started interesting itself on how biometric signals (e.g. eye-tracking, electrocardiograms (ECG) and skin conductivity) and, among them, electroencephalograms (EEG) could help understand design thinking in a formal and scientific way.

The analysis of biometric signals in the context of Design Engineering was undertaken

in a series of publications. The Design Lab has more specifically focused on mental stress, mental effort and workload. It has also focused on the study of creativity and solution generation in relation with mental stress.

In the context of gesture analysis, [TZ09] discuss the use of kinesics in the study of mental stress in the conceptual design process. It is found that mental stress is closely related to body movement (kinesics). A combined study of EEG and Heart Rate Variability (HRV) is proposed in [NZ14b]. It is found that mental effort is at its lowest when stress is at its highest. [XNZ14] discuss the use of Galvanic Skin Response (GSR) in the study of mental workload as a determinant factor affecting creativity. It is found that GSR values vary significantly from rest state to workstate. In [NXZ13], HRV, EEG and gesture analysis are used in combination to study the relationship between design activities and mental stress. More specifically, it was found that design activities were less predominant when stress increases, while no correlation was found between types of design activities and mental stress. In the analysis, the design protocols were segmented and HRV data were associated to the segments; classification was then used to distinguish levels of stress. In [NZ16b], self-rated reports on stress and mental effort were compared with EEG frequency domain features measuring the same states (i.e. using the beta bandwith). Mental stress was again assessed using EEG and eye-tracking experiments in [PDY$^+$09]. Strong correlation between emotional states and recorded physiological signals was found.

In direct relation to our current research, the idea that design protocols can be segmented using EEG was brought forth in [NZ10a]. Frequency domain features were used on different channels. It is found that the subjects spent more effort in visual thinking during the solution generation than that in solution evaluation. Clustering of EEG frequency domain features was studied in [NZ12a]. Clusters were associated to design activities such as *solution expression*, *solution generation*, *knowledge search*, *requirements analysis* and *requirement evaluation*. A recent paper of the Design Lab [LNZH16] discusses how Principal Component Analysis (PCA) can be used to find relationships between different EEG frequency domain

features. Fixation in design was studied in [NZ16a].

1.2 New Contributions

In our work, we extend the work done by the Design Lab on biometric signal analysis of design (more specifically, using EEG) with new EEG methods of analysis. More specifically, we propose a measure of mental effort based on transient microstates [NNZ15a]. Microstate analysis was pioneered by D. Lehmann in [LOP87]. We propose a new method to segment EEG using transient microstates. EEG segmentation is typically too high frequency to be useful in protocol analysis, so we developed an algorithmic layer to associate EEG segmentations of EEG feature curves to protocol data [NNZ15b]. We also propose a method to validate and compare EEG based segmentation with protocol segmentation performed by human experts [NNZ17c]. We found that EEG based segmentation compares well with basic segmentation performed by human experts while being able to detect cognitive state that were invisible to the human expert in the underlying video protocols. We also propose a method to compare and validate different EEG feature curves with each other. More specifically, we find that different EEG metrics of fatigue do not correlate with each other necessarily, which leads to believe that different EEG metrics of fatigue measure different types of fatigue [NNZ16]. We propose a general algorithmic framework to monitor effort, fatigue and concentration during the design process and test our analysis against different results in the cognitive and design literature on effort, fatigue and concentration [NNZ17a]. Finally, we use the LORETA source localization algorithm to determine if creativity in design activates regions of the brain related to verbalization or insight (left-right hemisphere theory). An open question in the design literature is whether nonverbalizable processes are significant during the conceptual design process [NNZ17b].

Chapter 2

Background

2.1 Design Theories

The clothing iron can be seen as an example, albeit trivial, of how design theories and methodologies impact design itself. The history of the clothing iron dates back to 1st century BC China. Irons were initially heated on charcoal before the idea of incorporating the charcoal itself in the iron was discovered (cf. Figure 2.1). Ironing was then performed by specialized people. In XIXth century Europe, charcoal was replaced by fuel (gas or kerosene). The devices were hefty and heavy. With the emergence of plastic and polymers, the design of irons was made lighter and electricity then allowed for heated elements to replace the hazardous fuel. Modern irons are therefore cost effective and safe to use and ironing can be even performed by an unexperienced person. These modern irons even incorporate water as a means to smooth out the cloth.

The evolution of the design of the iron clearly follows the evolution of the history of technical capabilities (fuel, electricity, plastic) but is not solely determined by it. Indeed, the evolution of the iron may shed some light in design theory and methodology.

A common adage in design history is “Form follows Function”. In the case of the evolution of the iron, all models had the same end function (to iron clothing) and it is

(a) Early iron design (b) Charcoal iron (c) Modern iron

Figure 2.1: Different design of the clothing iron. Early models (a) were heated on charcoal before incorporating the charcoal in the design (b). The modern iron (c) is multi-functional, safe and easy to use.

safe to say that the adage would need to be upgraded to multi-functional purposes to be still valid (as the modern iron is clearly a combination of multiple functions). In terms of design theories, Adaptable Design [GHN04] focuses on reusing existing designs to increase the lifetime of a product design. This reuse is stated as an iterative and recursive process of design in contemporary design theories such as Axiomatic Theory of Design Modeling (ATDM) [Zen02] or C-K Theory [HW09]. C-K Theory splitting functions [LHW15] let us see the hybrid nature of the modern iron from the perspective of management of innovation (e.g. is the modern iron an iron or a water sprayer). The iterative nature of design creativity is stressed in the Nonlinear Theory of Design creativity of [NZ12c] as an extension theory of ATDM. As different instances of the clothing iron appear in the history of its design, we see an additional iteration in the design process occurring. The problem domain changes and the solution domain follows. Other perspectives can be taken on the evolution of the clothing iron. Axiomatic Design [Suh90] would stress out the existence of customer requirements (e.g. the iron needs to spray water) while Environment Based Design [Zen11] iteration would generate a ROM diagram [Zen08] stressing out environment constraints arising from the design of the modern iron (e.g. the iron needs to be used in a domestic environment and hence be safe).

The study of design and design theories or methodologies allows us to understand and improve the design process. While the case of the clothing iron may be only a toy example, complex products, processes and services would follow the same reasoning grids. Design is a pre-development phase of product engineering and good designs can save money, time and provide added-value to products, processes and services. It is therefore important to understand design as theories and as methodologies to improve the overall product development and lifecycle. The design of products furthermore impacts society as a whole by providing the tools and processes with which it realizes itself.

Although design theories and methodologies may seem reasonable, they sometimes need to be validated scientifically. The validation of design theories and methodologies is a field where physiological studies of design may provide a solution.

From the second half of the 20th century and the early 21st century, there have been numerous attempts at defining design theory in engineering ranging from prescriptive models to formal models and generative models. Early design theories attempted to provide formal processes and prescriptive background for the study of design (60's, 80's and early 90's) while later theories (2000's) attempt at defining generative frameworks where design is actuated.

2.1.1 Early Theories: Prescriptive Models

The Theory of Inventive Problem Solving (TRIZ) is a first notable theory and was sketched in 1947 and published later on by [Alt84]. It is an early prescriptive model of design aimed at understanding and defining hard problems by proposing a range of solution strategies classified in 40 principles. Strategies are formal and include contradiction matrices. Among the contradictions that can be found in the TRIZ analytical model are administrative contradictions (e.g. contradictions between needs and abilities), technical contradictions (i.e. contradictions within the technology used) and physical contradictions (i.e. contradictions in the physical requirements of a product). The Analysis, Synthesis and Evaluation Model (ASE) by [Jon63] is another early prescriptive model defining the design process as a

linear process involving analysis, synthesis and evaluation. The Analysis phase consists in "listing all design requirements and the reduction of these to a complete set of logically related performance specification" [Jon63] (much akin to functional and non-functional requirements). The Synthesis phase consists in "finding possible solutions for each individual performance specification and building up complete designs from these with least possible compromise" [Jon63]. The notions of *least possible compromise* already echoes a later design theory, Decision-Based Design. The Evaluation phase consists in "evaluating the accuracy with which alternative designs fulfill performance requirements for operation, manufacture and sales before the final design is selected" [Jon63]. A variation of the ASE model proposes a cyclical process involving analysis, synthesis and evaluation which may remind of more contemporary design theories insistence on iterative and recursive processes.

2.1.2 Formal Approaches

Following these early models, a set of formal approaches were devised. The General Design Theory [Yos81] is an early precursor theory which defines the theory of design through mathematics [Rei95] that was initially conceived to construct CAD systems in a scientific manner. The Theory of Technical Systems [HE88] and Systematic Design Theory [GWW88] are models where the goal is to "derive rules for the development of technical systems from the system elements and their relationships" [PBFG07]. It brings forth in design theory the notion of interrelated atoms. Axiomatic Design [Suh90] analyzes the production of functional requirements from customer requirements. Axiomatic Design incorporates two general axioms: first, functional requirements should be functionally independent and, second, the design should be compact. The Function-Behavior-Structure (FBS) Model [Ger90] defines an ontology (a computer-processable semantic definition) which is often used in protocol analysis to extract information pertinent on Function, Behaviour and Structure as its constructing atoms. By defining an ontology, protocol analysis can be extended to analyze behaviour in design, design modeling and design processes through operators on its base atoms. Total

Table 2.1: Chronology of a few remarkable design theories

Theory Name	Authors	Notable Publication Name	Year
Theory of Inventive Problem Solving (TRIZ)	G.S. Altshuller	Creativity as an Exact Science: The theory of the solutions of inventive problems	1947
Analysis, Synthesis and Evaluation (ASE)	J.C. Jones	A Method of Systematic Design	1963
General Design Theory	H. Yoshikawa	General Design Theory and CAD System	1981
Extended General Design Theory	T. Tomiyama and H. Yoshikawa	Extended General Design Theory	1985
Theory of Technical Systems	V. Hubka and W. Eder	Theory of Technical System	1988
Systematic Design Theory	G. Pahl, W. Beitz and K. Wallace	Engineering Design: A systematic approach	1988
Set Based Design	A. C. Ward	Mechanical Design Compilers	1989
SBF Model	A. Goel	The Principles of Design	1990
Axiomatic Design	N. Suh	The Principles of Design	1990
FBS Model	J. Gero	Design Prototypes: A Knowledge Representation Schema for Design	1990
Total Design	S. Pugh	Total Design: Integrated methods for successful product engineering	1991
Recursive Logic of Design	Y. Zeng and G.D. Cheng	On the Logic of Design	1991
Decision-Based Design Theory	G.A. Hazelrigg	Systems Engineering: An approach to information-based design	1996
Formal Design Theory	D. Braha and O. Maimon	A Mathematical Theory of Design: Foundations, Algorithms, and Applications	1998
Artificial intelligence-Based Design	J. Gero	Artificial Intelligence in Design '00	2000
Science-based Product Design	Y. Zeng and P. Gu	A Science-based Approach to Product Design Theory (Part I and II)	1999
Axiomatic Theory of Design Modeling	Y. Zeng	Axiomatic Theory of Design Modeling	2002
Coupled Design Process	D. Braha and Y. Reich	Topological Structures for Modeling Engineering Design Processes	2003
C-K Theory	A. Hatchuel and B. Weil	C-K Design Theory: An advanced formulation	2003
Environment-Based Design (EBD)	Y. Zeng	Environment-Based Formulation of Design Problem	2004
Adaptable Design	P. Gu, M. Hashemian, and A.Y.C. Nee,	Adaptable Design	2004
Infused Design	O. Shai and Y. Reich	Infused Design: I. Theory	2004
Affordance Based Design	J.R.A. Maier and G.M. Fadel	Affordance Based Design: A relational theory for design	2009

Design [Pug91] aims at defining customer requirements. In the words of its author, "Total Design is the systematic activity necessary, from the identification of the market/user need, to the selling of the successful product to satisfy that need an activity that encompasses product, process, people and organization". Decision-Based Design Theory [Haz96] models the design process as a set of decision, hence incorporating the large compendium of work from decision sciences. A decision is seen as a selection-compromise pair.

2.1.3 Contemporary Theories: Generative Models

Following these formal approaches, a set of generative approaches can be found in the literature where design is seen as a set of atoms on which operators are applied. These approaches are often based on mathematical formulations of design. A contemporary first formulation of design using abstract algebra and recursive logic can be found in [ZC91]. Applications of the theory to product design can be found in [ZG99a, ZG99b]. Formal Design Theory [BM98] brings a formal model of design based on set theory [Zen02]. Bringing set theory to design theory was precursor of C-K Theory and Axiomatic Theory of Design Modeling (ATDM). Coupled Design Process [BR03] is a clarification of Formal Design Theory which takes the General Design Theory as a special case of the framework. By recasting the ASE model and Axiomatic Design's focus on specification, it describes an iterative process of refinement of specification, synthesis and refinement of solution in a set-theoretical framework. ATDM [Zen02] brings recursive logic in design theory models such as ASE and like Formal Design Theory is set theoretical (however, uncertainty is handled by removing the membership function [Ngu16] - hence becoming a set theory without the Axiom of Choice). In computational sciences, it is well-known that a recursive language is Church-Turing complete. ATDM therefore brings set theoretical theories to the level of computational completeness. Infused Design [SR04] formally describes how collaboration and concurrent engineering occurs in design through the use of the concept of combinatorial-representations. Exchange of information is multidisciplinary. C-K Theory [HW03, HW09] is a generative approach similar

to Chomsky linguistics with a focus on management of innovation. Chomsky's generative approach was a criticism of structuralism and post-structuralist theories and although it is largely seen as correct, the definition of a general set of effective generating functions for language, and by extension conceptual design, remains ill-defined, a case-by-case study. Generative approaches can be paralleled with computation theory where the generating function is a recursive language. C-K Theory splitting function [LHW15] aims at defining a base operator for C-K theories and the Twizy vehicle by Renault is largely seen as a productive example of the method by fuzzifying concepts: is the Twizy a motorcycle? is it a car? Environment-Based Design (EBD) [Zen04, Zen11] extends ATDM to incorporate environment as an element of analysis by identifying conflict and through a dialectical and recursive approach generate a solution. Like C-K Theory and the earlier ADTM, the approach is recursive and generative but, rather than focusing on the concept-knowledge pair, takes the general concept of an environment as its ambient space. The ROM diagram [Zen08] is an artifact of the EBD method. The generative operators of EBD are the structure operator, the union operator and the interaction operator which effectively define a recursive dynamic system of the design process.

An interesting initiative for design theory can be found in the Artificial Intelligence-Based Design model [Ger00] aimed at incorporating the significant advances in computational sciences to the field of design theory. Other less theoretical and more pragmatic methods include Adaptable Design [GHN04] which addresses the lifecycle of the product by proposing the notions of design and product adaptability (how proven processes and designs can be reused and how products are reused to extend their service life).

Table 2.1 lists major contributions to design theory we have discussed.

Table 2.2: Some publications on the use of EEG analysis in design protocol analysis and the study of the conceptual design process

Authors	Title and publisher	Keywords
R. Riedl & P.M. Léger (2016)	Fundamentals of NeuroIS: Information Systems and the Brain, *Springer*, 2016	Design science research, neuroscience, NeuroIS
T. A. Nguyen & Y. Zeng. (2016)	Effects of Stress and Effort on Self-Rated Reports in Experimental Study of Design Activities, *Journal of Intelligent Manufacturing*, 2016	Cognitive effort, psychological stress, subjective rating, skin conductance, EEG design
P. Nguyen & T. A. Nguyen & Y. Zeng (2016)	Quantitative Analysis of the Effort-Fatigue Tradeoff In the conceptual design process: A Multistate EEG Approach, *Proceedings of the ASME DETC/CIE Design Theory and Methodology Conference (DTM)*, 2016	conceptual design process, EEG, fatigue
V. Goel & I. Eimontaite & A. Goel & I. Schindler (2015)	Differential Modulation of Performance in Insight and Divergent Thinking Tasks with tDCS, *Journal of Problem Solving*, 2015	Enhancing creativity, tDCS, insight, fluency, semantic spread, mental set shift, temporal lobes
S. Jaarsveld & A. Fink & M. Rinner & D. Schwab & M. Benedek & T. Lachmann (2015)	Intelligence in Creative Processes: An EEG study, *Intelligence*, 2015	Intelligence, creativity, EEG-Alpha synchronization, complex problem solving, ill-defined problem space
P. Nguyen & T. A. Nguyen &Y. Zeng (2015)	Measuring the Evoked Hardness of Design Problems Using Transient Microstates, *Proceedings of the ASME DETC/CIE Design Theory and Methodology Conference (DTM)*, 2015	conceptual design process analysis, functional microstate analysis, problem solving, effort
P. Nguyen & T. A. Nguyen & Y. Zeng (2015)	Physiologically Based Segmentation of Design Protocol, *Proceedings of the 20th International Conference on Engineering Design (ICED 15) Vol 11: Human Behaviour in Design, Design Education*, 2015	Design cognition, protocol data analysis, EEG based segmentation, problem hardness
P. Seitamaa-Hakkarainen & M. Huotilainen & M. Mkela? & C. Groth & K. Hakkarainen (2014)	The Promise of Cognitive Neuroscience in Design Studies, *Design Research Society, DRS2014*, 2014	Design process, cognitive science, brain imaging methods, embodiment
V. Goel (2014)	Creative Brains: Designing in the real world, *Frontiers in Human Neuroscience*, 2014	Architecture, creativity, drawing, representations, cognition, neuropsychology, lesion studies, hemispheric asymmetry
S. S. Shankar & R. Rai (2014)	Human Factors Study on the Usage of BCI Headset for 3D CAD Modeling, *Computer Aided Design*, 2014	Brain computer interfaces (BCI), human factors, natural CAD interfaces

T. A. Nguyen & Y. Zeng (2014)	A Physiological Study of Relations Between Designers Mental Effort and Mental Stress During Conceptual Design, *Computer Aided Design*, 2014	EEG, mental stress, heart rate variability (HRV), design activity, design creativity
J. Vom Brocke & R. Riedl & P.M. Léger (2013)	Application Strategies for Neuroscience in Information Systems Design Science Research, *Journal of Computer Information Systems*, 2013	Design science research, neuroscience, fMRI, EEG, affective computing, neuroergonomics
M. Steinert & K. Jablokow (2013)	Triangulating Front End Engineering Design Activities With Physiology Data and Psychological Preferences, *Proceedings of the 19th International Conference on Engineering Design (ICED13)*, 2013	Physiology sensors, EEG, cognitive problem solving preference
T.A. Nguyen & Y. Zeng (2012)	Clustering Designers Mental Activities Based on EEG Power, Proceedings of Tools and Methods of Competitive Engineering (TMCE), 2012	Design cognition, clustering, EEG, electrical brain signal, protocol analysis
J. Vom Brocke & R. Riedl & P.M. Léger (2011)	Neuroscience in Design-oriented Research: Exploring New Potentials, *Proceedings of the 6th International Conference on Design Science Research in Information Systems and Technology*, 2011	Design science research, design theory, brain, neuroscience, fMRI
B. Sylcott & J. Cagan & G.Tabibnia (2011)	Understanding of Emotions and Reasoning During Consumer Tradeoff Between Function and Æsthetics in Product Design, *Proceedings of the ASME DETC/CIE Design Theory and Methodology Conference (DTM)*, 2011	Product design, brain, decision making, networks, testing, magnetic resonance imaging
C. Liapis & S. Chatterjee (2011)	On a NeuroIS Design Science Model, *Service-Oriented Perspectives in Design Science Research: 6th International Conference*, 2011	Design Science, neuroscience, design science research methodology, human threading, EEG, information systems
V. Goel (2010)	Neural Basis of Thinking: Lab Problems vs. Real-World Problems, *Cognitive Science*, 2010	Psychology, reasoning and decision making, neuroscience, cognition
T.A. Nguyen & Y. Zeng (2010)	Analysis of Design Activities Using EEG signals, *Proceedings of the ASME DETC/CIE Design Theory and Methodology Conference (DTM)*, 2010	Design cognition, EEG, protocol analysis
K. Alexiou & T. Zamenopoulos & J.H. Johnson & S.J. Gilbert (2009)	Exploring the Neurological Basis of Design Cognition Using Brain Imaging: Some Preliminary Results, *Design Studies*, 2009	Design cognition, problem solving, design problems, research methods, cognitive neuroscience
H. Petkar & S. Dande & R. Yadav & T. A. Nguyen & Y. Zeng (2009)	A Pilot Study to Quantify Designers Mental Stress from Eye Activity and EEG During Stroop Test, *Proceedings of the ASME DETC/CIE Design Theory and Methodology Conference (DTM)*, 2009	Stress , electroencephalography
M.H. Goöker (1997)	The Effects of Experience During Design Problem Solving, *Design Studies*, 1997	Design cognition, design knowledge, design research, psychology of design, design experience

2.2 Physiological Studies of Design: Effort, Fatigue and Concentration

As medical and physiological research becomes widespread and accessible, the usage of physiology to understand human-centric phenomena using human-centric approaches becomes of interest. A list of EEG studies of design can be found in Table 2.2. Physiological studies of design research have coexisted with the timeline of important design theories since the late 90's, with a surge in the 2010's, by offering human-centric definitions and measurements of an inherently human-centric phenomenon, design. They are scientific studies of design aiming at using the measurable physiology of the designer to reveal patterns in the design process. They provide an objective glimpse into the human phenomenon. The object of study is a design protocol where human physiological signals are measured. Physiological studies of design methods can be seen as empirical bottom-up approach where the design protocol and the patterns extracted from the physiological signals constitute the base of analysis.

2.2.1 Cognitive Aspects of Mental Effort

Effort can be commonly defined as how hard someone tries to do something [Sta04]. It is described as "spending energy and consequently experiencing a feeling of strain, thus ultimately investing a limited energetic resource to perform a mental task" [OZG93]. The notion that effort is like a feeling, "a conscious appraisal of one's own state", is discussed in [Dam99, OZG93]. Mental effort is also often defined in terms of cognitive resource allocation [Hee86] measured through subjective ratings [HRC+15, ZPR+12]. The Rating Scale Mental Effort (RSME) [OZG93] is such a subjective rating framework.

It is interesting to define mental effort through its immediate correlates. Mental effort is often associated to cognitive load. [Swe88] defines cognitive load as "the total amount of mental effort being used in the working memory" and it was initially used to study problem

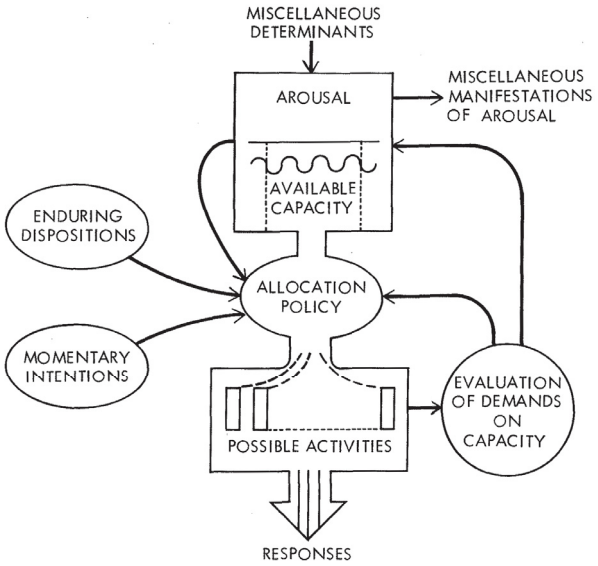

Figure 2.2: Kahneman's capacity model theory [Kah73]: A mental state is an activator that regulates the capacity of another mental state.

.

solving. [Swe88] defines three types of cognitive loads: intrinsic (inherent level of difficulty of a task), extraneous (caused by the manner in which information is presented) and germane (associated to schema learning and automation). Cognitive load theory is often used in instructional sciences and aims at decreasing extraneous mental load and increase germane load [Swe88]. [DM08] measures cognitive load through self-report scales, response time to a secondary visual monitoring task and a difficulty rating scale. [Kre15] proposes to replace the concept of Cognitive Load (CL) with Mental Load (ML) and Mental Effort (ME). Mental effort is also shown to highly correlate with perceived task difficulty [Sta04]. Kahneman shows that effort is tightly linked to performance [Sta04]. [Fai01, Sta04] note that [Kah73] was "the first to conclusively link mental effort to attention control within an information processing model". [Kah73] also discusses a capacity model between effort and arousal: high levels of arousal increase the capacity for effort and vice-versa. By doing so, he effectively initiated capacity theories of mental states. Figure 2.2 illustrates the capacity theory of mental states. Following this capacity model theory, [YN04, Sta04] argue that motivation, performance and, by extension, effort (effort being correlated to performance measured

as the number of successful tasks executed divided by the total number of tasks) follow a capacity model. [Kah73] also argued that the best physiological concomittant for effort was pupillary dilation while providing cases where such a concomittant fails (i.e. autonomic responses, muscle strain and anxiety also cause pupillary dilation). A bell-curve relation between mental effort and stress was found in [NZ14b]. Effort and stress were also linked to kinesics and eye-tracking experiments in [TZ09].

Many metrics of mental effort have been proposed. Subjective ratings are discussed in [PV93]. Heart rate and blood pressure are addressed in [FCH+05]. Task-involved pupillary response is advocated in [GASD96, Kah73]. Metabolic measures (more specifically, blood glucose) are proposed in [FH04]. [WFG+15] monitors brain (with EEG) and physiological (ECG, Galvanic Skin Response (GSR)) signals to assess mental effort produced by users performing 3D object manipulation tasks. [HRC+15] discusses the use of Subjective Rating of Mental Effort (SRME) and Simple Reaction Time (SRT) on a vibrotactile stimulus-monitoring secondary task as means to measure mental effort. [ZPR+12] confirms that performance correlates with mental effort measured through rating scales, pupillary responses or heart-rate variability.

It is known that effort aggregates from sustained mental strain on given tasks [De 05]. Hypothesis 3 addresses the problem of defining activation patterns and loci of effort in the conceptual design process.

As a challenge to Hypothesis 4, [De 05] argues that mental fatigue and effort should correlate positively. Our research shows evidence of a capacity model of fatigue and effort. This discrepancy is mainly due to a difference in the definition of effort. [De 05] defines effort as a decrement or increment in performance whereas we define it as an allocation of cognitive resources (transient microstates). The question is: does the relationship between fatigue and effort correlates positively or follows a capacity model (negative correlation) (cf. Hypothesis 4). Following the capacity theory of mental states, higher levels of fatigue would produce less capacity for effort and inversely less fatigue would produce more capacity for

effort.

[OZG93] argue that being aware of levels of mental effort investment provides information about the sustainability of a current activity. This becomes invaluable in the context of design problem solving, quality and performance. [Fai01, Sta04] argue that "an increase of mental effort is associated with an increased fidelity of self-monitoring, effective memory retrieval, and analytical processing of a problem space".

2.2.2 Cognitive Aspects of Fatigue

Physical fatigue is defined in [CN14] as "the temporary physical inability of a muscle to function normally" while mental fatigue is "the temporary inability to maintain optimal cognitive performance". [De 05] defines mental fatigue through its correlates as a decrement in performance due to excess effort. In an early work on fatigue, [Ara12, KDKM12] find that "difficult and disagreeable continued work brings about a decrease in the efficiency of the function exercised". Mental fatigue has been studied extensively in cognitive science in the context of medical research as it often co-occurs with significant medical conditions and diseases [SGD$^+$14, ÖBrW05, TJD$^+$04]. Sleep disorder have been extensively studied using EEG and fMRI in [HDVDS10, DDVS$^+$09, DVDP$^+$07]. In medical practice, the mainstream approach to diagnosing fatigue still remains symptomatic (e.g. fever, pain, nausea) and based on disease and medical condition co-occurrence (e.g. pregnancy, HIV, Thyroid function tests) [Dav16]. [Hoc13,De 05] argue that fatigue is a multidimensional concept (cf. Hypothesis 5). They note that different types of fatigue are routinely confused in research.

Subjective rating tests of fatigue remain the main tool in medical research. Psychomotoric Vigilance Test (PVT), the Stanford Sleepiness Scale (SSS), Digit Symbol Substitution Task (DSST) and Serial Addition/Sub-Traction Task (SAST) are used in [VMMD73] to measure mental fatigue in a study of the effect of sleep depravation and fatigue on cognitive performance. These tests are post-hoc and not monitored in real-time due to the required interaction with subjects. [NZ16b] shows how stress and effort can impact post-hoc self

assessment tests.

In industry, fatigue has been said to be the main cause of industrial accidents. More specifically, “most of the spectacular failures in process control that have resulted in the world’s largest industrial accidents have occurred in the small hours of the morning when the circadian rhythm is lowest and operator fatigue itself peaks” [Des12]. [BRSU09] shows that sleep depravation reduces the performance (in terms of accuracy and response time) of subjects performing number comparison tasks. In this context, physiological metrics of fatigue have been integrated as fatigue detection systems in vehicles [SB15].

2.2.3 Cognitive Aspects of Concentration

Concentration “means a work state where cognitive resources are assigned to target work” [SOM+13]. The definitions of concentration and attention are often blurred. “Attention is a multidimensional term that refers to at least three different cognitive processes -concentration or effortful awareness, selectivity of perception, or the ability to coordinate two or more skills at the same time” [Mor12]. According to [Kah73], arousal and attention follow the same capacity model as arousal and effort. Dysfunction in attention control (i.e. aberrant salience) is theorized to be diagnosed in schizophrenic disorders [Kap03]. In the medical literature, concentration is mostly studied in the context of learning disorders [DCMG01]. The Attention Network Test (ANT) is a measure of attention used in medical research (in the context of Attention Deficit Hyperactivity Disorder (ADHD) and is described in [ASL08]. In EEG analysis, concentration is associated to the beta band [BBGW08]. A terminological distinction should be made about beta waves: while the physiology literature often associates the beta waves with ”arousal”, we can safely infer that this is not the same arousal as the one mentioned in [Kah73] as there is no clear correlate between beta waves and pupillary dilation. Furthermore, our research shows no positive correlation between beta waves and mental effort which should occur in a capacity model theoretical setting if beta waves be associated to arousal.

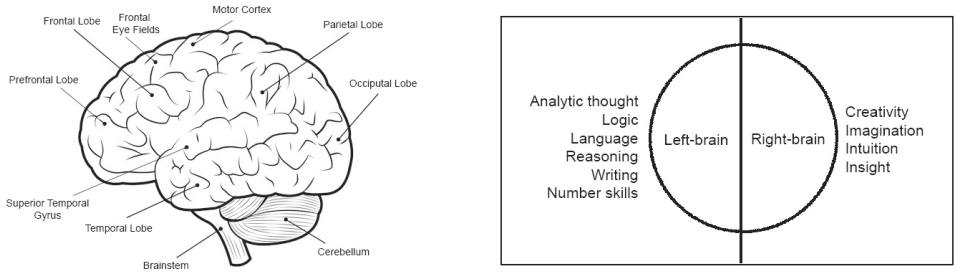

Figure 2.3: (left) Regions of the brain. (right) Functions of the left/right hemispheres.

.

In [Cro01], "an aspect of cognitive strategy that emerges from several studies is that, especially during creative periods of conceptual design, designers alternate rapidly in shifts of attention between different aspects of their task, or between different modes of activity". More specifically, these shifts, termed "modal shifts", seem to be indicative of designer creativity. "The apparent importance of frequent shifts of attention or activity mode in influencing either the creativity or overall quality of the design concepts produced" is discussed in [Cro01, CCD94]. [NZ12c] describes creativity as a sequence of iterates that can fall into a chaotic state. In our research, we found that concentration (beta band) was better understood using the concept of "modal shifts" as segments of the protocol data where subjects were performing *tabula rasa* sequences (erasing their prior design and replacing it with a new one) were associated with high levels of short duration segments in the beta feature segmentation (cf. Hypothesis 6).

2.3 Neurological Aspects of Creativity

The left/right brain paradigm was pioneered by Robert Sperry using the so-called "split brain" experiment [Gaz67]. "Split brain" experiments are cognitive experiments on subjects whose corpus callosi (the neurological structure that connects the left and right hemisphere of the brain) has been severed surgically notably as a treatment for epilepsy. More specifically, when such subjects were presented with a visual stimulus to their left brain, they were unable

to verbalize it as information was not transferred to their right hemisphere which is known to process visual information. Using these type of experiments, it was found (cf. Figure 1(right)) that the left hemisphere is responsible for analytic though, logic, language, reasoning and writing whereas the right hemisphere is responsible for creativity, imagination, intuition, insight, holistic thought, music and form recognition [Orn77]. Also, the left hemisphere controls the sensory functions of the right side of the body while the right hemisphere controls the sensory functions of the left side of the body.

In recent functional imaging experiments, it is found that the prefrontal cortex (PFC) plays a crucial role in creative tasks [dGT$^+$14, GYdL$^+$13]. In these assessments, creativity was often measured using standardized tests of divergent thinking or the Torrance Test of Creative Thinking [Tor04]. Subjects affected with neurodegenerative diseases of the frontal lobes often saw a decrease in their Torrance test score although some notable exceptions to the rule were reported (perhaps due to neuroplasticity). [JSB$^+$10] correlates cortical thickness to higher performance in Creative Achievement Questionnaire (CAQ) tests. Furthermore, it was found that activation of subregions in the lingual gyrus correlated negatively with the Composite creativity Index (CCI) while the right posterior cingulate correlated positively. [HNB03, Die04] discuss whether creativity engages predominantly the frontal lobes or posterior brain regions and subcortical structures (basal ganglia).

Evidence that creativity is hard to verbalize can be found in such the concepts that go as far back as the Wechsler Intelligence Scale [Wec44], insight (Aha! experience) [JBBH$^+$04] and creative "flow" (the feeling of being fully immersed and focused in an activity [Csi96]). More specifically, the Wechsler Intelligence Scale also emphasizes non-verbal performance in contrast to other scales such as the Binet test which overly emphasizes on language and verbal skills. In an fMRI study, [JBBH$^+$04] finds that subjects solving problems using insight solutions (Aha! experience) had increased sudden flashes of activity in the right hemisphere anterior superior temporal gyrus. In another fMRI study, [LCX$^+$04] shows that improvising musicians (i.e. nonverbalizable and insight task) saw lower activity in their

dorsolateral prefrontal cortex and increased activity in their medial prefrontal cortex (cf. Figure 2.3(left)).

2.4 Design Protocol Analysis and Automated Methods

In the movie HER (2013), Theodore is a lonely writer who develops an unlikely relationship with his operating system, Samantha. One of the scenes that impressed viewers occurs while Theodore is playing a next-generation immersive video game:

> THEODORE (playing a video game): I have been going in circles for an hour...
>
> SAMANTHA OPERATING SYSTEM (giggles): Ok... You have got... You are just not being very optimistic... You are being very stubborn right now... Stop walking the structure... It is the other way!
>
> THEODORE: Hum...
>
> SAMANTHA OPERATING SYSTEM: Thank you... thank you... The tunnel on the left is the only one we haven't tried...
>
> THEODORE: No, I think that's the one you sent me where I suddenly fell down the pit...
>
> SAMANTHA OPERATING SYSTEM: OK... I don't think so...
>
> THEODORE: Hum... Yeah... This is different...

What impressed most computer scientists, engineers and video game fans is the way the AI's in the movie were able to sense the emotions of their users and the environment they are evolving in. In the conversation above, the Samantha OS is clearly sensing Theodore's perception of the game's hardness and interacting with him based on this evoked hardness. One of the problems posed by the Samantha OS paradigm is the measurement of a problem's perceived hardness. Measuring a problem's perceived hardness is effectively a window into human intelligence and ability.

The above dialogue is also an instance of a design protocol. More specifically, it is an instance of an informal reporting design protocol. The dynamics of affect and effect are clear in this dialogue.

A design protocol is an artifact resulting from a design process. Like in the Samantha-Theodore dialogue quoted above, an individual playing a video game is also creating a design protocol artifact. While a design protocol can take the form of an audio or video recordings, a sketch or a report, analyses of design protocol data can be an annotated video of a design process, coarse encodings [USD87], structured encodings of the design process [EG87, MGW98, GM98] or a diagram such as a linkograph [Gol90, KG08, KG09] or a spiderweb [MES$^+$09].

Three main techniques for creating design protocols are discussed in the literature on the subject: *simultaneous thinking aloud techniques* (concurrent verbal protocols) during which a subject performing a design task simultaneously describes and comments on his design process [EG87, MGW98], *informal reporting* in which an observer takes notes and asks question to the subject performing a design task [EG87] and *retrospective protocol analysis* techniques in which the subject comments on his design process after having performed it [EG87].

The Delft protocols are a set of design protocols typically recorded from engineering and architectural design meetings. The Delft protocols are an example of experiments where different researchers were asked to reflect on a set of design protocols [CCD96]. More recent work has revisited the concept [ML09].

A recurring problem in design protocol analysis is to then segment the design protocol into logical and semantic units. Different types of logical and semantic units can be found in the literature on the subject. Earlier papers such as [USD87] proposed *coarse functional breakdowns* as a means to segment the design protocol data. Later papers such as [EG87, MGW98, GM98] proposed coding schemes such as *problem domain*, *microstrategies* (e.g. problem analysis, solution synthesis and evaluation), *macrostrategies* (e.g. top-down, bottom-up, decomposing the problem, backtracking and opportunistic) and *FBS encodings* (Function-Behaviour-Structure). It can be noted that FBS encodings are ontologies and typical ontology tools and techniques may be applied. The particular encoding of a design

episode into atoms is first agreed upon by domain experts and then used to segment the design protocol. The process is manual and often iterated to alleviate imprecisions. More recent papers such as [KG08] discuss the dynamics of design protocols by adding temporality and interaction to these design atoms: the design protocol data is segmented into *design moves* and these design moves are linked together depending on what move is a predecessor or successor to another move. The resulting diagram is called a *linkograph*. More specifically, linkographs can be applied to design processes which have multiple participants. The linkograph then measures the extent to which the participants cooperated by measuring the extent to which a design move from a given participant was a predecessor or a successor of another participant's design move. Furthermore, [KG09] discusses linkographs built over FBS segmentations. In this particular case, it is interesting to note that links between a Structure segment and a Behaviour segment are said to be illustrative of the analysis process. Function-Function links or Behaviour-Behaviour links are then analyzed to be reflection on a Function or on Behaviour respectively. If the FBS encoding has 3 codes (in some cases FBS encodings have more than the basic Function, Behaviour and Structure codes), then 9 such links are possible each carrying particular semantics. These links are qualified by the authors as *process types*. Another diagram used in design protocol analysis is the *spiderweb* discussed in [MES$^+$09]: topics extracted from a design protocol are organized around a spiderweb and links between topics denote that the topic is being discussed at a given time. The time dimension is then radial to the spiderweb and the diagram can illustrate succinctly how topics re-emerge during the design protocol. The logical unit of the analysis is then the *design topic*. Spiderweb diagrams are to be put in contrast to more linear depictions of conversation.

Encoding design protocols is a fundamental approach used in many analysis techniques [ML09]. While the FBS ontology is a known and generally applicable method [KG09], researchers often develop encodings based on the problem or hypothesis at hand. [Aki09] discusses an encoding of a design protocol involving architects to test the hypothesis that

architects design by operating *bread-first* and *depth-next*. In the language of the FBS model, the encoding is used to detect a *macrostrategy*. [DKV09] encodes a design protocol to detect appraisal based on linguistic coding strategies. Computational linguistics methods are prevalent. [BC09] proposes the use of *hedge words* such as *like* to detect analogical thinking, *I think* to detect mental simulation and *I guess* or *sort of* to detect uncertainty. These *hedge words* are then used to encode the design protocol. Another example comes from [DD09] where mechanisms of valuation are studied by encoding the protocol data into *design values* (form, material, aesthetic), *human values* (spirituality, respect, family), *requirements*, *narrative* and *processes*. Different participants of the design protocol are then measured against their use of these concepts and this is used to determine levels of value transfers occurring in the design protocol. Conversation analytical methods such as interruptions and unfinished turns delineation have also been used in [Mat09] to detect social order among participants. External object references are extensively researched in [SEE09]. Encodings in the design literature are often performed manually by domain experts. More than one domain expert is often also used to alleviate subjective ratings. In some cases, encoding was performed by the same person but each encoding session was separated by a time lag [KG09]. Other encoding strategies are described in the Delft protocol workshop [CCD96, KG09].

[KG08] proposes a segmentation of design protocols into *design moves* and provides a complex linkography between those design moves. [MGW98, KG09] propose the use of the FBS (Function-Behavior-Structure) ontology. The FBS ontology is a structured encoding of design segments that uses coding schemes such as *problem domain*, *microstrategies* (e.g. problem analysis, solution synthesis and evaluation), *macrostrategies* (e.g. top-down, bottom-up, decomposing the problem, backtracking and opportunistic). Typically, design researchers construct different coding schemes depending on the subject and domain of their study. For example, [DD09] proposes a coding scheme based on *form*, *material*, *æsthethics*, *uniqueness*, *solitude* and *purity* to study human values in an architectural design meeting. [DKV09] analyzes subjectivity and language constructs indicating subjectivity to study the language

of appraisal in the same architectural meeting dataset. Both these analysis were done on transcripts of a design meeting.

While textual analysis of design protocols can provide invaluable information on design processes, some aspects of design cognition remain obfuscated by a natural language barrier. While domain experts can easily notice subtexts and inferences in a design transcript, there remains large regions of semantical and physiological information that are untaped by these methods. Some researchers may alleviate these limitations by studying, for example, video recordings in which they can annotate the gestures or movements of the participants in the design session. [Vis09] proposes such an analysis. However, we can safely say that this is only the tip of the iceberg with respect to the cognitive map of a subject involved in a design task.

Design protocols come in different media of communication. Textual protocols are widespread in the research literature. Most of the work on design protocol analysis is done on textual protocols (e.g. audio recordings or transcripts of design meetings) [CCD96, ML09]. Video protocols form the bulk of non-textual protocols. They are commonly used to analyze gesture and other visual cues in design protocols [Vis09]. Non-content based non-textual design protocols methods refer to data gathered during a design episode which is not the design protocol per say but which correlates with states and properties of the design protocol. These include clickstreams, eye-tracking experiments, electrocardiogram (ECG) and electroencephalogram (EEG) monitoring. The latter form the basis of the methods we will investigate in this research. More specifically, we will study the use of EEG in design protocol analysis.

A survey of methods used in design protocol analysis can be found in [JY09].

2.4.1 Content Based Analysis Methods for Textual Protocols: Ontologies

When the design protocol is textual data, well-known methods such as automated taxonomy induction (ATI) or automated ontology extraction (AOE) exist. A survey of automated

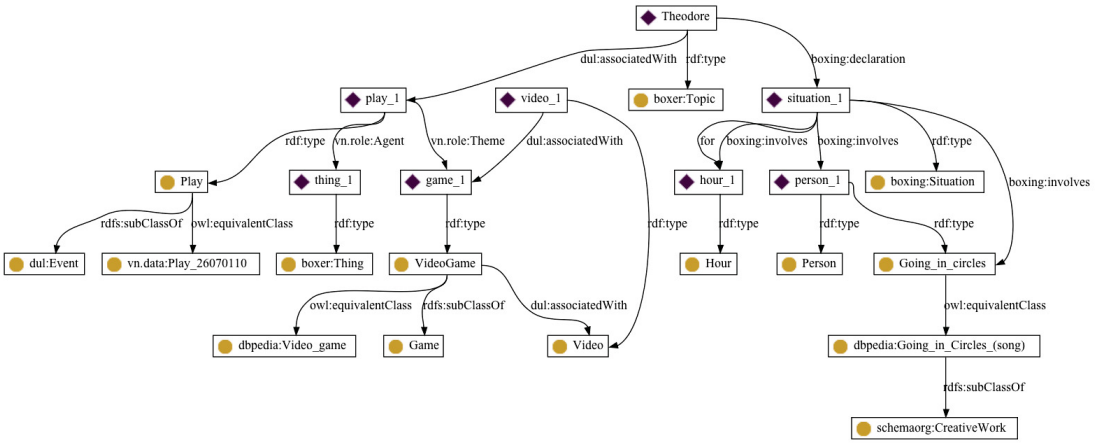

Figure 2.4: Ontology generated using FRED for the first conversation line of the Samantha-Theodore dialogue.

ontology extraction techniques can be found in [WLB12]. The Recursive Object Model (ROM) is such an ontological method that has been applied to design science [Zen08, WZCE13]. It can be noted that since audio recordings can be translated into text using speech-to-text methods, we consider audio recordings as being textual protocols. Figure 2.4 illustrates an ontology generated automatically using the FRED tool for automatically producing RDF/OWL ontologies [PDG12] on the first line of the Samantha-Theodore dialogue quoted before. Concepts such as *turning in round* and *video game* are tracked properly using this tool. The FRED tool also is capable of detecting that the *object* Theodore is in a *situation* (turning in round) and that he has the *role* Play of *subtype* Video_Game. In the context of analysing design protocol data, this information may be invaluable.

Furthermore, since ontologies can be commonly created on textual data, methods such as ontology matching can be used [ES07]. An FBS based design protocol analysis solution would then perform an ontology alignment between the ontology of Figure 2.4 and the FBS ontology. For example, the term *Play* could be matched with a Function that has the Behaviour of *Going_in_circles*. The Behaviour in this case, would be a *derived* behaviour in contrast with an *expected* behaviour [KG09]. In this example, the Structure component would be *Theodore* and *Video_Game*. This solution outline effectively solves the problem of

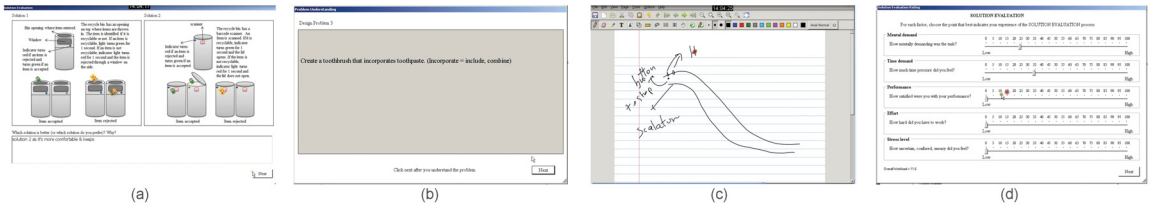

Figure 2.5: (a) displays a typical answer question segment, (b) a read question segment, (c) a design object segment and (d) a rate problem segment.

automatically segmenting a design protocol using the FBS model [KG09]. Different ontology alignment techniques could be used from lexical synonymy techniques to knowledge bases or concept matching measures.

This technique would however not be able to encode more complex concepts such as affects and emotions [DKV09], micro and macrostrategies [GM98] or design and human values [DD09]. In the case of emotions, more complex Natural Language Processing (NLP) techniques such as emotion mining, sentiment analysis or opinion mining could be of service [PL08].

2.4.2 Content Based Analysis Methods for Non-Textual Protocols: Image Processing and Pattern Recognition

A typical non-textual protocol would be a video recording of a design meeting or of a design task executed on a touchpad. Multimedia data does not lend itself to the same ontology or NLP techniques used for textual data. However, a set of tools from computational and engineering sciences are available as for textual data. Techniques from image processing and pattern recognition may be used and specific applications and implementations may vary depending on the exact nature of the data since these techniques are typically data-oriented.

If we examine the example of the design protocol data gathered by the Design Lab of the Concordia Institute for Information Systems Engineering during the past years [ZYZ07, NZ10b, NZ12a, XNZ14], design sequences in the design protocol video have particular attributes. Some of these typical sequences are described in Figure 2.5. Since these *answer*

question, *read question*, *design object* and *rate problem* segments have particular image attributes, having been designed with a particular UI, typical data mining techniques, such as supervised classification or unsupervised clustering, can be used to segment the overall video into such segments. In this design protcol, the *read question* segment is typically a gray screen with a text in it and the *design object* segment is typically a white screen with touchpad drawings in it. Such characteristics are discerning enough for a classifier to separate the segments properly. For example, using a Support-Vector Machine (SVM) classifier, we could train the classifier function using the prototypical screens of Figure 2.5 and then use it to classify the screens of the overall design protocol video into segments. Such a segmentation remains rough and complex information such as concepts and affects would be lost. However, it is not complicated to imagine methods that could evaluate automatically the level of complexity of a drawing from childish sketches to professional drafts. It is clear that analyzing different types of data using different methods (textual and non-textual data) yields different domains of information.

2.4.3 Non-Content Based Analysis Methods for Non-Textual Protocols: Physiological Methods

Non-content based methods are termed as such because the object of study (e.g. design protocol data) is not the data to be analyzed (e.g. physiological signal). Physiological approaches have been devised in the past to study the hardness of design problems. Heart-rate variability and task hardness have been experimented with by [MOK+92] in the context of medical research and [NZ10a, NZ14b] in the context of design sciences. [TZ09] propose to measure movements (kinesics) to parameterize problem hardness and mental effort. Eye-tracking experiments, clickstream and gesture analysis are commonly used in psychology, cognitive and design sciences to analyze protocol data or other engineering tools and artifacts.

Physiological methods have the benefit of being hands-free and purely quantitative. They lend themselves to be utilized in engineering systems and devices. Such examples range from

BCI tools to lie detection systems and medical diagnosis systems [GAP10, HBJ10, DJJ+97]. Immersive Brain-Computer Interfaces (BCI) are not pure science-fiction and they have been well-studied in the past decades in the context of not only next-generation immersive video games, but also medical devices, smart home design, CAD/E systems and design sciences. Such applications can be found in [GAP10] and [CGT+12]. Cognitive methods in next-generation video games for the cloud were recently proposed in [CZLC13] where click-streams and intelligent resource allocation methods are being extensively used to monitor Quality of Experience (QOE). The importance of measuring environment-based parameters for the development of these next-generation smart systems is non-negligible. The idea is to layer traditional AI and machine-learning techniques with human-centric dimensions such as collaboration, conceptualism, creativity and cognition stated in [GVWH12].

It can be noted that current commercially available BCI headsets such as the EMOTIV EPOCH or the MUSE headset are able to measure mental stress and strain in addition to eye and head movements using built-in accelerometers and algorithms. The EMOTIV EPOCH is commonly used to navigate and play video games.

With respect to design protocol analysis methods, the logical step forward from textual and content-based methods would be to use physiological methods to detect patterns unavailable to the latter methods or rely on the objective rating provided by such methods. While traditional protocol data analysis methods rely heavily on the transcripts of the design meeting or solution, physiological methods are conjectured to offer a *peak* into the *unseen*.

2.5 Weaknesses of Verbal Protocols

[KP00] argues that concurrent verbalization techniques are more complete (i.e. measured as the number of protocol segments) than retrospective protocol analysis while the latter gains by not interfering in the conceptual design process. Furthermore, retrospective protocol analysis suffers from post-hoc imprecisions as the quality of verbal protocols is known to

decrease (i.e. no longer describe a cognitive process) as the memory of task leaves a subjects short term memory [ES84]. Encodings in the design literature are often performed manually by domain experts. More than one domain expert is often also used to alleviate subjective ratings. In some cases, encoding was performed by the same person but each encoding session was separated by a time lag [KG09].

Verbal protocols are known to bear some weaknesses. [Wil84, KP00] note that verbal protocols do not trace cognitive processes that are not part of "focal attention", such as "subliminal stimulus" (i.e. "subliminal primes") or thoughts that do not reach the verbalization process. Furthermore, [Wil84] argues that concurrent verbalization changes the sequence of thought processes (i.e. "the reactive effects of verbal protocol"). [SOKB93] run four sets of experiments to show that verbalization interferes with problem solving by showing that subjects asked to verbalize their problem solving strategies were significantly less successful than control subjects. [WLS+13, SOKB93, FS93, WS91, SRR91, SE93, Wil84] all argue that verbalization affects performance. [SOKB93] states that "certain thoughts have a distinctly nonverbal character" such as creative thoughts and insights (i.e. unexpected problem solutions that just happen). Furthermore, facial recognition is studied by the authors as an example of a task that requires large amounts of information that cannot be easily verbalized [SOKB93]. creativity and insight are then argued to "have occurred in the absence of words" [SOKB93]. [WS91] discusses how verbalization increases the salience of verbal attributes and "overshadows" non-verbal attributes (e.g. affective judgment is often ignored using verbalization). Verbal overshadowing was then defined as a subject's focus on verbally relevant information to the detriment of information that is not easily verbalized. Subjectivity of verbal protocols (e.g. self-presentational concerns) are also discussed in [Wil84]. Fabrication problems in design protocols are discussed in [KP00]. [Sma89] also reports that subjects have a hard time verbalizing while manipulating objects. [CS10] argues that verbal protocols showed limitations in their experiments by contradicting the assumption that stimuli increases concept creativity. The authors then raise three concerns related to verbal protocols:

time and resource intensiveness (i.e. the technical setup of verbal protocols), data validity and the fact that some tasks are not conducive to verbalization (e.g. task parallelism impacts verbalization that is inherently sequential and automaticity [RJ91, Gor92]). [SOKB93, Met86] note that, in the context of insight problem solving, "subjects who believe that a solution is imminent are engaging in a 'gradual rationalization process' that focuses them on an inaccurate yet reportable approach". [SOKB93] lists of few types of insight problem solving tasks as follows: memory retrieval tasks, spreading activation tasks (i.e. how the brain navigates in a network of thoughts), constraint relaxation (i.e. how we remove a constraint on a problem that is false) and perceptual reorganization (e.g. Necker cube illusion). They form a group of "difficult-to-report perceptual and memory processes" [SOKB93]. [ES84] argues that concurrent verbalization is qualitatively correct while only decreasing the overall performance of problem solving while [SOKB93] argues that in the case of insight problem solving, verbalization impedes cognitive processes as it "overshadows" nonreportable processes. This latter approach is clearly gestaltist.

When hidden cognitive processes are of concern, [Wil84] concludes that verbal protocols cannot be "taken on faith": there are some tasks where verbal protocols yield poor quality results such as creative tasks, insight (e.g. the Aha experience, gestalt psychology), affective judgment, memory retrieval tasks or automated tasks (e.g. facial recognition, visual recognition tasks). These tasks are sometimes termed as nonreportable processes [SOKB93]. More specifically, [Wil84] argues that while verbal protocols are not "completely invalid", they do not provide "a perfect window into the mind" and by doing so, challenges the positions long held in [ES84] where it is believed that research has "overestimated the extent of nonconscious processing".

Chapter 3

EEG Analysis

Physiological methods for the study of design constitute a new and emerging option made possible with EEG and other physiological measuring techniques. Physiological methods are purely quantitative and may provide additional insight where investigative and descriptive techniques do not. They rely on metrics of the human mind and body and can provide a powerful retroactive or real-time analysis tool that is non-invasive to the design process while being precise if interpreted properly. In this line of work, [MHM+14] have successfully segmented images into subobjects using EEG signals of subjects presented with these images. Segmenting design protocol data, like images, using EEG data is an instance of an inverse problem since the problem is to reconstruct, at least tentatively or partially, a thought process from its output, the EEG signal. This inverse problem is non-trivial as it is currently unknown to what extent information is lost from the initial thought process to the electrical measurement.

Electroencephalogram (EEG) signals and scalp field maps have been widely used in the context of medical research since the works of H. Berger in 1937 who described them as a window into the brain [Ber37, MKB+09]. Other physiological measurement apparatuses and techniques that predate the Berger electroencephalogram are galvanic skin response techniques, the Marey-Lippmann capillary electrometer (1870) and string galvanometers

for electrocardiograms (1900) [SRQ00]. Currently, commercial EEG devices measuring different states of mind and facial movements have gained acceptance with applications to Brain-Computer Interfaces (BCI) for paralytic patients and immersive video game interfaces. EEG measurements excel at measuring states of mind.

The quantitative analysis of electroencephalograms (EEG) draws from many fields of computing, mathematics and engineering. Techniques used in the detection of well-known waves such as P100, P300 and N400 for the study of the human decision making processes typically make use of pattern recognition and signal processing methods such as wavelets, multiresolution and spectral analysis [SB10, KASR13]. The preprocessing of EEG signals usually involves filtering techniques used to distinguish between different frequency bands such as alpha, beta, delta and gamma waves. Machine learning techniques such as classification and clustering are gaining momentum [GAP10]. Basic statistical techniques such as normalization and hypothesis testing are common while more complex concepts such as Granger causality [BS01, KB91] are also encountered in the related literature. Electrical neuroimaging techniques also encompass a large range of well-known tools and methods. Typical techniques are noise and artifact removal using heuristic, statistical or stochastic methods such as Gaussian noise filtering, principal and independent component analysis (PCA, ICA) [JHL$^+$08, VC02]. Source localization techniques are used to map a scalp field to locations in the brain. Such techniques described in [LMPM$^+$97] include low resolution electromagnetic tomography. Classification techniques such as Support Vector Machines (SVM) or Naive Bayes classifiers and clustering techniques such as k-means are used to discover new patterns in EEG data [BTV$^+$10, DT11]. An end goal of these techniques is to extract significant features from EEG data.

The goals of EEG analysis in design sciences involve the extraction of valuable and reproducible information from EEG signals for the scientific validation of design theories and methodologies and further our understanding of the conceptual design process. In

engineering, EEG analysis is an evolved and mature field of study. For instance, Brain-Computer Interfaces (BCI) have gained momentum over the past decade as next-generation immersive Human Computer Interfaces (HCI). Interfaces for paralytic patients are under development and are shown to be more accurate every year [GAP10], next-generation immersive video game interfaces are now commercially available [ALCJ14] and smart devices for smart homes are being researched extensively [CGT$^+$12]. Medical devices based on electrical neuroimaging now cover a large range of application domains from the diagnosis of mental disease such as Alzheimers [DJJ$^+$97] or schizophrenia [KLM$^+$99, SLF$^+$12] to the prediction of epileptic seizures and stress [LMPM$^+$97]. Hands-free control systems are being researched in the context of aircraft and cars [LWC11, Pow13, Wai11].

3.1 Fundamentals of EEG

Given a set of N measurements at time $t = 1, \ldots, N$ and n electrode locations, a scalp field map is a sequence of n electrode potential values at a given time t. More specifically, if an epoch consists of a function $f(x, t)$ measured at $x = 1, \ldots, n$ and $t = 1, \ldots, N$, a scalp field map is given by $f(x, t)$ for some value $t \in [1, N]$. For some value t, such a scalp field map will be denoted by $f(x)$ with x defining an electrode label, for conciseness. When electrode positions are required, a scalp field map will be aternatively denoted by $f(\mathbf{x})$ with $\mathbf{x} = (x, y)$ defining electrode locations in the Cartesian plane. There are $n(n-1)/2$ such pairs of electrodes, each combination yielding polarity and magnitude information.

It is common to pre-process the raw scalp field data. Typical pre-processing methods include average references, bandpassing and averaging (often used in Event-Related Potential (ERP) techniques). Bandpassing the data is done to recover specific frequency bands. These frequency ranges are indicative and may vary in practice.

The literature [Leh71, LOP87] reports the following additional indices computed on scalp field maps: *global field power* and *map hilliness*. Averaging techniques are typically

performed on different sets of measurements (epoch) or on all electrodes of a scalp field map. Well-known preprocessing techniques are described in Table 3.1.

Microstates are prototypical patterns in scalp field maps that are conjectured to provide information on human thought processes. In practice, they are computed on experimental datasets using methods such as clustering, principal component analysis and other such data mining techniques [Leh71, LOP87, PMML95, KLM+99, KPL+02]. Microstate clustering and segmentation are novel neuroscience techniques and have been notably studied in the context of the quantitative diagnosis of mental diseases. Such diagnoses are often highly subjective and the path towards quantifiable diagnoses is arduous. Significant work is being published in the area [KLM+99], outlining advances and new challenges. Unusual thought processes can then be measured using EEG signals and are indicative of brain diseases or re-allocative dysfunctions in neurological maps. The same challenges that apply to clustering techniques then also apply to microstate segmentation.

Microstates can also be applied to the analysis of a creative process measured through an EEG signal [NZ14b]. Microstate segmentation should then be capable of identifying segments where inherent thought processes and mechanism occur while a subject is asked to perform a creative task.

3.1.1 Stochasticity and Fractality

It is an open debate as to whether complex nonlinear time series, such as EEG signals or stock market tickers, are stochastic in nature or fractal. A stochastically modeled signal integrates noise and stochasticity in its formulation while a fractal signal integrates order finding and scale.

From the perspective of stochasticity, the pairwise electrode polarity/orientation of a scalp field map can be modeled using the stochastic differential equation:

$$d\mathbf{X}_{\sigma,t} = \sigma \mathbf{U}_{kt} dt + d\mathbf{W}_t \tag{3.1}$$

Table 3.1: EEG scalp field map pre-processing techniques

Name	Description	Function
Average reference	Subtracting an average of all potential values of a map from a given potential value	$\mathbf{x}_k - \overline{\mathbf{x}}$
Electrode averaging	Averaging the values of all potentials of a map	$\frac{1}{n}\sum_{k=1}^{n}\mathbf{x}_k$
Epoch averaging	Averaging a potential at a given electrode over a set of m epochs $\mathcal{E}$ (often used in ERP techniques)	$\frac{1}{m}\sum_{k\in\mathcal{E}}\mathbf{x}_k$
Map hilliness	Average absolute amplitude per electrode	$\frac{1}{n}\sum_{k=1}^{n}\lvert\mathbf{x}_k - \overline{\mathbf{x}}\rvert$
Global field power	n-weighted standard deviation of potentials at all electrodes with respect to a given electrode	$\left(\frac{1}{n}\sum_{k=1}^{n}(\mathbf{x}_k - \overline{\mathbf{x}})^2\right)^{1/2}$
Bandpassing	Bandpassing a signal by frequency range r and sample rate s	$\mathrm{FILTER}(\mathbf{x}, \mathrm{r}, \mathrm{s})$

where $\mathbf{W}_t$ is a Wiener process and σ a parameter defining the process range. For a biased uniform random process $\mathbf{U}_t = (u_1, u_2, \ldots, u_t)$ with $u \in [0, 1]$, $\mathbf{U}_{kt}$ is rescaled to a window size k/t. It can be noted that the derivative of a Wiener process with respect to time is a white noise process and Equation 3.1 describes a biased uniform process perturbated with white noise. The non-noisy and non-random component of the process is then the extent to which the process is biased.

The pairwise magnitude of a scalp field map can be modeled similarly using a jump-diffusion process with constant mean.

The stochasticity of EEG signals is argued in [GRSA13].

On the other hand, it can be noted that research has shown that EEG signals are signals with time-varying Hurst indices indicating long-range dependencies, hinting at their fractal

nature. More specifically, the EEG of newborns can be estimated to have Hurst indices bell-curved between 0.2 and 0.8 with an average of 0.5 [SRMB07] while the EEG of adults in a resting state can be estimated to have Hurst indices between 0.5 and 0.8 [VBM10]. This reveals long-range dependencies in EEG signals. Signals with long-range dependencies tend to either correlate strongly or anti-correlate with each other. This phenomenon is discussed in Section 3.5 and Figure 3.7.

Also, it is safe to posit that EEG signals have a dual stochastic-fractal nature. While noise is an inherent property of measurement and the dynamicity of the system, multiscale fractal behaviour can be denoted in such signals. The perspective taken to EEG signals should reflect the nature of the problem to solve. For instance, when denoising needs to be performed, a stochastic approach may be well suited while when classification or simulation needs to be performed, a fractal and nonlinear systems approach can be well suited.

3.1.2 Analyticity and Interpolation

A common routine performed on scalp field maps is to interpolate the EEG measurements on the x, y-plane for better visualization. Interpolation of EEG scalp field maps falls under the category of scattered point interpolation problems since the electrode positions constitute a scattered set of points associated to a value, the scalp field potential. Many interpolation methods exist such as Hermite interpolation, Voronoi interpolation or B-spline interpolation. In the case of B-spline interpolation, the result is a differentiable manifold in $\mathcal{C}^{d-1}$ for an interpolation of order d. The literature reports that, using B-spline interpolation, maxima and minima of interpolated scalp field potentials may no longer fall on electrode locations [MKB$^+$09]. In general, topographical data is well suited for radial basis function interpolation methods. Without loss of generalities, we address the 2-dimensional case. Let $f(\mathbf{x})$ define a scalp field map interpolated at position $\mathbf{x} = (x, y)$ and measured at electrode

positions $\mathbf{x}_k = (x_k, y_k)$, the radial basis function interpolation equation is given by:

$$f(\mathbf{x}) = \sum_{k=1}^{N} c_k \varphi\left(\|\mathbf{x} - \mathbf{x}_k\|_2\right) \tag{3.2}$$

The coefficients c_k are obtained by solving the linear system:

$$\begin{bmatrix} f(\mathbf{x}_1) \\ f(\mathbf{x})_2 \\ \vdots \\ f(\mathbf{x})_n \end{bmatrix} = \begin{bmatrix} \varphi\left(\|\mathbf{x}_1 - \mathbf{x}_1\|_2\right) & \dots & \varphi\left(\|\mathbf{x}_1 - \mathbf{x}_n\|_2\right) \\ \varphi\left(\|\mathbf{x}_2 - \mathbf{x}_n\|_2\right) & \dots & \varphi\left(\|\mathbf{x}_2 - \mathbf{x}_1\|_2\right) \\ \vdots & \vdots & \ddots \quad \vdots \\ \varphi\left(\|\mathbf{x}_n - \mathbf{x}_1\|_2\right) & \dots & \varphi\left(\|\mathbf{x}_n - \mathbf{x}_n\|_2\right) \end{bmatrix} \begin{bmatrix} c_1 \\ c_2 \\ \vdots \\ c_n \end{bmatrix} \tag{3.3}$$

The index n gives the number of electrodes in the EEG measurements. In compact notation, we have:

$$f(\mathbf{x}) = \Phi \cdot \mathbf{c} \tag{3.4}$$

The matrix Φ is effectively a distance matrix of all electrode positions (x_1, y_1), $(x_2, y_2), \dots,$ (x_n, y_n) in Cartesian coordinates. In practice, the Moore-Penrose pseudo-inverse method may be used to avoid ill-conditioned matrices. In those cases, the approximation is exact if the conventional inverse is well-defined.

The radial basis function $\varphi(\cdot)$ is a set of smooth orthogonal functions. Typical functions are described in Table 3.2.

Radial basis functions such as Gaussians are effectively in $\mathcal{C}^\infty$ and although, for some choices of radial basis functions, the method provides exact reconstruction of a signal, in practice, spurious datasets may exist and numerical conditioning needs to be applied.

3.1.3 Gradient Fields

Gradient fields of an EEG signal's epoch measure the rate of change between different scalp field maps at successive time indices. Such fields are shown in Figure 3.1. They are best described as an $N \times n$ matrix of measurements with N describing the epoch length and n

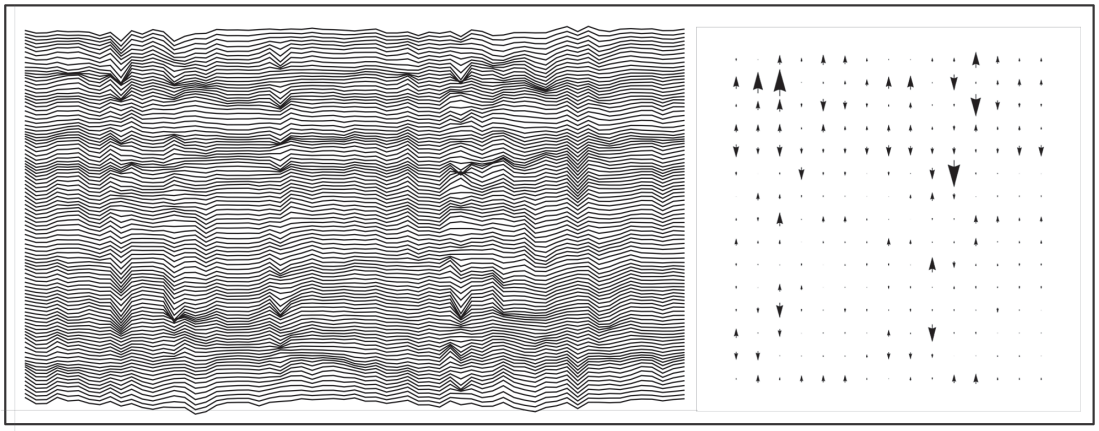

(a) EEG epoch of length 100 using 63 electrodes (left) and its gradient field in the time direction (right).

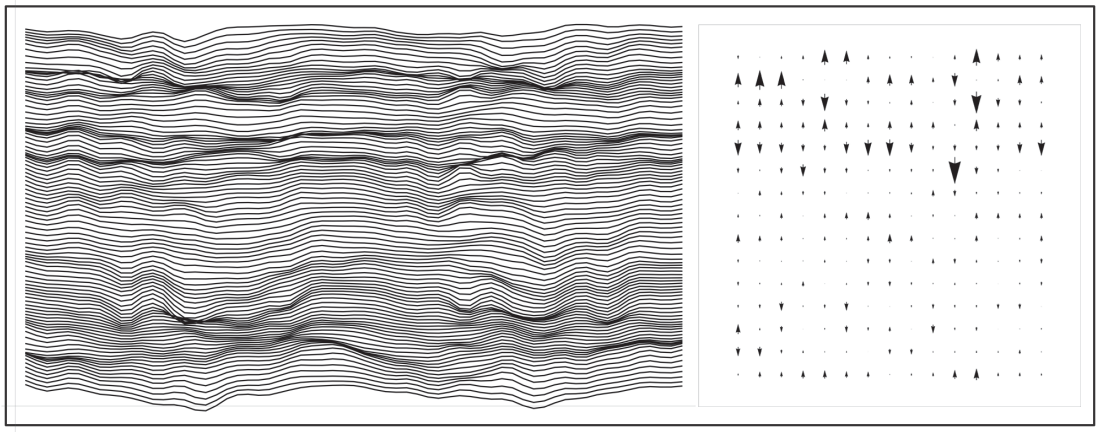

(b) EEG epoch of length 100 using 63 electrodes that were alpha-bandpassed (8-13Hz at a sample rate of 500 samples/s) (left) and its gradient field in the time direction (right).

Figure 3.1: Both plots show the channel labels $(1, 2, \ldots, n)$ on the x) axis and time on the y axis for convenience. The gradient field of an EEG epoch is computed using the directional derivative in the time direction. Smaller arrows or blanks denote small changes in potential or no changes in potential while larger arrows show larger changes in potential. Here the subject was asked to close his eyes for 1 minute and clear his mind. The EEG signals show an sequence of 0.2 seconds taken at the beginning of the epoch of 1 minute.

Table 3.2: Radial Basis Functions

Method	Function $\varphi(r)$	Parameter ϵ
Gaussian	$e^{-2\epsilon^2 r}$, $e^{-(\epsilon r)^2}$	$\sqrt{\text{Median}(\Phi)}$
Thin plate spline	$\begin{cases} 0, & r = 0 \\ \dfrac{r \log r}{2 - \log \epsilon}, & r \neq 0 \end{cases}$	$\sqrt{\text{Median}(\Phi)}$
Inverse multiquadrics	$\dfrac{1}{\sqrt{r + \epsilon}}$	$\text{Median}(\Phi)$
Multiquadrics	$\sqrt{r + \epsilon/4}$	$\text{Median}(\Phi)$

the number of electrodes. Let x index the set of electrodes as $1, 2, \ldots, n$, the function $f(x, t)$ defines the $N \times n$ matrix of measurements and $f(x, t)$ effectively contains the information of a given scalp field map at time t and electrode x. In practice, the gradient field is a directional derivative. The directional derivative of a differentiable function $f(x, y)$ in the direction of the unit vector $\mathbf{u} = \cos\theta\ \mathbf{e}_1 + \sin\theta\ \mathbf{e}_2$ is given by:

$$\begin{aligned} D_{\mathbf{u}} f(\mathbf{x}, k) &= (f_x(\mathbf{x}, k), f_y(\mathbf{x}, k)) \cdot \mathbf{u} \\ &= f_x(\mathbf{x}, k) \cos\theta + f_y(\mathbf{x}, k) \sin\theta \end{aligned} \tag{3.5}$$

for $\mathbf{x} = (x, y)$ and time $t = k$. The gradient is defined as usual as:

$$\begin{aligned} \nabla f(\mathbf{x}, k) &= f_x(\mathbf{x}, k)\ \mathbf{e}_1 + f_y(\mathbf{x}, k)\ \mathbf{e}_2 \\ &= (f_x(\mathbf{x}, k), f_y(\mathbf{x}, k)) \end{aligned} \tag{3.6}$$

We then have:

$$D_{\mathbf{u}} f(\mathbf{x}, k) = \nabla f(\mathbf{x}, k) \cdot (\cos\theta, \sin\theta) \tag{3.7}$$

The general problem of defining the directional derivative of an epoch on the scalp field maps themselves can be addressed as follows. Without loss of generalities, let $f(x, y)$ be a radial basis function with coefficients $c_1, \ldots c_n$, distance matrix Φ and Gaussian function

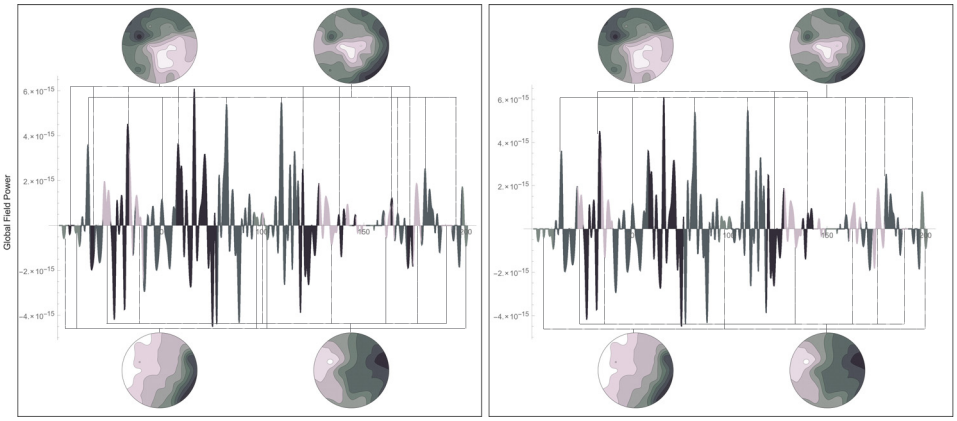

Figure 3.2: Scalp field maps associated to points on the global field power curve of an EEG. The subject was asked to perform an acitvity.

$e^{-(\epsilon r)^2}$, the following holds:

$$\begin{aligned} f_x(\mathbf{x},t) &= \frac{\delta}{\delta x}\sum_{k=1}^{n} c_k e^{\left(-\epsilon\sqrt{(x-x_k)^2+(y-y_k)^2}\right)^2} \\ &= -2\epsilon^2\sum_{k=1}^{n} c_k e^{-\epsilon^2((x-x_k)^2+(y-y_k)^2)}(x-x_k) \end{aligned} \tag{3.8}$$

$$\begin{aligned} f_y(\mathbf{x},t) &= \frac{\delta}{\delta y}\sum_{k=1}^{n} c_k e^{\left(-\epsilon\sqrt{(x-x_k)^2+(y-y_k)^2}\right)^2} \\ &= -2\epsilon^2\sum_{k=1}^{n} c_k e^{-\epsilon^2((x-x_k)^2+(y-y_k)^2)}(y-y_k) \end{aligned} \tag{3.9}$$

Using Equation 3.5, the directional derivative on parameters (x, y, θ) is then given.

In practice, we may want to compute the directional derivative at larger time increments. This is then done as follows:

$$_{\mathbf{u},k}f(\mathbf{x},t) = f(\mathbf{x},t+k) - f(\mathbf{x},t) \tag{3.10}$$

with $\mathbf{u} = (0,1)$ and for some constant k defining a reference window. This is shown in Figure 3.1 (left).

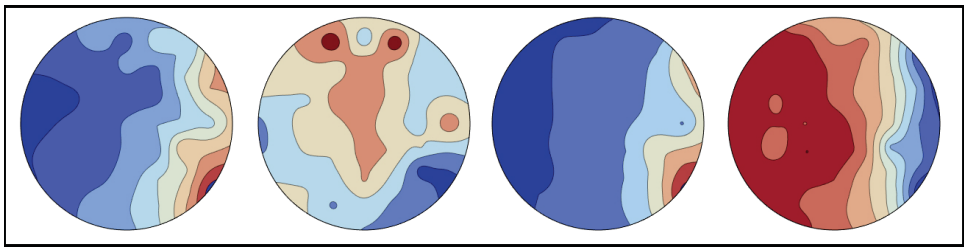

(a) Microstates obtained from Lloyd's k-means algorithm

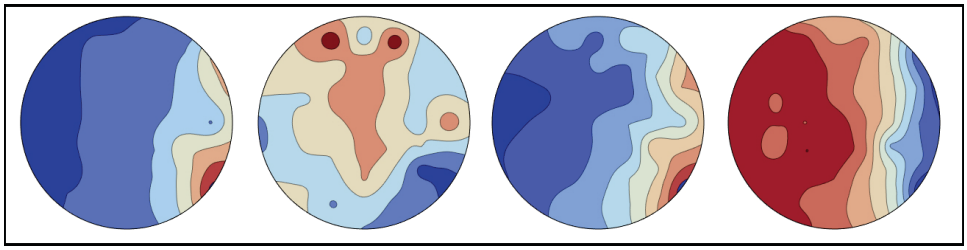

(b) Microstates obtained from a built-in k-means algorithm

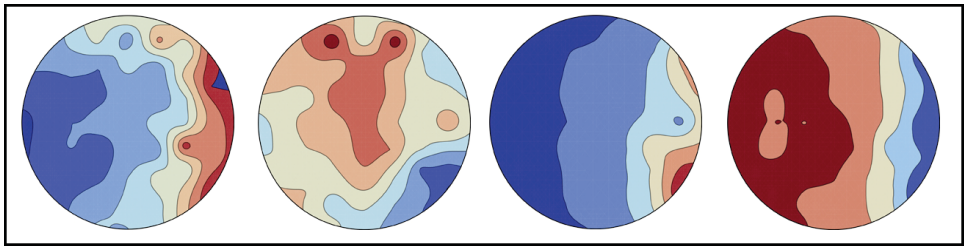

(c) Microstates obtained from the fuzzy c-means algorithm

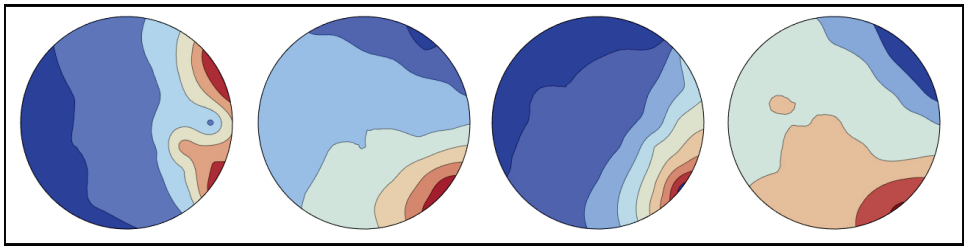

(d) Microstates obtained from the P2ML algorithm (first run)

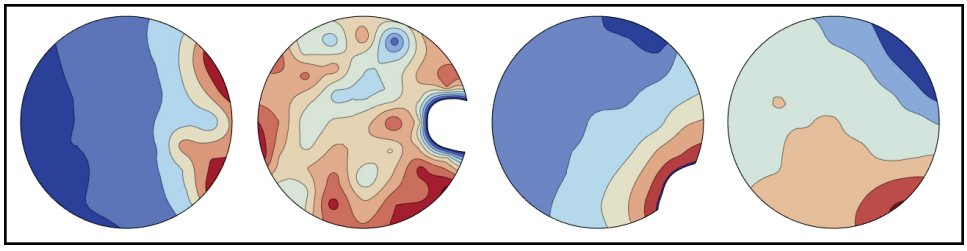

(e) Microstates obtained from the P2ML algorithm (second run)

Figure 3.3: Microstates obtained from different algorithmic implementations.

3.2 Spatio-Temporal Features: Microstates

3.2.1 Unsupervised Clustering of Scalp Field Maps: Comparisons

Many methods exist to segment EEG data: some of them are frequency based and others spatio-temporal. Microstate analysis form a set of spatio-temporal techniques that apply to multichannel EEG recordings. Microstates are features of an EEG epoch extracted using clustering-like methods. Since microstates are sub-second quasi-stable configurations of scalp field map potential values that quickly change to another quasi-stable configuration, it makes sense to cluster the scalp field maps into representative cluster centroids. Experimentally, this number of representative cluster centroids was found to be 4 on subjects with eyes closed [PMML95]. [BTV$^+$10] proposes different machine learning techniques to obtain these centroids. [PMML95] proposes the P2ML algorithm, an optimized clustering technique based on eigenvalues and Lagrangians. The orthogonal squared distance between different scalp field maps is used and the objective function then finds the patterns that are closest to some cluster centroids. The cluster centroids are initially guessed and iteratively set to converge to an optimum which may be a local optimum and may not be a global optimum. Using the P2ML algorithm, the strength of the system's eigenvalues can be used to estimate the number of needed cluster centroids. The strength of the eigenvalues then measures the number of eigenvectors needed to represent the system.

Given an EEG signal, a global power field curve can be computed. Each point on the global field curve corresponds to a sample which in turn corresponds to a scalp field map. This is shown in Figure 3.2. The theory of functional microstates states that these scalp fields are stable for subsecond periods and that these stable configuration reoccur. This in turn means that the scalp field maps of an EEG signal can be clustered into representative centroids and that, in turn, these centroids can provide a means to segment an EEG signal.

Many algorithms to cluster data exist. The k-means and fuzzy c-means algorithms are popular methods. In the context of functional microstate analysis, the Pascual-Marqui,

Michel and Lehmann (P2ML) algorithms, which come in a regularized and non-regularized version, are also popular. The k-means algorithm is a simple algorithm to implement and iterates by optimizing the orthogonal squared distance between centroids and a dataset. The centroids are refined through the iteration process. While being simple, the Lloyd's implementation of the k-means algorithm is known to be NP-hard and, for high dimensional datasets such as EEG scalp field maps, the performance of the algorithm is slow if not unpredictable. Scalp field maps measured in a laboratory typically have 64 sensors and by extension have 64 dimensions while scalp field maps measured on general purpose commercial devices may have 4 to 16 sensors. The fuzzy c-means algorithm is similar to the k-means algorithm but provides the additional information contained in the membership functions. Membership functions say to what extent a data value is a *member* of a given cluster centroid. For example, given 4 centroids, a data value can be a member of the first centroid with membership value 0.6, of the second centroid with a value 0.25, a third centroid with a value 0.1 and a fourth centroid with a value 0.05. Such membership functions are shown in Figure 3.4 for the centroids obtained in Figure 3.3c. The fuzzy c-means algorithm has a reported complexity ranging from linear to quadratic [Kol02].

Figure 3.3 shows the different results obtained when using two different implementations of the k-means algorithm, Lloyd's algorithm and a built-in implementation (Figure 3.3(a-b)), the fuzzy c-means algorithm (Figure 3.3(c)) and the P2ML algorithm (Figure 3.3(d-e)). The EEG data was generated from an experiment conducted by the Design Lab at the Concordia Institute for Information Systems Engineering. While the k-means algorithms are sensitive to initial seeds, the P2ML algorithm may converge to local minima while also being sensitive to initial seeds. The advantage of using the P2ML algorithm over a traditional k-means approach is to avoid the computational complexity of Lloyd's k-means which is NP-hard even for low-dimensional datasets higher or equal to 2. The P2ML is guaranteed to converge and in practice may take between 20 to 60 iterations to converge. The bottleneck of P2ML is bounded by the computation of an eigensystem and a distance matrix. Figure 3.4 shows

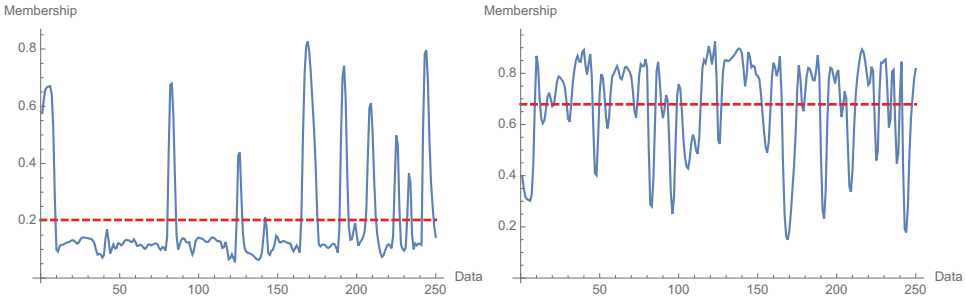

(a) Membership of the first centroid

(b) Membership of the second centroid

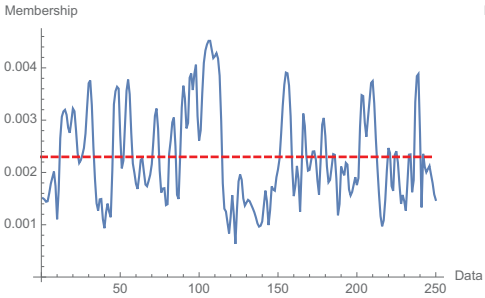

(c) Membership of the third centroid

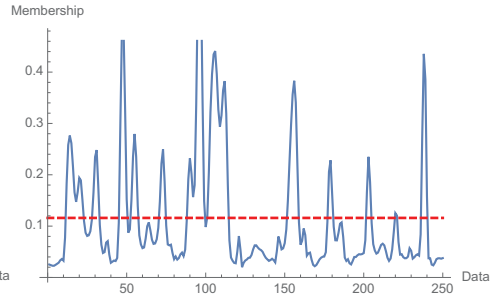

(d) Membership of the fourth centroid

Figure 3.4: Fuzzy membership functions of the first 250 samples of an EEG clustered using fuzzy c-means. The strongest component is clearly the second centroid. The first and the fourth centroid follow whereas the third centroid has a low average membership.

the fuzzy membership functions of the centroids obtained using the fuzzy c-means clustering algorithm. The third centroid has low membership function values because it is similar to the first one to which samples are more likely to cluster. The centroids obtained using k-means and the fuzzy c-means algorithms are similar while the P2ML centroids are slightly different. In terms of functional microstates analysis, the centroids obtained using the P2ML algorithm (first run) are smoother and less sensible to noise while the second run of the P2ML algorithm (Figure 3.3(e)) are similar to the centroids obtained using the k-means or the fuzzy c-means algorithms. Membership functions computed using the fuzzy c-means is shown in Figure 3.4.

The k-means algorithm is described in Algorithm 3.1 while the fuzzy c-means algorithm is described in Algorithm 3.2. The normal and regularized P2ML algorithms are described in Algorithms 3.3 and 3.4.

3.2.2 The P2ML Algorithm: An Outline

D. Lehmann, C.M. Michel, Koenig, R.D. Pascual-Marqui et al. in a series of papers [Leh71, LOP87, Leh90, PMML94a, PMML95, KLM+99, KPL+02] developed the notion of functional microstate analysis of the brain based on machine learning algorithms over the spatial-domain EEG signals. [Leh90] describes the latter as being the atoms of thought. Functional microstates of the brain are prototypical patterns of the scalp field maps and, in terms of pattern recognition, can be seen as the cluster centroids of an EEG signal. Large scale statistical studies have shown that most human have the same 4 microstates when EEGs were measured on subjects at rest with eyes closed. They were initially studied by D. Lehman *et al.* in the context of medical diagnosis as it was shown that deviant microstates were statistically correlated with psychiatric disorders. Furthermore, microstates have been shown to vary depending on age groups [KPL+02]. Microstates constitute the main technique of analysis of spatio-temporal analysis of EEG signals [MKB+09, BMM11]. Since D. Lehman's seminal paper on microstates [Leh71], a few techniques have been proposed to compute these microstates [BTV+10, BMM11, PMML95] based on various feature extraction techniques, segmentation and clustering methods. One of the first such method proposed in [LOP87] measured the orientation of scalp field maps based on maximum and minimum potential values. CARTOOL [BMM11] is an open-source tool to perform functional microstate analysis. A well-studied method by Pascual-Marqui, Michel and Lehman (P2ML) proposes two ways to compute functional microstates, a non-regularized version which is sensible to transient microstates and a regularized version which smoothes out transient microstates [PMML95]. These transient microstates have be shown to carry significant physiological information.

In the following, we describe the two P2ML algorithms. For a set of k given microstates $\mathbf{M}_k$ and potential values $\mathbf{V}_t$ at time t, the P2ML objective function is:

$$\arg\max_{\mathrm{k}} \left\{ (\mathbf{V}_{\mathrm{t}} \cdot \mathbf{M}_{\mathrm{k}})^2 \right\} \tag{3.11}$$

$\mathbf{V}$ is a matrix containing all the potential measurements at time t and $\mathbf{V}_t$ is a vector of a

Algorithm 3.1: K-Means Algorithm

Data: potential data $\mathbf{V}$, number of centroids k and convergence parameter ϵ
Result: k centroids $\mathbf{M}$

```
Set each k centroids M_k to a random value;
while true do
    For each M_k, compute all the closest points in V to M_k;
    Compute the new centroids M'_k of points in V that clustered to M_k
    if ||M_k − M'_k||_2 ≤ ε then
        Break;
    else
        M_k = M'_k
Return M;
```

Algorithm 3.2: Fuzzy C-Means Algorithm

Data: potential data $\mathbf{V}$, number of centroids k and convergence parameter ϵ
Result: k centroids $\mathbf{M}$ and membership function $\mathbf{W}$

```
Set each k centroids M_k to a random value;
Set each value in the membership N × k matrix W to a random value;
while true do
    Compute the new centroid M'_k as the mean of all j-th points multiplied by their
    membership value W_jk to M_k
    Update the membership function W' with M'
    if ||W_k − W'_k||_2 ≤ ε then
        Break;
    else
        M_k = M'_k;
        W_k = W'_k;
Return M,W;
```

measurement at time t containing n electrodes.

Using vector geometry [Fre03], the orthogonal squared distance between V_t and M_k is:

$$d^2(\mathbf{V}_t, \mathbf{M}_k) = (\mathbf{V}_t \cdot \mathbf{V}_t) - (\mathbf{V}_t \cdot \mathbf{M}_k)^2 \tag{3.12}$$

The objective function is effectively minimizing the orthogonal squared distance between $\mathbf{V}_t$ and $\mathbf{M}_1, \ldots, \mathbf{M}_k, \ldots$ by maximizing the $(\mathbf{V}_t \cdot \mathbf{M}_k)^2$ term of the equation.

Algorithm 3.3: P2ML Algorithm

Data: potential data $\mathbf{V}$, number of centroids k and convergence parameter ϵ
Result: segmentation $\mathbf{S}$ and centroids $\mathbf{M}$

1 Set each centroid $\mathbf{M}_k$ to a normalized random vector;
2 Set the current variance σ_0 to a zero-vector or length k ;
3 For each $\mathbf{M}_k$, compute the segmentation $\mathbf{S}_i = k$ as the closest value of points in $\mathbf{V}$ to $\mathbf{M}_k$;
4 **while** *true* **do**
5 For each $\mathbf{V}_t$ in segment $\mathbf{S}_k$, set $\mathbf{M}_k$ as the eigenvector with largest eigenvalue of $\sum_t \mathbf{V}_t \mathbf{V}_t^T$;
6 For each M_k, compute the segmentation $S_i = k$ as the closest value of points in $\mathbf{V}$ to $\mathbf{M}_k$;
7 Compute the variance of the new system σ_1^2;
8 **if** $|\sigma_{0,k}^2 - \sigma_{1,k}^2| \leq \epsilon\sigma_{0,k}\ \forall k$ **then**
9 Break;
10 **else**
11 $\sigma_{0,k}^2 = \sigma_{1,k}^2$;
12 Return $\mathbf{S}$;

Note that, in Algorithm 3.3 , the product $\mathbf{V}_t \mathbf{V}_t^T$ of vectors of length n (the number of electrodes) yields a matrix $n \times n$ and these matrices are summed over t before the computation of the related eigensystem.

The regularized objective function of the P2ML method is:

$$\arg\min_{\mathrm{k}} \left\{ \frac{\left(\mathbf{V}_\mathrm{t} \cdot \mathbf{V}_\mathrm{t} - (\mathbf{V}_\mathrm{t} \cdot \mathbf{M}_\mathrm{k})^2\right)}{2\mathrm{e}(\mathrm{N}-1)} - \lambda \mathrm{E} \right\} \tag{3.13}$$

where λ is a regularization parameter and E is a smoothness penalty function given by:

$$E = \sum_{i=t-w}^{t+w} \delta(\mathbf{S}_i, n), \quad n = 1, \ldots, k \tag{3.14}$$

Algorithm 3.4: Regularized P2ML Algorithm

Data: potential data $\mathbf{V}$, number of centroids k, convergence parameter ϵ, smoothness penalty λ and window size w

Result: segmentation $\mathbf{S}$

```
Set the current variance σ_0 to a zero-vector or length k ;
For each M_k, compute the segmentation S_i = k as the closest value of points in V to M_k;
Compute the error parameter e;
while true do
    For each sliding window of length 2w, compute the smoothness penalty E;
    Compute S using the regularized objective function;
    if |σ²_{0,k} − σ²_{1,k}| ≤ ϵσ_{0,k} ∀k then
        Break;
    else
        σ²_{0,k} = σ²_{1,k};
Return S;
```

for a segment number $\mathbf{S}_i$ (the numerical index k of the microstate $\mathbf{M}_k$) and a delta function given by:

$$\delta(x, y) = \begin{cases} 1, & x = y \\ 0, & \text{otherwise} \end{cases} \tag{3.15}$$

The regularization parameter is λ and the smoothness penalty factor is E. It increases when segments are long and decreases when segments are short based on a window size parameter w. Therefore, the regularized objective function has low values for smooth segments and high values for non-smooth segments, effectively penalizing transient microstates.

Figure 3.5(a) shows the segmentation of a global field power curve into 4 microstates. The P2ML algorithm computed 32 segments. Figure 3.5(b) shows the segmentation of the same global field power curve using the regularized P2ML algorithm and 4 microstates. The regularized P2ML algorithm computed 21 segments.

The number of microstates in the P2ML algorithm is a parameter which is often estimated using the number of significant eigenvalues in the system which are the number of dimensions useful in explaining the variance of a system. Typical numbers of microstates are 4 [LOP87, PMML95]

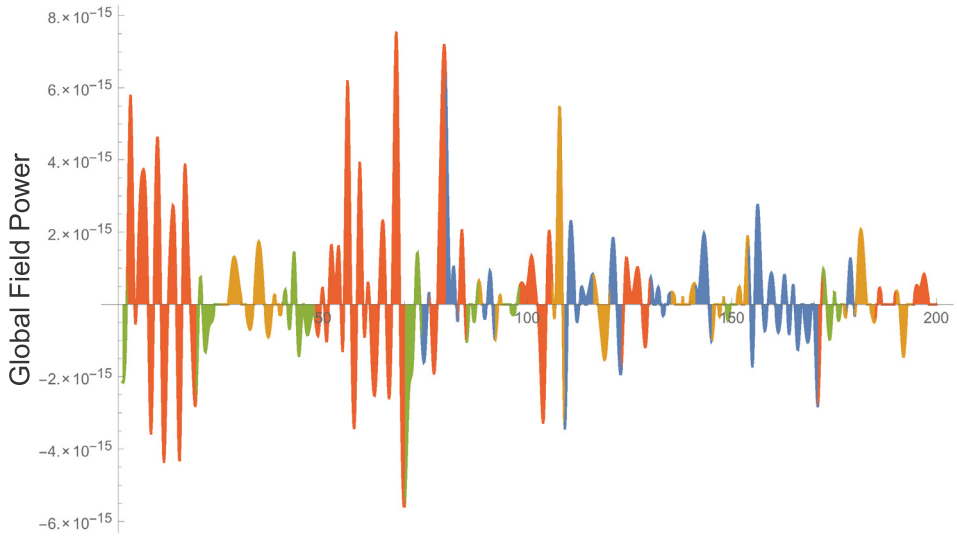

(a) Non-regularized segmentation.

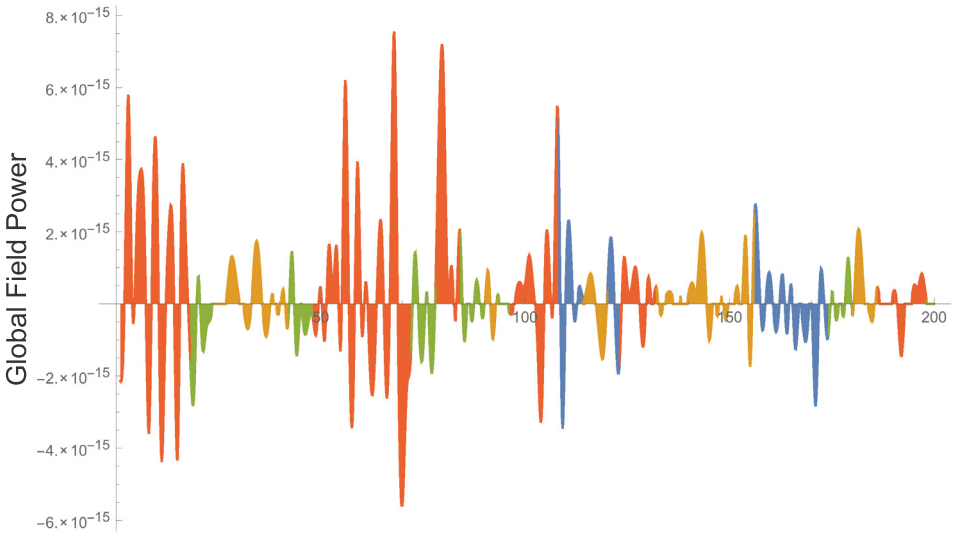

(b) Regularized segmentation.

Figure 3.5: Global field power curve with non-regularized (a) and regularized (b) microstate segmentation of an epoch of length 200. The subject was asked to keep his eyes closed.

Following the definition of the regularized and non-regularized microstate algorithms, we can define the transient microstate percentage (T.M.%) as follows:

$$T.M.\% = \frac{(Segments - SmoothSegments)}{N} \tag{3.16}$$

The number of transient microstates is a significant feature which finds ground in the medical literature and EEG analysis.

For example, let an EEG signal have 10 samples. The non-regularized segmentation of an EEG signal based on 4 microstates could be: $(1, 1, 1, 1, 3, 3, 3, 2, 4, 4)$. The sample segmented to microstate 2 has a transient duration of only one sample. Assume the regularized segmentation is then: $(1, 1, 1, 1, 3, 3, 3, 4, 4, 4)$. The segment at index 8 has been smoothed out and the associated transient microstate percentage is 10%.

3.3 Frequency-Domain Features

Frequency-domain features are typically computed on the Fourier transforms or the wavelet (multiresolution) transforms of an EEG signal. In EEG analysis, a popular and common method is based on power spectral densities (PSD). The usual frequency ranges in neurosciences are the alpha band, the beta band, the delta band and the theta band whose exact frequency values (that may change depending on authors) are given in Table 3.3. Other less used frequency bands are the gamma (somatosensory cortex) and mu bans (sensorimotor cortex). Furthermore, combinations of frequency ranges are used by researchers to narrow down different characteristics such as fatigue and concentration.

The PSD can be computed using correlograms or periodograms. Many algorithms exist to approximate PSD values. The modulus of the Discrete Fourier Transform (DFT) is a simple method given by:

$$PSD_{range} = \sum_{\tau \in range} \left| (DFT_\tau(\mathbf{x})) \right| \tag{3.17}$$

Table 3.3: EEG frequency-domain features

Features	Characteristics	Range (Hz)
alpha	relaxed, eyes closed, brain non-arousal	$8-15$
beta	focused, brain arousal, concentration, fatigue	$16-31$
delta	slow-wave sleep, dreaming	<4
theta	drowsiness, inhibition, idling	$4-7$
gamma	somatosensory cortex	>32
mu	sensorimotor cortex	8-12
(theta+alpha)/beta	fatigue	
alpha/beta	attention, fatigue	
(theta+alpha)/ (alpha+beta)	fatigue	
theta/beta	fatigue	

for a given sample $\mathbf{x}$ within a specific frequency range (Hz).

For example, let $(1,2,2,3,5,2,1,4,5,6,3,2)$ be the modulus of the DFT of a signal in the frequency range $1-12$ Hz with 1 Hz as base unit. Computing the $4-5$ Hz frequency range is done by summing $3+5=8$ Hz.

In contrast to microstates (which are computed on multichannel measurements of an EEG), PSD is usually computed on a given electrode such as FP1 (left frontal area). PSD is a one-dimensional method and has been widely used to detect eye-blinking artifacts, sensorimotor artifacts, sleep cycles and states of mind such as fatigue, concentration and relaxation

3.4 Source-Localization

Source localization is an indeterminate inverse problem for which may exist an infinity of approximations. Effectively, the associated forward problem is to map densities in a 3D model of the brain (of M voxels cf. Figure 3.6(right)) to a 2D scalp field map (of N

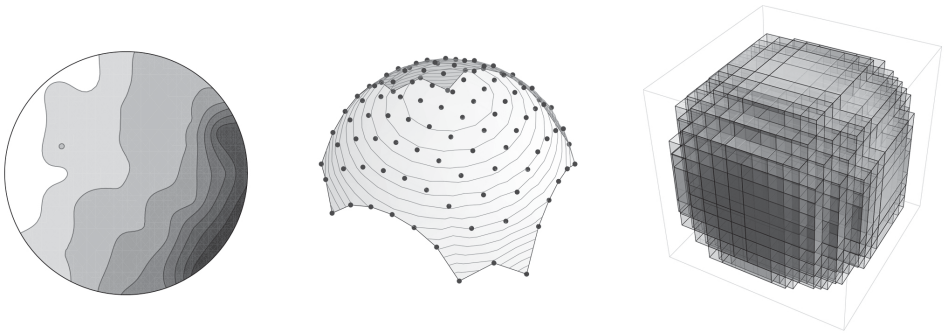

Figure 3.6: (left) 2-D scalp field map. (center) Interpolated 3D scalp field map using 107 points. (right) Voxels representing the brain using 452 voxels.

electrodes cf. Figure 3.6(left)):

$$\mathbf{\Phi} = \mathbf{KJ} \tag{3.18}$$

where $\mathbf{\Phi}$ is the N-by-1 vector representing the 2D scalp field map, $\mathbf{K}$ is a transfer matrix and $\mathbf{J}$ are the M densities associated with the M voxels model of the brain. Since M is usually much greater than N, solving Equation 3.18 for $\mathbf{J}$ is indeterminate. The approximation for the inverse equation is then given by:

$$\tilde{\mathbf{J}} = \mathbf{T\Phi} \tag{3.19}$$

where $\tilde{\mathbf{J}}$ is an approximation of the densities associated with the 3D voxel model of the brain and $\mathbf{T}$ is a resolution matrix. Using the LORETA technique [PMML94b], the resolution matrix is given by:

$$\mathbf{T} = \mathbf{W}^{-1}\mathbf{K}^T \left[\mathbf{K}\mathbf{W}^{-1}\mathbf{K}^T\right]^+ \tag{3.20}$$

where $\mathbf{K}$ is a lead field matrix (in our experiments, for simplicity, we used the lead field of a homogeneous conducting sphere in air with conductivity 0.185 S/m -grey matter conductivity) given by, for scalp positions $\mathbf{s}_i$ and voxel positions $\mathbf{v}_j$ [PM07]:

$$\mathbf{K}_{ij} = \frac{1}{4\pi\sigma}\left(2\frac{(\mathbf{s}_i - \mathbf{v}_j)}{\|\mathbf{s}_i - \mathbf{v}_j\|^3} + \frac{\mathbf{s}_i\|\mathbf{s}_i - \mathbf{v}_j\| + \|\mathbf{s}_i\|(\mathbf{s}_i - \mathbf{v}_j)}{\|\mathbf{s}_i\|\|\mathbf{s}_i - \mathbf{v}_j\|(\|\mathbf{s}_i\|\|\mathbf{s}_i - \mathbf{v}_j\| + \mathbf{s}_i^T(\mathbf{s}_i - \mathbf{v}_j)}\right) \tag{3.21}$$

and $\mathbf{W}$ is a positive definite matrix given by

$$\mathbf{W} = (\mathbf{\Omega} \otimes \mathbf{I}_3)\mathbf{B}^T\mathbf{B}(\mathbf{\Omega} \otimes \mathbf{I}_3) \tag{3.22}$$

with $\mathbf{\Omega}$, a diagonal matrix on $i = 1 \dots M$ and $\mathbf{k}_{ij} \in \mathbf{K}$, given by:

$$\mathbf{\Omega}_{ii} = \sqrt{\sum_{j=1}^{N} \mathbf{k}_{ij}^T \mathbf{k}_{ij}} \tag{3.23}$$

and with $\mathbf{B}$ given by the discrete spatial Laplacian operator:

$$\mathbf{B} = \frac{6}{d^2}\, \mathbf{A} - \mathbf{I}_{3m} \tag{3.24}$$

with the following:

$$\mathbf{A} = \mathbf{A}_0 \otimes \mathbf{I}_3 \tag{3.25}$$

$$\mathbf{A}_0 = \frac{1}{2} \left(\mathbf{I}_M + [diag\,(\mathbf{A}_1 \mathbf{1}_M)]^{-1} \right) \mathbf{A}_1 \tag{3.26}$$

$$[\mathbf{A}_1]_{ij} = \begin{cases} 1/6, & \|\mathbf{v}_i - \mathbf{v}_j\| = d \\ 0, & \text{otherwise} \end{cases} \tag{3.27}$$

Here, + denotes the Moore-Penrose pseudo-inverse. While many source localization techniques exist [JNKFB14], the LORETA solution is said to yield the "smoothest solution capable of explaining the data" [PMML94b]. Since we did not have access to MRI data, we interpolated 2D scalp field maps (Figure 3.6(left)) to an intermediate 3D scalp representation (Figure 3.6(center)) using a radial basis interpolating function for scattered data. Furthermore, our brain topology was simplified by using a voxelized sphere (Figure 3.6(right)).

3.5 Mathematical Validity of Machine Learning Algorithms on EEG Data

Machine learning and data mining algorithms such as P2ML often rely on similarity (i.e. correlation) or distance metrics such as the ℓ_p norm (where ℓ_2 is the usual Euclidean distance) to perform their operations. Vectors that are closer to each other are clustered or segmented together. Whenever these distance metrics fail to provide discerning information, the underlying machine learning or data mining algorithm fails altogether. Therefore, before

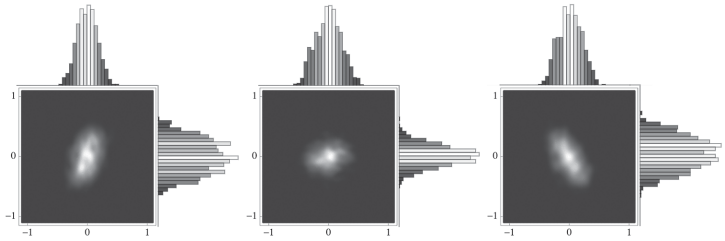

(a) H=0.1, n=100, N=1000

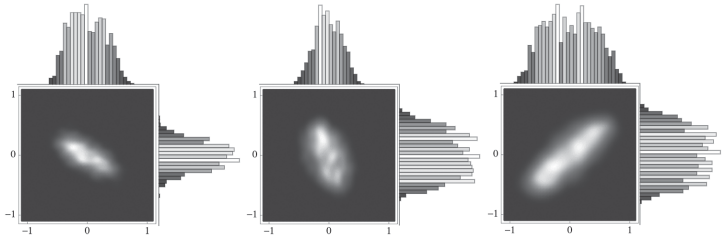

(b) H=0.2, n=100, N=1000

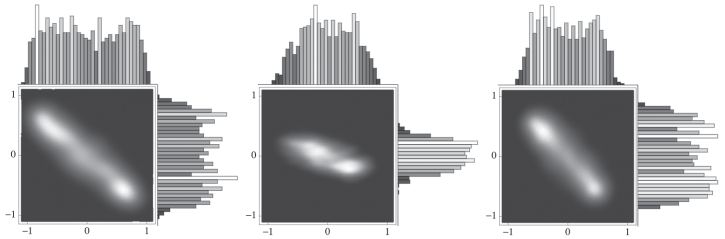

(c) H=0.3, n=100, N=1000

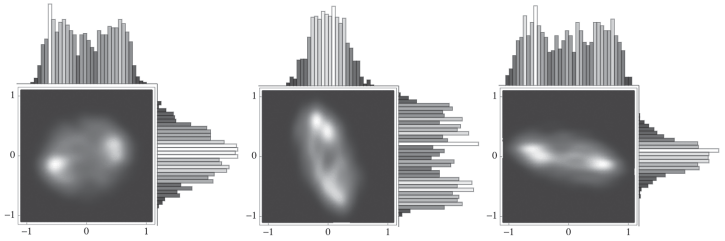

(d) H=0.4, n=100, N=1000

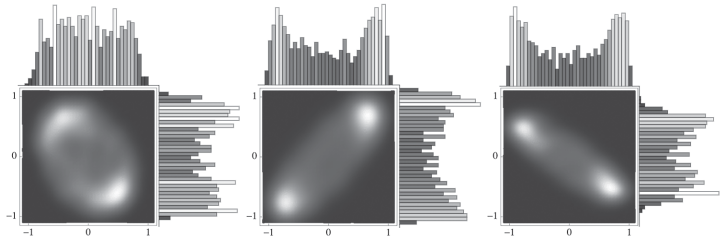

(e) H=0.5, n=100, N=1000 (Brownian motion case)

Figure 3.7: Computed probability density functions on different Hurst indices with sythetic data simulating n electrodes and an epoch-length of N. Lower Hurst indices tend to aggregate around low correlation scores ($\rho < 0.5$).

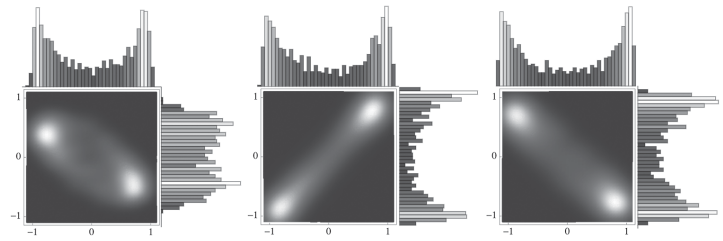

(f) H=0.6, n=100, N=1000

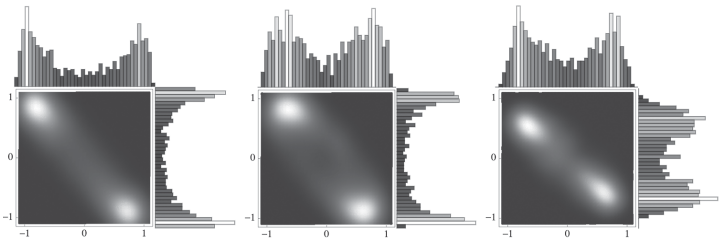

(g) H=0.7, n=100, N=1000

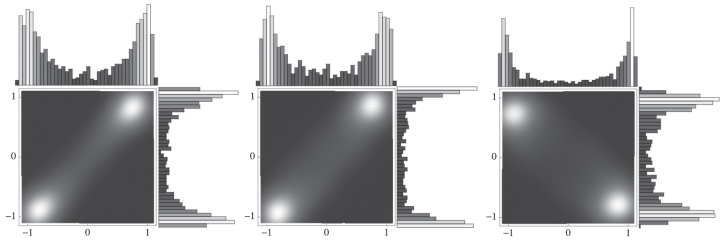

(h) H=0.8, n=100, N=1000

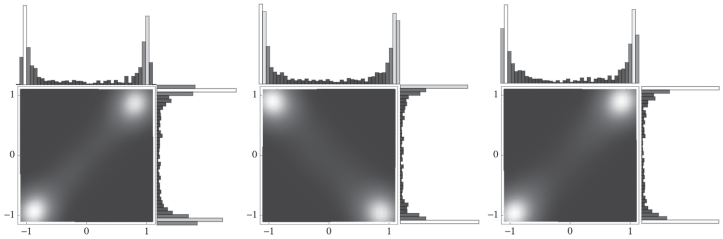

(i) H=0.9, n=100, N=1000

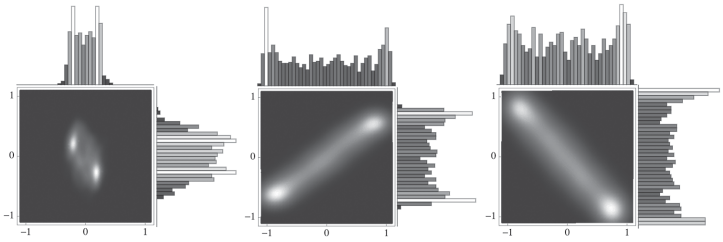

(j) H=U(0.001,0.999), n=100, N=1000 (uniformly chosen indices)

Figure 3.7: (continued) Higher Hurst indices tend to aggregate around higher absolute value correlation scores ($\rho \approx (-1, 1)$).

applying these techniques to a data set, it is important to verify if the metric used provides discerning information for the underlying data set.

3.5.1 Concentration of Measure

A well-studied case, and perhaps the single most important one, where ℓ_p norms fail, is known as the concentration of measure phenomenon [DP09, Pes11, FWV07, VP09]. A measure phenomena occurs when the underlying generating distribution of a datasets impacts the measure used to distinguish the data. A well-known measure phenomena occurs when computing the ℓ_p norm of high dimensional independent and identically distributed (*i.i.d.*) vectors [FWV07, VP09]. More specifically, we have:

$$\lim_{n\to\infty} \|\mathbf{x}_i - \mathbf{x}_j\|_p = k \tag{3.28}$$

for some constant k and $\mathbf{x}_i, \mathbf{x}_j \in \mathbf{X}_n$, an *i.i.d.* random generator of dimension n. In those cases, since all vectors have a pairwise distance that tends to a constant, the discerning value of the ℓ_p norm is greatly diminished, if not completely useless. Therefore, using an ℓ_p norm-based machine learning or data mining algorithm is not advisable as it will mostly generate spurious results. This phenomenon also occurs when using correlation (cosine similarity).

3.5.2 Experimental Validation

In the context of the EEG data analysis we perform, the metrics used are the orthogonal squared distance, the Euclidean distances and correlation. EEG data can be considered high dimensional as we often deal with 64-dimensional vectors corresponding to the number of electrodes on the EEG system. EEG data can be modeled as an fBm (fractional Brownian motion) process [SRMB07]. In practice, to validate the usage of norm-based machine learning algorithms on such data, we then only need to verify if the distance between two high dimensional vectors generated using an fBm process for different Hurst exponents

tends to a constant. If it does tend toward a constant, the plot of the pairwise distances will tend towards a single dot. If it does not, the data will be spread out. To plot such distances, we generated a random fBm vector and measured its distance (in Figure 3.7, correlation was used) to two other random fBm vectors (one for each axis of the plot). Figure 3.7 shows that concentration of measure does not occur for fBm processes and therefore distance-based machine learning and data mining algorithms on such processes are valid. In fact, our plots show that the distribution of distances seems to follow a Gaussian mixture distribution.

Chapter 4

Approaches to Quantifying EEG Features

4.1 Experimental Protocol

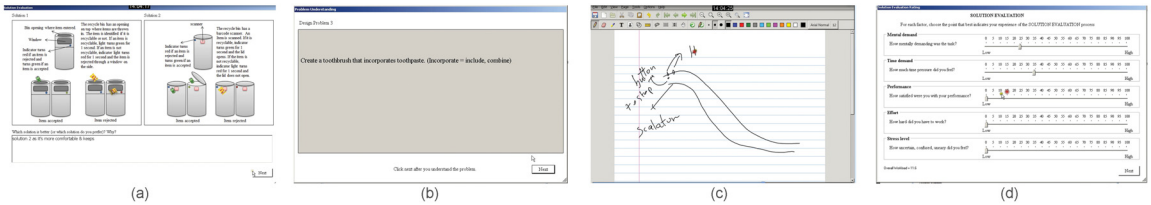

Figure 4.1: Screenshots of various stages in our experimental protocol: (a) multiple choice question, (b) read question, (c) sketch a solution and (d) rate the hardness of the question

In the past years, the Design Lab has conducted a set of experiments where subjects were asked to solve various design problems while having physiological signals monitored (e.g. EEG, ECG, eye-tracking, heart-rate variability (HRV) or skin conductance). The experimental data we used in this thesis is EEG-based. It consists of EEG recordings monitored on subjects executing design tasks on a touchpad. These problems are listed in Table 4.1. Subjects were asked to solve design problems of variable difficulty, ranging from trivial tasks to more complex tasks.

Table 4.1: Experimental Design Protocol Problem List

Problem	Description
Design Problem 1	Make a birthday cake for a five year old kid. How should it look like?
Design Problem 2	Sometimes, we don't know which items should be recycled. Create a recycle bin that helps people recycle correctly.
Design Problem 3	Create a toothbrush that incorporates toothpaste.
Design Problem 4	In many cities, people on wheelchair cannot use the metro safely because most metros only have stairs or escalators. Elevators are not an option because they are costly. You are asked to create an efficient solution to solve this problem.
Design Problem 5	Employees in IT companies sit too much. The company wants their employees to stay healthy and work efficiently at the same time. You are asked to create a workspace that can help employees to work and exercise at the same time.
Design Problem 6	There are two problems with standard drinking fountains: a) filling up water bottles is not easy, b) people too short cannot use the fountain and people too tall have to bend over. Create a new drinking fountain that solves these problems.

The design protocol was as follows. For each design problem, subjects were asked to sketch a solution for the problem. After the sketch was done, subjects were asked a multiple choice question where they were asked to choose the best between two different solutions for the problem. After the multiple choice question, they were asked to rate the hardness of the problem. The strict sequence in which problems were presented to the subject was kept intact to facilitate comparisons between subjects as if we had randomized the problems, a different sequencing of problems may have yielded problems with comparing different subjects. The dataset consisted of the recordings on 8 subjects which ranged between 30 minutes and 2 hours.

As listed in Table 4.1, the difficulty of the problems to solve were of varying difficulty ranging from trivial (design a birthday cake for a child) to complex (design an escalator for a person in a wheelchair).

Figure 4.1 displays various screenshots taken from a video recorded from a sketchpad

while a subject was having its EEG monitored.

The Human Research Ethics and Compliance of our university approved our research protocol. All subjects were volunteers and all of them were graduate students from the Quality System Engineering program at Concordia University. Subject selection was randomized and no gender considerations were taken. The subjects' age ranged from 25 to 35. A gift card of 100$ was given as compensation to the best design.

4.2 Problem Hardness and Transient Microstate Percentages

Next generation CAD\E systems are aiming to be more *collaborative, conceptual and creative* [GVWH12]. Furthermore, immersive, behavioral and telepathic subsystems are being widely studied. In this context, the Design Lab of the Concordia Institute for Information Systems Engineering has in the last years effectively conducted a series of experiments on mental effort in the design process [NZ10b,NZ12a,NZ14b,NZ14c]. A series of datasets were then made available to us involving subjects who were asked to perform simple to complex design tasks while having their EEG monitored. The output of the subject's design task was also recorded and synced to the EEG signals.

The hardness of a mental task can serve as a measure of how alert and active the brain is and has multiple applications in engineering systems that interface with the human mind. The perceived hardness of a problem solving is effectively a window into human intelligence. For example, measuring how alert is the mind during a task such as driving a car is such an application. Another example can be found in video game AI: the level of hardness of the game can be automatically and parametrically adjusted according to the mental effort and alertness detected by an EEG subsystem. Alertness is then measured against fatigue and task hardness can effectively monitor both. Next generation CAD\E systems augmented with BCI technologies were studied in [BDRE13,SVR13]. Figure 4.2 shows a typical feedback loop in a BCI subsystem.

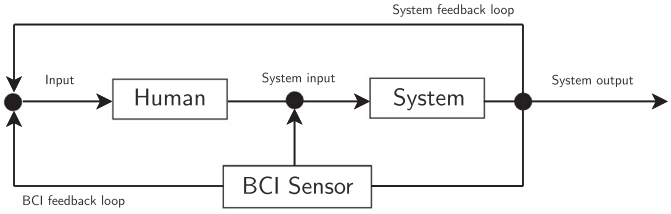

Figure 4.2: Feeback loops in a typical BCI subsystem.

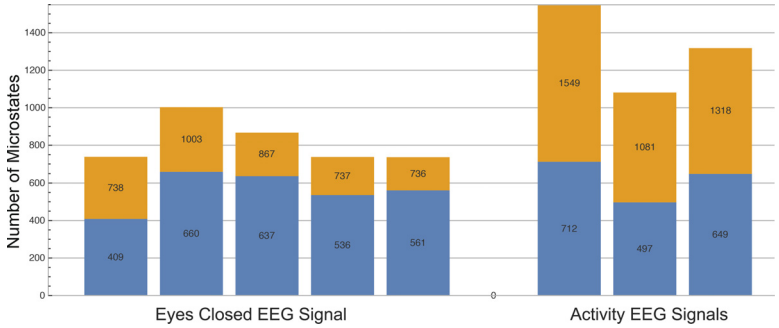

Figure 4.3: The number of transient microstates is computed using segment regularization and is defined as the difference between the number of segments in the non-regularized microstate segmentation (yellow) and the number of segments in the regularized segmentation (blue). The number of transient microstates (yellow) is significantly higher for EEG signals during an activity (right) than an EEG signal recorded eyes closed (left).

In this context, we have implemented the P2ML algorithm for microstate segmentation [PMML95] as a means to study design task hardness. As a heuristic, we considered that different tasks have different levels of perceived hardness and require different levels of alertness. Tasks can be broken down into subtasks and applying the same measurement method for task hardness, we have developed a means to segment subtasks in the creative process. Our data consisted of video sequences of subjects performing different tasks and the EEG recordings associated to the task. A major problem involved the segmentation of the task videos into subtasks using EEG recordings in a way that preserved the intrinsic logic of the videos.

4.2.1 Experiments

The data obtained during the experiments held by the Design Lab were a set of EEG signals monitored on subjects who were asked to perform design tasks of varying hardness and length. The execution of the tasks themselves were recorded on a touchpad. The perceived hardness was measured using a short survey after each tasks. The EEG signals measured the evoked potentials of the subjects faced with the design tasks. In short, the experiments consisted of two types of questions: a first asked the subject to chose the best design solution to a problem while a second asked the subject to design on a sketchpad a solution to a design problem. After each question, the subject was asked to rate the hardness of the task.

In a first set of experiments, we computed the segmentation of these EEG signals using the P2ML algorithm. The number of transient microstates was then computed using the regularized P2ML algorithm. The number of transient microstates for sequences of $8,782$ samples was then compared between signals obtained from subjects who were asked to keep their eyes closed and subjects who were asked to perform various design tasks of short duration (a few seconds to a few minutes). Figure 4.3 shows the results of these first set of experiments.

In a second set of experiments, we computed the transient microstate percentage of EEG sequences of subjects who were asked to close their eyes, then perform a task and then close their eyes again. In the first of these experiments, the task segment lasted about half a minute while in the second experiment, the task segment lasted a few seconds. This is illustrated in Figure 4.4 (left, center-left).

In a third set of experiments, we computed the transient microstate percentage of subjects submitted to tasks of varying hardness. The goal was to support the idea that the transient microstate percentage effectively measures the perceived hardness of a task. Higher transient microstate percentage averages yield harder tasks. Figure 4.4 illustrates these experiments (center-right, right). It can be noted that tasks that were rated as average were typically

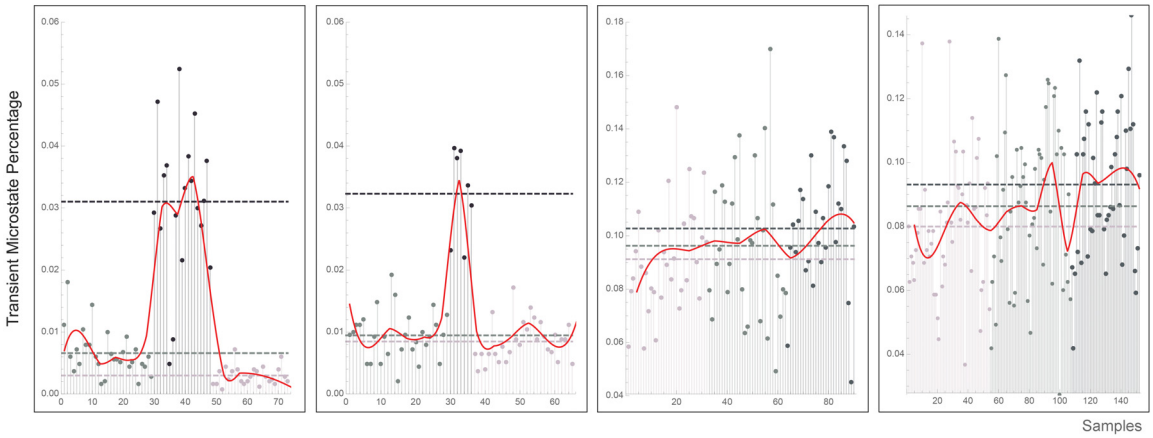

Figure 4.4: The plots show the time-varying transient microstate percentage of EEG signals of subjects asked to perform tasks of varying difficulty. In the leftmost and center-left figures, a subject was asked to close his eyes (gray) and the perform an activity (black) and then close his eyes (light gray). In the center-right and rightmost figure, a subject was asked to perform tasks of varying difficulty: he rated the tasks as easy with a score of 5 (lightgray), average with a score of 10 (gray) and hard with a score of 15 (black). The window size used was 1,000.

composed of segments with high transient microstate percentages and low percentages. This would be in line with the assumption that an average problem may be composed of hard subtasks and easy subtasks.

The transient microstate percentage of a subject with eyes closed typically ranges from near 0% to 1% while the transient microstate percentage of a subject who is asked to perform tasks ranges from 3% to 18%. Easy tasks range in the lower spectrum while harder tasks range in the higher spectrum.

It can also be noted that experiments show that the transient microstate percentage is not sensitive to the window size used.

4.2.2 Discussion

The performance of the P2ML algorithms is displayed in Tables 4.2 and 4.3 using basic indicative *Mathematica* implementations. All computations were performed with a convergence parameter of 0.0001. Larger matrices than those tested with take significantly more

time to execute.

As the datasets grow larger, the performance of the P2ML algorithm decreases significantly although large sequences are rarely needed when computing the transient microstate percentage. Since the transient microstate percentage only requires the number of segments rather than the microstate labels to which the segments are linked, a natural improvement would be to use gradient fields rather than the P2ML algorithm. The underlying idea would be to use polarity changes in the directional derivatives of the EEG epoch to mark the changes in segmentation.

The transient microstate percentage is highly correlated with the perceived hardness of a task or a subtask. According to our experiment, it may also be correlated with the level of fatigue exerted on the subject by a given task. Specifically, the transient microstate percentage dynamically measures the number of short-duration microstates of an EEG epoch. These short-lasting microstates were shown in the literature to have significant physiological meaning [KLM$^+$99, KPL$^+$02]. When the duration itself is known in advance, a simple optimization is to count microstates of duration less than some threshold. This threshold is itself usually not available beforehand and may need to be computed dynamically in accordance to the data to be analyzed. Such an approach is however well suited for real-time systems design by alleviating the need of computing the regularized P2ML segmentation.

The segmentation of the transient microstate percentage curve is not hard but statistical. A hard segment in the task has on average more hard-valued percentages while it may contain some segments that were categorized average or even easy. The segmentation of the transient microstate percentage curve is a trend. Such trends are shown in Figure 4.4.

In the experiments of Figure 4.4, the average transient microstate percentage seem to follow the rule that harder tasks have higher transient microstate percentages while easier tasks have lower transient microstate percentages. The tasks that were categorized by the subject as average display spikes in its transient microstate percentage curve which would lead to believe that the tasks should be measured as harder than the task that was

Table 4.2: Performance benchmarks of the P2ML Algorithm

Problem Size	Performance (s)
$1,000 \times 63$	4.024826
$5,000 \times 63$	36.005031
$10,000 \times 63$	73.726073
$50,000 \times 63$	90.152978

Table 4.3: Performance benchmarks of the regularized P2ML Algorithm

Problem Size	Performance (s)
$1,000$	0.483603
$5,000$	2.511616
$10,000$	5.148033
$50,000$	25.474963

categorized as hard. However, the averages classify properly the tasks. This could mean that the task classified as average is a mixture of segments perceived as easy and segments perceived as hard. A limitation of this method is that the signal-to-noise ratio of the transient microstate percentage curves is high in the case where we are trying to differentiate easy and medium or medium and hard tasks (Figure 4.4 center-right and right). We posit that this is mainly due to intra-segment variations in the measured evoked hardness.

For this analysis, we had a set of 7 experiments on different subjects. Out of the 7 subjects, 5 showed a clear linear correlation between the subjective ratings and the transient microstate percentages. In recent work [NZ15], it was found that subjective rating might not be very accurate.

Following our experiments on transient microstate percentage, it can be noted that the human brain seems to be using $1 - 20\%$ of its transient microstate capacity. The transient microstate percentage of an EEG signal cannot be larger than 100% and experimentally camps between $1 - 20\%$.

4.3 Segmentation of Design Protocols Using EEG

4.3.1 Physiologically Based Segmentation

While microstate segmentation effectively segments an EEG, the problem of segmenting design protocol data stems from another application domain. The heuristic we use to perform the segmentation of design protocol data is that the expected perceived hardness of two different subtasks is different. We therefore segment the protocol data into windows of a given time length and aim at measuring the hardness of these subtasks to distinguish them. Adjacent segments of similar measured hardness are then considered to be part of the same subtask. Obviously, this is a necessary condition to make a proper segmentation, which may result in a segment consisting of different types of activities. We propose a physiological approach to measuring this perceived hardness, based on which the hardness of a task is given by the transient microstate percentage. The transient microstate percentage is given by:

$$T.M.\% = \frac{(Segments - SmoothSegments)}{N} \tag{4.1}$$

The number of segments is given by the number of discontinuous segments obtained using the P2ML algorithm while the number of smooth segments is given by the number of segments obtained using the regularized P2ML algorithm. For example, the segmentation (1,1,1,2,2,3,4,1) has 5 discontinuous segments. In Figure 3.5(a), the P2ML segmentation has 37 discontinuous segments while the regularized P2ML segmentation in Figure 3.5(b) has 22 discontinuous segments. The transient microstate percentage effectively measures the number of short duration flashing microstates. These microstates were determined in the related literature to be significant physiologically and were characterized as being the atoms of thought. This number is always positive and can be shown experimentally to camp between 1% and 20% on average. A clear gap can be found between the transient microstate percentage of a subject who was asked to keep his eyes closed and a subject who was asked

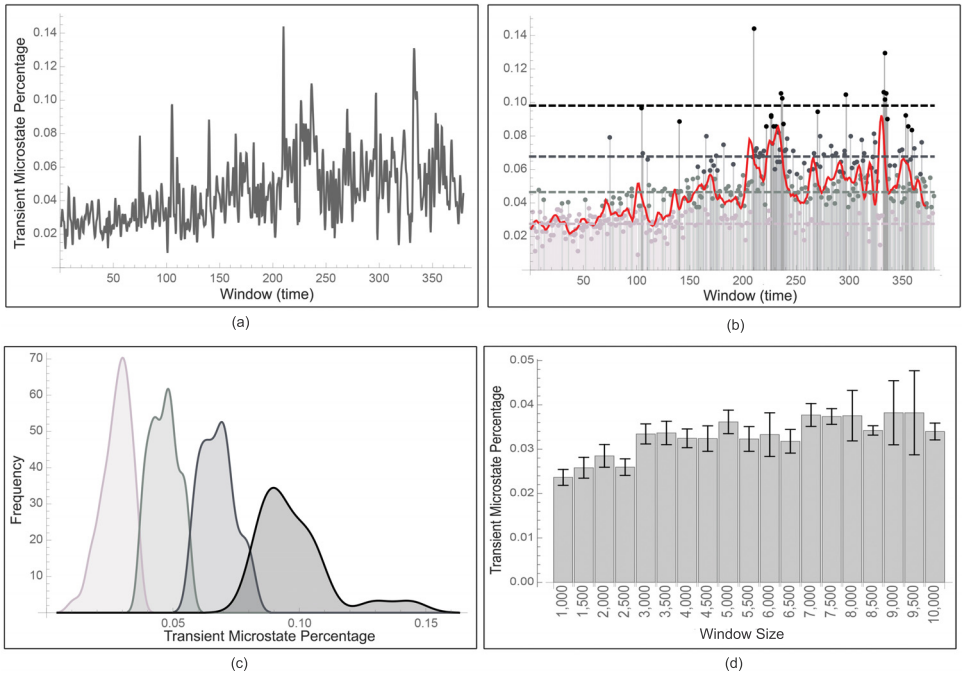

Figure 4.5: (a) shows the time-varying transient microstate percentage of EEG signals of a subject who was asked to perform a set of tasks over 30 minutes. In (b), the transient microstate percentage curve was classified into low segment (lighter gray) medium segments (light gray), high segments (gray) and very high segments (black). A trending curve was added. In (c), histograms were computed. Lower microstate percentages correlated with easier tasks while higher microstate percentages correlated with harder tasks. In (d), the transient microstate percentage was computed on a subject with eyes closed using different window sizes. The percentage shows stability with respect to window size.

to solve a design problem. We posit that tasks perceived to be easy are shown to have a lower transient microstate percentage than tasks perceived to be hard.

Once the transient microstate percentage curve is computed on an EEG signal (typically a signal of a given sample size such as 2,500 samples), these values are aggregated into groups of windows (e.g. 5 windows) and the data is clustered. Since the clustering algorithm is evaluating single values, no significant performance penalty is incurred. Different segments are then defined as clusters with different cluster neighbours.

4.3.2 Experiment and Analyses

The data that was used in this study contained video sequences of a subject who was asked to perform a set of design tasks on a touchpad while having his/her EEG monitored. After each task, the subject was asked to grade the level of difficulty of the task. The experiment lasted around 30 minutes. Details of experimental setting and experimental tasks can be found in [Ngu16, XNZ14]. In summary, the subjects were asked to alternate between 2 types of tasks: answering multiple choice questions on design problems that presented different alternatives to solve a given problem and designing a solution to a design problem by drawing a sketch. After each tasks, the subjects were asked to rate the hardness of the problem as they perceived it.

In a first set of analyses, we computed the transient microstate percentage of longer EEG epochs by using the P2ML and regularized P2ML algorithms for the subject. Figure 4.5(a) shows these percentages. The transient microstate percentage is a stronger figure than the number of transient microstates because it can be used when two sequences do not match in length and it can be shown to not be sensible to sequence length.

In a second set of analyses, the time-varying transient microstate percentages of the EEG sequence was used to segment the task execution video obtained on a touchpad into subtasks. The dataset used in Figure 4.5(a) is the same as the dataset used in Figure 4.5(b) and was obtained by measuring the EEG of a subject who was asked to perform various tasks for a duration of about 30 minutes. The epoch of 30 minutes was then divided into windows of 2,500 samples at a sample rate of 500 samples per second and the transient microstate percentage of each window of about 2.5 seconds was computed. The transient microstate percentage curve was segmented into four categories: resting/very easy, easy, average and hard. Figure 4.5(c) shows that the very easy category peeks at a transient microstate percentage value of 0.025, the easy category at 0.045, the medium category at 0.065 and the hard category at 0.10.

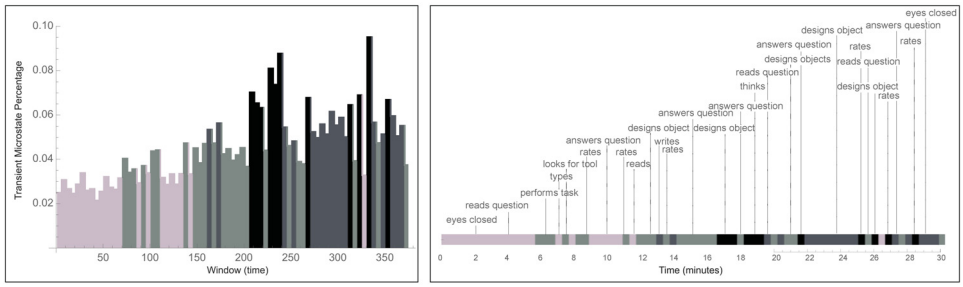

Figure 4.6: Coarse-grained segmentation of design protocol video based on the transient microstate percentage. A window size of 5 (25 seconds) was chosen. Values in the window were averaged. The resulting values were clustered into 4 clusters.

In a third set of analyses, we tested the stability of the transient microstate percentage with respect to the window size. We computed the transient microstate percentage of a subject with eyes closed over different window sizes. We expected that the transient microstate percentage remain within the same range. Figure 4.5(d) illustrates this analysis.

In a fourth and last set of analyses, we compared the segmentation of the design protocol data obtained using transient microstate percentages with the actual video of the protocol data. These experiments are illustrated in Figure 4.6.

4.3.3 Discussion

Our design protocol data was a set of videos taken from the touchpad on which subjects were asked to perform various design tasks of varying hardness. Screenshots of the experiment are shown in Figure 4.1. The EEG of the subjects was monitored and, after each task, a short questionnaire on the perceived hardness of the task was handed.

Such design protocols were a sequence of segments where the subjects were asked to keep their eyes closed and segments where the subjects were asked to perform tasks.

By characterizing a segment of a design protocol dataset by its perceived hardness, we have effectively introduced a metric to perform the segmentation of these protocols using monitored EEG signals. Harder tasks have harder levels of transient microstate and easier tasks have lower levels of transient microstate. The transient microstate percentage of a

subject with eyes closed typically ranges from near 0% to 4% while the transient microstate percentage of a subject who is asked to perform tasks ranges from 5% to 18%. Easy tasks range in the lower spectrum while harder tasks range in the higher spectrum.

When using the transient microstate percentage to segment design protocol videos, the accuracy was surprisingly high in detecting, within a given range, segments such as read question, rate question, design object and answer question. The think segment in the experiment was defined as a sequence in the video where the subject paused while designing an object or answering a question. More specifically, we noticed that the rate segments were classified as having high transient microstate percentage. Furthermore, design segments were classified on average as having larger transient microstate percentages. The design protocol data started and ended with an eyes closed segment. The first eyes closed segment was detected as having a low transient microstate percentage while the second segment had a mid- transient microstate percentage. This may be due to the fact that, following the 30 minutes experiment, the subject was not thoroughly resting. It was however properly segmented. Some expected segments were properly classified while others were not, which may be resulted from the fact that the proposed segmentation criterion (hardness) is only a necessary condition for a proper segmentation. Furthermore, unexpected segments were discovered, which may be because in conducting a design activity a designer may experience different levels of difficulty for the activity period. Like in most data mining approaches, false positives are to be expected.

4.4 Validation of EEG Based Segmentation of Design Protocols

4.4.1 Physiologically Based Segmentation Using Transient Microstates

The transient microstate percentage effectively measures the percentage of short duration microstates with respects to the total number of samples in the signal. This number is

always positive and smaller than 1. Transient microstates are deemed to be a significative metric in EEG signal processing and were characterized as being the atoms of thought [Leh90, KLM+99, KPL+02].

A first step in our method is then to compute the transient microstate percentages of small segments of the EEG signal. Once these percentages are computed, they are aggregated into small contiguous groups. The length of these groups gives a window size which can be adjusted based on the required sensitivity of the experiment. Figure 4.5(a) shows such a transient microstate percentage curve. The values in the groups are averaged and the resulting data is clustered. Different segments are then defined as clusters with different cluster neighbours. Figure 4.5(b) shows such a segmentation.

4.4.2 Experiments and Analysis

4.4.2.1 Experimental Protocol

To evaluate the correctness and precision of EEG based segmentation, we adopted the following strategy. First, 3 domain experts were asked to segment the 8 videos manually. Second, a set of 9 algorithms using 2 different window parameters (for a total of 18 algorithms) were used to segment the videos. In addition to the segmentation we proposed using transient microstates and we used Power Spectral Densities, which are commonly used in EEG analysis. A summary of those PSD algorithms is provided in Table 4.5. We then compared the distance between different manual segmentations by domain experts, between manual segmentation and EEG based segmentation and between different EEG based segmentations to evaluate which algorithm performed best in comparison to manual segmentation. Also, it was expected that manual segmentation would perform the best (since comparing manual segmentations with themselves is tautological) but it was unknown to what extent. Furthermore, the relationship between different algorithms was also an unknown.

When comparing manual segmentations to manual segmentations, we evaluate if manual

Table 4.4: Segmentation of the design protocol video into design moves. Underlined rows were detected by means of the automated physiological method. Non-underlined rows were expected design moves in the segmentation that were not detected by the method.

Segment	Time	Design Move Description
1	0:00	Eyes closed, resting state
2	4:20	Reads a question
3	4:41	Designs an object on the touchpad
4	6:05	Adds some object to the drawing on the touchpad
5	7:20	Writes on the touchpad
6	7:45	Consults the experiment instructions
7	8:10	Rates the hardness of the problem
8	8:35	Reads a question
9	9:25	Answers a question
10	9:55	Rates the hardness of the question
11	11:30	Reads a question
12	11:55	Thinks about a solution
13	12:20	Designs an object on the touchpad
14	13:35	Rates the hardness of the problem
15	14:00	Reads a question
16	14:25	Answers the question
16	14:50	Pauses to think
17	15:43	Rates the hardness of the problem
⋮	⋮	⋮

segmentation is self-consistent. When comparing automated segmentations with manual segmentations, we actually evaluate to what extent automated segmentation is aligned with manual segmentation. Finally, when comparing automated segmentations with automated segmentations, we evaluate if automated segmentation *sees* something that manual segmentation does not. If automated segmentation is self-consistent while yielding other results than manual segmentations, this may hint at an underlying structure that manual segmentations cannot *see*. EEG brain patterns would then be able to identify cognitive structures that simple observation cannot. Since the notion of *perfect* segmentation is ill-defined and may not truly exist, we attempt to relativize our analysis and determine if each method is consistent

Table 4.5: EEG Features

Features	Characteristics
alpha	relaxation, focus
beta	concentration, fatigue
(theta+alpha)/beta	fatigue
alpha/beta	attention, fatigue
(theta+alpha)/(alpha+beta)	fatigue
theta/beta	fatigue

and to what extent they are similar.

The distance metric we used to evaluate the distance between two segmentations was the following:

$$d(x, y) = \sum_i Abs(y_i - Nearest(x, y_i)) \tag{4.2}$$

This distance measure allows for segmentations of different lengths. However, it is a non-metric distance measure. To alleviate this, we only need to set x to be the longest or shortest segment and y to be the other remaining segmentation. Also, false and near positives are a necessary evil. If a segment has length 100 and the other 200, then it is clear that at least 100 points are false positives or near positives. This being said, false and near positives may be indicative that a segmentation contains more information than another.

The labels we used for each datasets in Figures 4.7-4.9 are listed in Table 4.6.

Power spectral densities were measured on the FP1 electrode of the EEG as commonly performed. The transient microstates were computed on all 64 electrodes of the EEG device. Table 4.5 shows the characteristics of the different PSD algorithms we chose.

Figure 4.7 shows the distance matrix of the 21 segmentations obtained (3 domain expert segmentations, 9 EEG based segmentations with window size parameter set to 1 and 9 EEG based segmentations with window size parameter set to 2. Each distance in the distance matrix was averaged from the segmentations obtained for each of the 8 datasets (FEB28,

Table 4.6: Segment Labels and Methods

Segment Label	Segmentation Method	Window Size
R1	Domain Expert 1	
R2	Domain Expert 2	
R3	Domain Expert 3	
TM1%	Transient Microstate	1
A1	Power Spectral Density Algorithm-FP1 (alpha)	1
B1	Power Spectral Density Algorithm-FP1 (beta)	1
C1	Power Spectral Density Algorithm-FP1 (delta)	1
D1	Power Spectral Density Algorithm-FP1 (theta)	1
E1	Power Spectral Density Algorithm-FP1 ((theta+alpha)/beta)	1
F1	Power Spectral Density Algorithm-FP1 (alpha/beta)	1
G1	Power Spectral Density Algorithm-FP1 ((theta + alpha)/(alpha + beta))	1
H1	Power Spectral Density Algorithm-FP1 (theta/beta)	1
TM2%	Transient Microstate	2
A2	Power Spectral Density Algorithm- FP1 (alpha)	2
B2	Power Spectral Density Algorithm-FP1 (beta)	2
C2	Power Spectral Density Algorithm-FP1 (theta)	2
D2	Power Spectral Density Algorithm-FP1 ((theta+alpha)/beta)	2
E2	Power Spectral Density Algorithm-FP1 (alpha/beta)	2
F2	Power Spectral Density Algorithm-FP1 (alpha/beta)	2
G2	Power Spectral Density Algorithm-FP1 ((theta + alpha)/(alpha + beta))	2
H2	Power Spectral Density Algorithm-FP1 (theta/beta)	2

	R1	R2	R3	TM1%	A1	B1	C1	D1	E1	F1	G1	H1	TM2%	A2	B2	C2	D2	E2	F2	G2	H2
R1	0.000	0.020	0.010	0.010	0.030	0.030	0.020	0.030	0.030	0.020	0.020	0.010	0.050	0.080	0.110	0.080	0.070	0.100	0.090	0.050	0.050
R2	0.020	0.000	0.020	0.020	0.040	0.080	0.030	0.060	0.060	0.030	0.050	0.020	0.110	0.140	0.150	0.100	0.090	0.100	0.090	0.080	0.130
R3	0.010	0.020	0.000	0.030	0.050	0.060	0.040	0.050	0.060	0.040	0.060	0.040	0.080	0.110	0.130	0.130	0.070	0.100	0.090	0.060	0.100
TM1%	0.010	0.020	0.030	0.000	0.020	0.020	0.020	0.020	0.020	0.020	0.020	0.020	0.010	0.010	0.010	0.010	0.010	0.010	0.010	0.020	0.010
A1	0.030	0.040	0.050	0.020	0.000	0.030	0.020	0.020	0.020	0.020	0.020	0.020	0.030	0.010	0.020	0.030	0.020	0.020	0.020	0.010	0.020
B1	0.030	0.080	0.060	0.020	0.030	0.000	0.020	0.030	0.020	0.020	0.030	0.020	0.040	0.020	0.010	0.030	0.030	0.030	0.030	0.020	0.040
C1	0.020	0.030	0.040	0.020	0.020	0.020	0.000	0.020	0.020	0.020	0.020	0.020	0.020	0.010	0.010	0.010	0.010	0.010	0.010	0.020	0.020
D1	0.030	0.060	0.050	0.020	0.020	0.030	0.020	0.000	0.030	0.020	0.020	0.010	0.030	0.020	0.030	0.040	0.010	0.020	0.040	0.020	0.030
E1	0.030	0.060	0.060	0.020	0.020	0.020	0.020	0.030	0.000	0.020	0.020	0.020	0.030	0.030	0.030	0.040	0.020	0.010	0.040	0.010	0.040
F1	0.020	0.030	0.040	0.020	0.020	0.020	0.020	0.020	0.020	0.000	0.020	0.020	0.020	0.010	0.020	0.020	0.020	0.010	0.010	0.010	0.020
G1	0.020	0.050	0.060	0.020	0.020	0.030	0.020	0.020	0.020	0.020	0.000	0.020	0.020	0.020	0.030	0.030	0.020	0.010	0.030	0.000	0.030
H1	0.010	0.020	0.040	0.020	0.020	0.020	0.020	0.010	0.020	0.020	0.020	0.000	0.020	0.010	0.010	0.010	0.010	0.010	0.010	0.010	0.010
TM2%	0.050	0.110	0.080	0.010	0.030	0.040	0.020	0.030	0.030	0.020	0.020	0.020	0.000	0.040	0.040	0.040	0.040	0.040	0.040	0.020	0.060
A2	0.080	0.140	0.110	0.010	0.010	0.020	0.010	0.020	0.030	0.010	0.020	0.010	0.040	0.000	0.060	0.040	0.040	0.060	0.040	0.030	0.040
B2	0.110	0.150	0.130	0.010	0.020	0.010	0.010	0.030	0.030	0.020	0.030	0.010	0.040	0.060	0.000	0.050	0.040	0.070	0.050	0.030	0.040
C2	0.080	0.100	0.130	0.010	0.030	0.030	0.010	0.040	0.040	0.020	0.030	0.010	0.040	0.040	0.050	0.000	0.040	0.050	0.050	0.020	0.060
D2	0.070	0.090	0.070	0.010	0.020	0.030	0.010	0.010	0.020	0.020	0.020	0.010	0.040	0.040	0.040	0.040	0.000	0.060	0.040	0.040	0.040
E2	0.100	0.100	0.100	0.010	0.020	0.030	0.010	0.020	0.010	0.010	0.010	0.010	0.040	0.060	0.070	0.050	0.060	0.000	0.050	0.030	0.050
F2	0.090	0.090	0.090	0.010	0.020	0.030	0.010	0.040	0.040	0.010	0.030	0.010	0.040	0.040	0.050	0.050	0.040	0.050	0.000	0.020	0.040
G2	0.050	0.080	0.060	0.020	0.010	0.020	0.020	0.020	0.010	0.010	0.000	0.010	0.020	0.030	0.030	0.020	0.040	0.030	0.020	0.000	0.040
H2	0.050	0.130	0.100	0.010	0.020	0.040	0.020	0.030	0.040	0.020	0.030	0.010	0.060	0.040	0.040	0.060	0.040	0.050	0.040	0.040	0.000

Figure 4.7: Figure 7: Distance matrix between various segmentation strategies averaged across the 8 datasets. Distances are measured in minutes (e.g. 0.01 is equivalent to 1 second). The first 3 rows show the distance between Domain Expert segmentation (R1, R2, R3) and algorithm segmentation (TM1%, A1, B1, . . . ,H2). Our nearest neighbor metric was used to compute deviations in seconds between different segmentations using different segmentation algorithms. See Table 4.6 for label descriptions.

	R1	R2	R3	TM1%	A1	B1	C1	D1	E1	F1	G1	H1	TM2%	A2	B2	C2	D2	E2	F2	G2	H2
R1	0.000	0.003	0.004	0.002	0.007	0.008	0.004	0.011	0.008	0.003	0.004	0.002	0.010	0.025	0.023	0.027	0.015	0.019	0.022	0.025	0.011
R2	0.003	0.000	0.002	0.002	0.011	0.029	0.005	0.016	0.018	0.004	0.016	0.002	0.019	0.042	0.029	0.014	0.020	0.019	0.010	0.030	0.041
R3	0.004	0.002	0.000	0.009	0.009	0.014	0.009	0.011	0.017	0.008	0.017	0.011	0.008	0.041	0.030	0.034	0.016	0.022	0.017	0.026	0.042
TM1%	0.002	0.002	0.009	0.000	0.003	0.001	0.002	0.002	0.002	0.002	0.004	0.004	0.001	0.002	0.001	0.001	0.001	0.001	0.001	0.005	0.001
A1	0.007	0.011	0.009	0.003	0.000	0.008	0.003	0.006	0.007	0.005	0.006	0.004	0.007	0.001	0.005	0.005	0.005	0.005	0.005	0.003	0.006
B1	0.008	0.029	0.014	0.001	0.008	0.000	0.002	0.006	0.004	0.002	0.005	0.004	0.008	0.007	0.001	0.007	0.007	0.005	0.006	0.004	0.010
C1	0.004	0.005	0.009	0.002	0.003	0.002	0.000	0.004	0.004	0.002	0.003	0.003	0.004	0.001	0.001	0.001	0.002	0.002	0.003	0.004	0.003
D1	0.011	0.016	0.011	0.002	0.006	0.006	0.004	0.000	0.008	0.004	0.005	0.002	0.007	0.008	0.013	0.017	0.001	0.004	0.015	0.003	0.011
E1	0.008	0.018	0.017	0.002	0.007	0.004	0.004	0.008	0.000	0.004	0.006	0.004	0.008	0.013	0.013	0.016	0.005	0.001	0.019	0.002	0.016
F1	0.003	0.004	0.008	0.002	0.005	0.002	0.002	0.004	0.004	0.000	0.002	0.003	0.004	0.003	0.005	0.004	0.003	0.002	0.001	0.002	0.002
G1	0.004	0.016	0.017	0.004	0.006	0.005	0.003	0.005	0.006	0.002	0.000	0.003	0.007	0.010	0.012	0.016	0.005	0.002	0.018	0.001	0.015
H1	0.002	0.002	0.011	0.004	0.004	0.004	0.003	0.002	0.004	0.003	0.003	0.000	0.004	0.002	0.005	0.004	0.002	0.002	0.002	0.002	0.001
TM2%	0.010	0.019	0.008	0.001	0.007	0.008	0.004	0.007	0.008	0.004	0.007	0.004	0.000	0.010	0.005	0.007	0.008	0.007	0.007	0.005	0.014
A2	0.025	0.042	0.041	0.002	0.001	0.007	0.001	0.008	0.013	0.003	0.010	0.002	0.010	0.000	0.019	0.009	0.011	0.011	0.007	0.011	0.008
B2	0.023	0.029	0.030	0.001	0.005	0.001	0.001	0.013	0.013	0.005	0.012	0.005	0.005	0.019	0.000	0.012	0.011	0.014	0.006	0.014	0.007
C2	0.027	0.014	0.017	0.001	0.005	0.007	0.001	0.017	0.016	0.004	0.016	0.004	0.007	0.009	0.012	0.000	0.007	0.008	0.008	0.004	0.019
D2	0.011	0.020	0.016	0.001	0.005	0.007	0.002	0.001	0.005	0.003	0.005	0.002	0.008	0.011	0.011	0.007	0.000	0.016	0.007	0.015	0.013
E2	0.017	0.019	0.022	0.001	0.005	0.005	0.002	0.004	0.001	0.002	0.002	0.002	0.007	0.011	0.014	0.008	0.016	0.000	0.007	0.011	0.013
F2	0.022	0.010	0.017	0.001	0.005	0.006	0.003	0.015	0.019	0.001	0.018	0.002	0.007	0.007	0.006	0.008	0.007	0.007	0.000	0.007	0.005
G2	0.025	0.030	0.026	0.005	0.003	0.004	0.004	0.003	0.002	0.002	0.001	0.002	0.005	0.011	0.014	0.004	0.015	0.011	0.007	0.000	0.017
H2	0.011	0.016	0.042	0.001	0.006	0.010	0.003	0.011	0.016	0.002	0.015	0.001	0.014	0.017	0.007	0.019	0.013	0.013	0.005	0.017	0.000

Figure 4.8: Standard error matrix associated to the distance matrix. See Table 4.6 for label descriptions.

FEB18, AUG5, APR18, APR16, APR8, APR23, APR21). Figure 4.8 shows the standard errors associated with the distance matrix resulting from the averaging process. Figure 4.9 shows the unaveraged results for the first 3 rows of the distance matrix corresponding to the distance between domain expert segmentation and EEG based segmentation.

Statistical significance was done against the hypothesis that the mean of the average difference was equal to 1 second. For domain expert (R2), the only domain expert segmentation to deviate from the 1 second mean, p-value was found to be 0.3467 which leads to acceptance of the null hypothesis. This means that differences between average differences for domain expert is not statistically significant. For the best scoring algorithm (A1), the

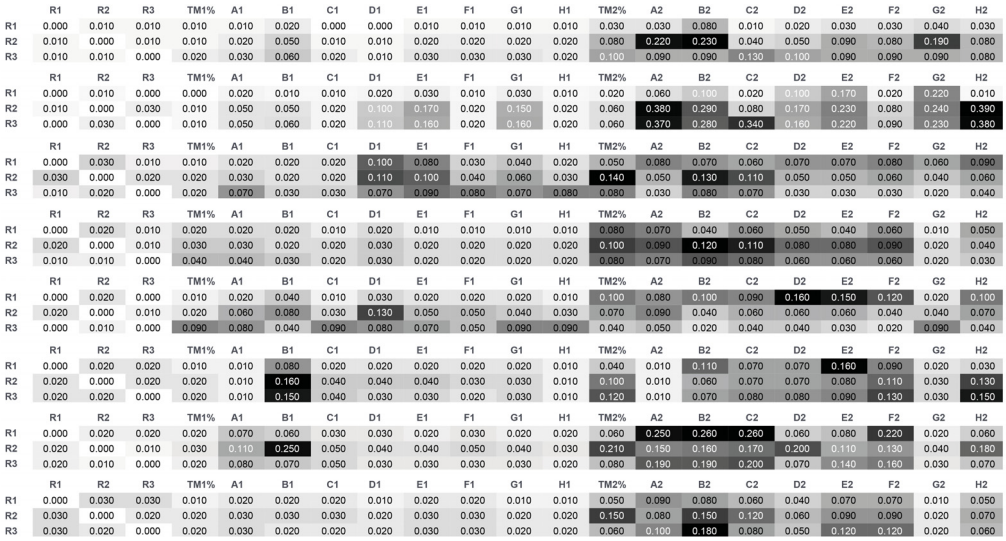

	R1	R2	R3	TM1%	A1	B1	C1	D1	E1	F1	G1	H1	TM2%	A2	B2	C2	D2	E2	F2	G2	H2
R1	0.000	0.010	0.010	0.010	0.010	0.020	0.000	0.000	0.010	0.010	0.010	0.010	0.030	0.030	0.080	0.010	0.020	0.030	0.030	0.040	0.030
R2	0.010	0.000	0.010	0.010	0.020	0.050	0.010	0.010	0.020	0.020	0.020	0.020	0.080	0.220	0.230	0.040	0.050	0.090	0.080	0.190	0.080
R3	0.010	0.010	0.000	0.020	0.030	0.060	0.020	0.010	0.030	0.030	0.030	0.020	0.100	0.090	0.090	0.130	0.100	0.090	0.090	0.090	0.080

	R1	R2	R3	TM1%	A1	B1	C1	D1	E1	F1	G1	H1	TM2%	A2	B2	C2	D2	E2	F2	G2	H2
R1	0.000	0.010	0.000	0.000	0.020	0.010	0.010	0.020	0.030	0.010	0.030	0.010	0.020	0.060	0.100	0.020	0.100	0.170	0.020	0.220	0.010
R2	0.010	0.000	0.030	0.010	0.050	0.050	0.020	0.100	0.170	0.020	0.150	0.020	0.060	0.380	0.290	0.080	0.170	0.230	0.080	0.240	0.390
R3	0.000	0.030	0.000	0.010	0.050	0.060	0.020	0.110	0.160	0.020	0.160	0.020	0.060	0.370	0.280	0.340	0.160	0.220	0.090	0.230	0.380

	R1	R2	R3	TM1%	A1	B1	C1	D1	E1	F1	G1	H1	TM2%	A2	B2	C2	D2	E2	F2	G2	H2
R1	0.000	0.030	0.010	0.010	0.020	0.020	0.020	0.100	0.080	0.030	0.040	0.020	0.050	0.080	0.070	0.060	0.070	0.070	0.080	0.060	0.090
R2	0.030	0.000	0.020	0.020	0.030	0.020	0.020	0.110	0.100	0.040	0.060	0.030	0.140	0.050	0.130	0.110	0.050	0.050	0.060	0.040	0.060
R3	0.010	0.020	0.000	0.020	0.070	0.030	0.030	0.070	0.090	0.080	0.070	0.080	0.080	0.030	0.080	0.070	0.030	0.030	0.030	0.020	0.040

	R1	R2	R3	TM1%	A1	B1	C1	D1	E1	F1	G1	H1	TM2%	A2	B2	C2	D2	E2	F2	G2	H2
R1	0.000	0.020	0.010	0.020	0.020	0.020	0.010	0.020	0.010	0.010	0.010	0.010	0.080	0.070	0.040	0.060	0.050	0.040	0.060	0.010	0.050
R2	0.020	0.000	0.010	0.030	0.030	0.020	0.020	0.030	0.020	0.020	0.020	0.020	0.100	0.090	0.120	0.110	0.080	0.080	0.090	0.020	0.040
R3	0.010	0.010	0.000	0.040	0.040	0.030	0.020	0.030	0.020	0.020	0.020	0.020	0.080	0.070	0.090	0.080	0.060	0.060	0.060	0.020	0.030

	R1	R2	R3	TM1%	A1	B1	C1	D1	E1	F1	G1	H1	TM2%	A2	B2	C2	D2	E2	F2	G2	H2
R1	0.000	0.020	0.000	0.010	0.020	0.040	0.010	0.030	0.020	0.020	0.020	0.010	0.100	0.080	0.100	0.090	0.160	0.150	0.120	0.020	0.100
R2	0.020	0.000	0.010	0.020	0.060	0.080	0.030	0.130	0.050	0.050	0.040	0.030	0.070	0.090	0.040	0.060	0.060	0.060	0.040	0.040	0.070
R3	0.000	0.010	0.000	0.090	0.080	0.040	0.090	0.080	0.070	0.050	0.090	0.090	0.040	0.050	0.020	0.040	0.040	0.030	0.020	0.090	0.040

	R1	R2	R3	TM1%	A1	B1	C1	D1	E1	F1	G1	H1	TM2%	A2	B2	C2	D2	E2	F2	G2	H2
R1	0.000	0.020	0.020	0.010	0.010	0.080	0.020	0.020	0.020	0.020	0.020	0.010	0.040	0.010	0.110	0.070	0.070	0.160	0.090	0.020	0.030
R2	0.020	0.000	0.020	0.020	0.010	0.160	0.040	0.040	0.040	0.030	0.030	0.010	0.100	0.010	0.060	0.070	0.070	0.080	0.110	0.030	0.130
R3	0.020	0.020	0.000	0.020	0.010	0.150	0.040	0.030	0.030	0.020	0.030	0.010	0.120	0.010	0.070	0.080	0.080	0.090	0.130	0.030	0.150

	R1	R2	R3	TM1%	A1	B1	C1	D1	E1	F1	G1	H1	TM2%	A2	B2	C2	D2	E2	F2	G2	H2
R1	0.000	0.020	0.020	0.020	0.070	0.060	0.030	0.030	0.020	0.030	0.020	0.020	0.060	0.250	0.260	0.260	0.060	0.080	0.220	0.020	0.060
R2	0.020	0.000	0.010	0.030	0.110	0.250	0.050	0.040	0.040	0.050	0.040	0.030	0.210	0.150	0.160	0.170	0.200	0.110	0.130	0.040	0.180
R3	0.020	0.010	0.000	0.020	0.080	0.070	0.050	0.030	0.030	0.030	0.030	0.020	0.080	0.190	0.190	0.200	0.070	0.140	0.160	0.030	0.070

	R1	R2	R3	TM1%	A1	B1	C1	D1	E1	F1	G1	H1	TM2%	A2	B2	C2	D2	E2	F2	G2	H2
R1	0.000	0.030	0.030	0.010	0.020	0.020	0.020	0.010	0.020	0.020	0.010	0.010	0.050	0.090	0.080	0.060	0.040	0.070	0.070	0.010	0.050
R2	0.030	0.000	0.020	0.020	0.030	0.030	0.030	0.020	0.030	0.030	0.020	0.020	0.150	0.080	0.150	0.120	0.060	0.090	0.090	0.020	0.070
R3	0.030	0.020	0.000	0.020	0.030	0.020	0.020	0.020	0.030	0.030	0.020	0.020	0.060	0.100	0.180	0.080	0.050	0.120	0.120	0.020	0.060

Figure 4.9: Distance matrix of each of the 8 datasets (from top to bottom: FEB28, FEB18, AUG5, APR18, APR16, APR8, APR23, APR21) with respects to the distance between the domain expert segmentation (R1,R2,R3).

average distance found of 2 seconds had p-value 0.002129 which leads to rejection of the null hypothesis. Differences between domain expert segmentation and algorithm segmentation were then found to be statistically significant.

4.4.2.2 Domain Expert Vs Domain Expert

As expected, the distance is the lowest for domain expert to domain expert comparisons (the first three columns): the average distance of the first domain expert segmentation to the two others was 1 second, the average distance of the second domain expert segmentation to the two others was 1.3 second and the average distance of the third domain expert segmentation was 1 second. In this experimental context, it was expected that domain expert segmentation perform the best. While subjectivity of segmentation (deciding if a given segment-event in the videos is worth notice) was a factor, the metric we used alleviated false and near positives. Therefore, a $1 - 1.3$ second deviation between different domain expert segmentations is expected and realistic. All domain experts were presented the same videos and their reactions to the videos was therefore expected to be similar.

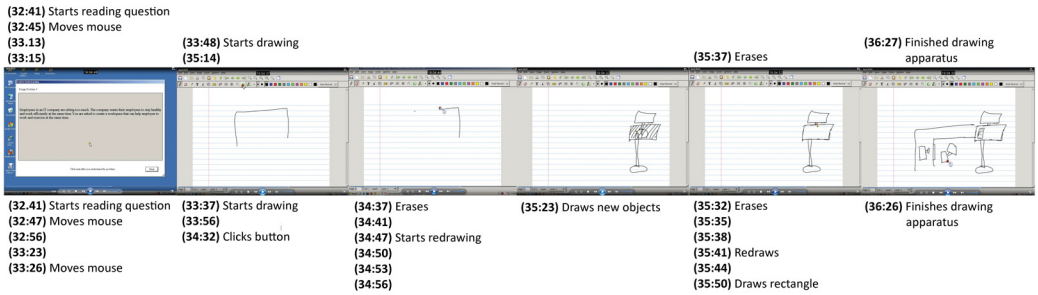

Figure 4.10: Sequence of screenshots from experimental protocol comparing manual segmentation and automated segmentations: (top) lists segments found by a domain expert; (bottom) shows segments found by the transient microstate algorithm with window size 1. Major segments (screenshot 1, 2, 5 and 6) are roughly aligned when comparing domain expert segmentation and automated segmentation. Automated segmentation is however much more fine-grained than manual segmentation. Unlabelled segments show segments that are observed to be a continuation of the previous segment label and for which not obvious observation can be made.

Domain expert to domain expert comparisons serves mostly the purpose of being a benchmark value: a $1 - 1.3$ second average deviation in segments is therefore expected to be a normal and natural deviation.

4.4.2.3 Algorithm Vs Domain Expert

The best EEG based segmentation had a 2 seconds deviation and was obtained by the transient microstate algorithm with window parameter set to 1. The worse result was a 12 seconds deviation and was obtained by the beta Power Spectral Density algorithm with window parameter set to 2. In the case of the best result, we determined that a 1 second difference between the average distance of domain expert and EEG based segmentations entailed that both segmentation methods were good. Microstate based segmentation (the best performing algorithm) is a holistic measure on all 64 electrodes of an EEG. Any movement in the EEG is recorded and accounted for in the microstate algorithm. The power spectral density algorithms did not perform as well averaging a difference ranging from 2.3 seconds in the best case (*theta/beta* formula) to 8.3 seconds (theta formula) for an average of 5.3 seconds on algorithms using a windows size of 1 and ranging from 7.7 (alpha/beta

formula) seconds to 12 seconds (beta formula) for an average of 9.7 seconds on algorithms using a window size of 2. It can be noticed that larger window sizes may have caused larger differences but also incur less false and near positives.

The higher differences recorded on power spectral density algorithms can be explained. As Table 4.5 shows, the PSD formulas used measure relaxation, focus, concentration, attention and fatigue. These characteristics are not easily visible in a video recording of a subject solving design tasks. Indeed, do concentration or fatigue translate themselves automatically into a pause in the video recording? Therefore, although average differences were higher with PSD based algorithms, this does not mean that PSD based algorithms provide erroneous segmentations. They rather provide complementary information on the design videos, more specifically, information that is not easily seen in the recordings.

Brain activities do not always align with their outward behaviour. Therefore, benchmarking EEG segmentation with domain expert manual segmentation may not be always significant.

Figure 4.10 compares manual segmentation by a domain expert and automated segmentation using the transient microstate algorithm by aligning screenshots from the experimental protocol with found segments.

4.4.2.4 Algorithm Vs Algorithm

By inspecting Figure 4.7, we notice that the average distance between domain expert segmentation and algorithms is higher than distances between different algorithms, which seems to point to a certain consistency between algorithms. Therefore, the 3 first rows and columns are labeled using a darker color as we move outwards while the submatrix composed of the other columns remains relatively within low values. By inspecting Figure 4.9, we also notice that on some datasets, some algorithms performed better that the best average algorithm (transient microstates), even yielding 0-distance values. Also, on average, EEG based segmentations using a window size of 1 performed better than those using a

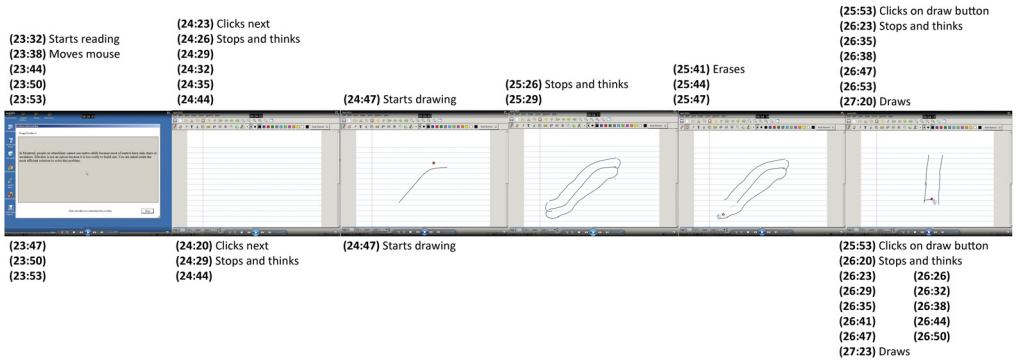

Figure 4.11: Sequence of screenshots from experimental protocol comparing two automated segmentations: (top) lists segments found by the transient microstate algorithm with window size 1; (bottom) shows segments found by the beta algorithm with window size 1. The beta algorithm misses a few segments and shows a slight deviation from the transient microstate algorithm. However, in screenshot 6, the beta algorithm showed a high level of granularity for the "Stops and thinks" segment. This can be explained by the fact that the beta range measures concentration.

window size of 2. This is partly due to the fact that lower window size values generate larger segmentations and therefore cause more false positives or near positives. However, as expected, domain expert segmentations are more similar to each others and the transient microstate algorithm with windows size 1 performs the best as it incorporates data from all the 64 electrodes of the EEG apparatus.

Different EEG based segmentations seem to correlate with each other. This may hint at the fact that while hardness of a design task increases, stress, fatigue or concentration may increase or decrease as well in a correlated manner. More specifically, the transient microstate algorithm (row 4 of Figure 4.7) seemed to remain in the range of $1-3$ seconds difference over all datasets while most other PSD based algorithms seemed to remain in the range of $1-6$ seconds when compared to each other with occasional spike in the $7-9$ seconds range.

While comparing domain expert segmentation to algorithm based segmentation provides insight into who well an algorithm aligns with the intuition of what a segmentation should be, comparing algorithms to each other provides additional information based on the characteristics that each algorithm measures.

Figure 4.11 compares two automated segmentation algorithms by aligning screenshots from the experimental protocol with found segments.

4.5 Fatigue as a Multidimensional Concept in EEG Analysis

Affective and cognitive engineering have recently gained momentum [BS15]. The goal of affective engineering is to *capture human emotion reactivity in engineering systems*. Clear applications to systems relying on user experience or design sciences and engineering can be found. In design sciences, it is often important to be able to get a glimpse at human behaviour and cognition from raw data such as design protocols or design artifacts [USD87, EG87, GM98, MGW98, KG08]. As for engineering systems, recent advances show that they are evolving towards more human-centric approaches.

One of the main challenges in affective or cognitive physiological engineering is to determine what a given physiological measurement means. What does a subject's eye blinking pattern mean, what does a higher skin conductivity or heart rate mean or what does it mean to have strong alpha channel measurement in an EEG signal. Researchers could imprint their own subjective interpretation to the physiological measurements but these could be erroneous or subjective. Furthermore, although all these measures have known documented clinical and medical interpretations, albeit leading to confusion [Hoc13], in the context of design sciences and engineering, interpretations may be lacking.

We propose to study the problem using a multistate approach by measuring different physiological signals and then analyze how they behave as an ensemble. Strong alpha channels in an EEG may mean that a subject is in a reflexive and meditative state according to the medical literature but it can also correlate with fatigue or effort and this correlation adds to the meaning and value of the measurement's interpretation. A multistate approach is then meant to analyze different physiological signals (in this thesis, EEG features) as an ensemble, a system of intercorrelated and interrelated metrics.

For example, many rules of thumb exist in design sciences regarding the relationship between effort and fatigue, effort and concentration or concentration and fatigue for example. However, these are rarely quantified clearly, assuming quantification is even possible. Intuitively, we can say that these pairs of states are either positively or negatively correlated. By using physiological measurements such as EEG signals, we can contribute to the analysis of these states of mind in the context of design sciences and quantify their relationship exactly. In this thesis, to do so, we use 9 time-domain and frequency domain features computed over EEG signals: a time domain feature, the transient microstate percentage, which was determined in the literature to measure hardness and mental effort [NNZ15a] and a set of 8 frequency domain features which measure diversely attention, fatigue and concentration [JLFB09]. The goal is to determine quantitatively the relationship between these features and their characteristics using a multistate approach.

It can also be noted that [Hoc13] describes fatigue as a poorly understood phenomenon in psychology and that different types of fatigue are routinely confused.

Monitoring physiological signals lends itself well to integration in engineering systems and subsystems. It adds a human, affective and cognitive perspective to engineering systems. These systems can alternatively be control systems in vehicles, video game user experience, feedback systems in health-oriented devices and other such control systems. Understanding how physiological signals behave as an ensemble is aimed at improving our understanding of design cognition, but also improving the usage of those signals in engineering systems and subsystems.

4.5.1 Multistate Analysis of EEG Signal

A multistate analysis of a set of physiological signals is composed of a set of features (states) extracted from the physiological signals. However, rather than analyzing these features separately as is often done in the research literature, multistate analysis focuses on analyzing these features as an ensemble (cf. Figure 4.12). Each feature is recorded in parallel on a

subject performing a given task and the features are put in relation to each other. The interrelations between the features are what define the system. Metrics are therefore relative rather than being absolute.

The goals of multistate analysis of physiological signals is to provide the following:

1. View physiological signals as an ensemble of interrelated signals rather than isolated metrics.

2. Provide aggregated statistics on these ensemble of physiological signals.

3. Identify loopholes and errors in the labeling of the characteristics of these physiological signals by analyzing their behaviour as an ensemble.

4. Provide a human-centric perspective to a given engineering problem.

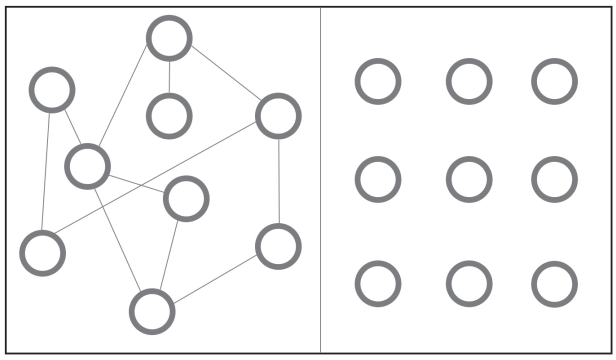

Figure 4.12: Features are analyzed as an ensemble of interrelated concepts (left) rather than isolated facts (right).

In this thesis, we use a correlation grid to measure relationships between different features across different subjects (cf. Figure 4.13). Signals that do not correlate are deemed to be independent signals and add an analytical dimension to the ensemble.

Two rules of thumb arise from multistate analysis:

1. Features that do not correlate add a dimension of interpretation to the system and features that correlate remove a dimension.

2. Features that refer to the same characteristic concept (label) should correlate.

Multistate analysis of EEG signals effectively differentiates spurious dimensions from

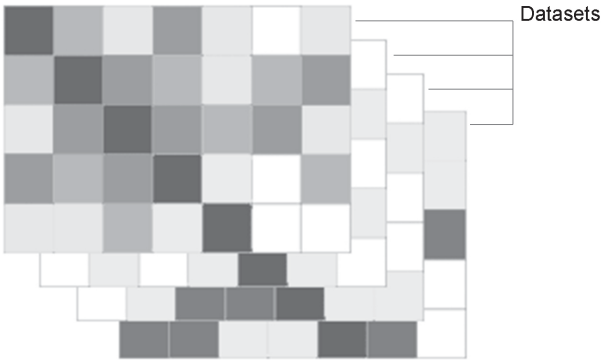

Figure 4.13: Multistate analysis provides a grid of interrelations between features of a set of physiological signals and are aggregate across different experiment datasets. The strength of the relationship is aggregated in a distance matrix.

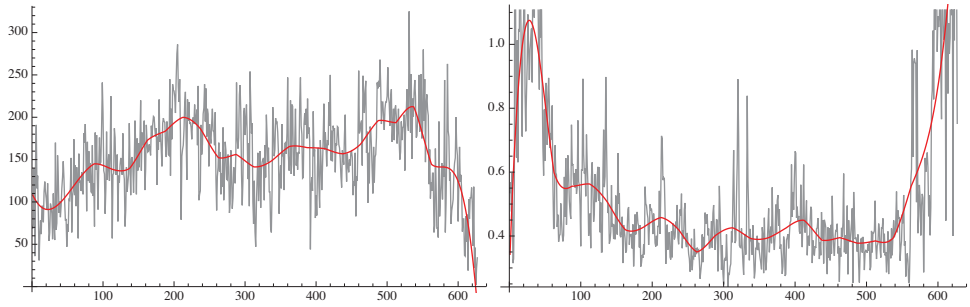

(a) Number of Transient Microstates (b) (theta+alpha)/beta (y-axis)

Figure 4.14: Figure (a) shows the number of transient microstates (y-axis) vs the segment label (x-axis). Figure (b) shows feature (theta+alpha)/beta (y-axis) vs the segment label (x-axis). A trended curve is given in red and shows a negative correlation between both Figure (a) and (b) curves.

non-spurious dimensions by correlating features and also validates characteristic labels associated to EEG features. It identifies features that move together in a given physiological system.

4.5.2 Experimental Results and Analysis

We have aggregated the results from 8 experiments lasting around 30 minutes to 1.5 hours during which subjects were asked to solve different design problems while being recorded on a touchpad and having their EEG monitored. EEG bandwidth was set at 500 samples per second.

	A	B	C	D	E	F	G	H	I
A	1.000	−0.816	−0.184	−0.604	−0.259	−0.847	−0.589	−0.586	−0.271
B	−0.816	1.000	0.290	0.676	0.300	0.962	0.718	0.642	0.429
C	−0.184	0.290	1.000	0.585	0.394	0.193	−0.094	−0.045	−0.327
D	−0.604	0.676	0.585	1.000	0.621	0.664	0.348	0.458	0.036
E	−0.259	0.300	0.394	0.621	1.000	0.311	−0.027	0.618	−0.347
F	−0.847	0.962	0.193	0.664	0.311	1.000	0.722	0.719	0.390
G	−0.589	0.718	−0.094	0.348	−0.027	0.722	1.000	0.393	0.707
H	−0.586	0.642	−0.045	0.458	0.618	0.719	0.393	1.000	0.037
I	−0.271	0.429	−0.327	0.036	−0.347	0.390	0.707	0.037	1.000

Figure 4.15: Correlations matrix between different EEG features: (A) transient microstate percentage, (B) alpha range - TYPE-1 Fatigue, (C) beta range, (D) theta range, (E) delta range, (F) (theta+alpha)/beta - TYPE-2 Fatigue, (G) alpha/beta - TYPE-3 Fatigue, (H) (theta+alpha)/(alpha+beta) - TYPE-4 Fatigue and (I) theta/beta - TYPE-5 Fatigue.

EEG related signals are often too noisy to be used as raw signals for analysis since the signal bandwidth is high. To alleviate this, we trend the signals using a window size. In our experiments, we have found that a window size of 25 works well as it is long enough to capture enough information while short enough to capture an adequate level of details. Figure 4.14 shows such trended curves.

We noticed that on most subjects, fatigue metrics were high at the beginning of the design sessions and at the end of the design sessions (cf. Figure 4.14). While it can be intuitive that fatigue be high at the end of a session, the high levels of fatigue at the beginning of the sessions can be explained by an “ice-breaking” phenomenon. Subjects were asked to be at rest with eyes closed before starting the design session and transition from rest to work most likely caused a spike in fatigue metrics before entering a ‘cruising-speed” mode. This hints at the fact that fatigue may be relative to the current state (physical and psychological) of a subject. In parallel, the transient microstate percentages (measuring effort) showed on most subjects an inverse bell curve shape (cf. Figure 4.14). It may be intuitive that at the beginning of the experiments, subjects showed less effort because, on one hand, the design problem (Design Problem 1) was trivial to solve and, on the other hand, subjects had just been in an eyes-closed rest state. However, the drop in the transient microstate percentage at the end of the design episode can only be explained by seeing the increase in fatigue

metrics. As fatigue increases, the available effort that a subject can provide decreases. We also noticed that local spikes in the fatigue feature curves and drops in the effort feature curve occurred when the subjects were solving non-trivial problems that required more of their attention.

Figure 4.15 displays a correlation matrix between different EEG features. In general, we can say that the transient microstate percentage showed negative correlation with the frequency-domain features that we have used. For these, the correlation coefficient ranged from -0.184 to -0.847. This would lead us to believe that effort (the characteristic label of the transient microstate percentage [NZ14b, NNZ15a]) is negatively correlated with fatigue, concentration and attention at various levels. This follows a rule of thumb intuition that a subject that is more fatigued can produce less mental effort. However, some correlation coefficients in this analysis were quite low. This also follows the popular belief that athletes are able to withstand larger efforts because they are not fatigued as quickly as non-athletes.

Perhaps, what is more intriguing is the correlation between different frequency-domain features which in the case of the beta range and the 4 composite features we used ((theta+alpha)/beta, alpha/beta, (theta+alpha)/(alpha+beta) and theta/beta) all measure to some extent fatigue. Since the correlation between these fatigue metrics is sometimes low, we can safely assume that what is measured is not the same type of fatigue. A multistate analysis enables us to discover that the fatigue metrics do not always correlate with each other and therefore must measure different types of fatigue. We label TYPE-1 Fatigue the beta feature, TYPE-2 Fatigue the composite (theta+alpha)/beta feature, TYPE-3 fatigue the composite alpha/beta feature, TYPE-4 Fatigue the composite (theta+alpha)/(alpha+beta) feature and TYPE-5 Fatigue the composite theta/beta feature. TYPE-1 Fatigue is reported in the related literature to measure a combination of concentration and fatigue while TYPE-3 Fatigue is reported to measure a combination of attention and fatigue. For example, since TYPE-1 Fatigue and TYPE-3 Fatigue only show a correlation coefficient of -0.094, they are assumed to be measuring a different underlying characteristic. Each type of fatigue is

then assumed to measure different characteristics.

The idea that fatigue is multidimensional is not new. [Hoc13] describes canonical types of fatigue in his monography on fatigue (e.g. mental, physical, sleepiness) stating that types of fatigue are routinely confused.

TYPE-1 Fatigue has a concentration flavour to it. Since TYPE-2 Fatigue is a composite of theta and alpha bands normalized on a beta band, we can assume that it incorporates relaxation, focus, concentration, drowsiness and inhibition. TYPE-3 Fatigue is an alpha band normalized with a beta band and measures the relaxation-concentration ratio in fatigue. TYPE-4 Fatigue measures the ratio between the theta band and the beta band augmented with the alpha band and therefore measures the concentration-drowsiness ratio in addition to relaxation and focus. TYPE-5 Fatigue measures the concentration-drowsiness ratio without correction factors. Following [Hoc13], TYPE-1 and TYPE-3 Fatigue would be more cognitive; TYPE-2, TYPE-4 and TYPE-5 would be a mix of cognitive fatigue and sleepiness.

Strong positive correlation (> 0.8) was found between the TYPE-2 fatigue and the alpha range (0.962) hinting at a relationship between relaxation and TYPE-2 Fatigue. Strong negative correlation (< -0.8) was found between the transient microstate percentage and the alpha range (-0.816) and TYPE-2 Fatigue (-0.847). This leads to an inverse relationship between effort and the relaxation-TYPE-2 Fatigue pair.

Medium range positive correlation (> 0.6) was also found between the alpha range and the theta range (0.676) and TYPE-3 (0.718) and 4 Fatigue (0.642). This hints at the loose relationships between relaxation and drowsiness and relaxation and fatigue. Medium range positive correlation (> 0.6) was also found between the theta range, the delta range (0.621) and TYPE-2 Fatigue (0.664). A loose relationship between drowsiness and TYPE-2 fatigue can then be seen. Medium range negative correlation (< -0.6) was found between effort and the theta range (-0.604). This leads to a loose inverse relationship between effort and drowsiness as effort would typically be negatively correlated with the latter. Fatigue metrics tend to correlate positively to each other albeit at different levels as they refer to the same

concept. Low correlation would however lead us to posit a multidimensional definition of fatigue.

Transient microstate percentage were shown to correlate significantly with some fatigue metrics but not with others. This strenghtens the idea that the fatigue characteristic in EEG features is no unidimensional but rather a multidimensional concept. Since features do not correlate with each other, each of them brings a new dimension to the problem domain. We could easily extend our intuition to the concept of mental effort. The transient microstate percentage, which measures effort, acts like a baseline where the other features can be compared and various measures of fatigue can differentiate themselves.

Multistate analysis of EEG signals allows us to differentiate different types of fatigue. In a single state analysis, we would have easily concluded that fatigue is negatively correlated with effort and hardness. A multistate analysis shows that different fatigue metrics behave differently as an ensemble and can therefore not measure the same characteristic. Each feature that does not correlate brings an analytical dimension to the problem domain.

It can be noted that the correlation matrix used in our approach uses trended signals (where noise is interpolated out). The relationship between this correlation matrix and its principal components is as follows:

$$\mathbf{w} = \frac{\lambda_{\mathbf{C}}}{\|\lambda_{\mathbf{C}}\|_1} \tag{4.3}$$

where λ are the eigenvalues of correlation matrix $\mathbf{C}$ and $\mathbf{w}$ is a vector yielding the contribution of each principal components to the overall variance in percentage.

4.6 Effort, Fatigue and Concentration In the Conceptual Design Process

Physiological studies of design provide scientific tools to validate and further our understanding of design theories and design methodologies. A fundamental tool in physiological studies are EEG measurements of the brain. Table 2.2 lists major work done in the hybrid

field of design sciences and neurosciences (EEG). Most of the work done in the field has mostly emerged in the 2010s to study design sciences (theory and methodology), design of information systems and psychological/cognitive aspects of design while some early work can be found in [Go7] (on the impact of experience on design problem solving). EEGs are more flexible than competing technologies such as fMRI and MRI as they can be readily integrated in an experimental protocol where subjects are asked to perform various design tasks while having their signals monitored. Since design is fundamentally a mental task, we argue that such EEG tools can provide insight in the conceptual design process. Another tool that is popular in the field of design sciences are design protocols. Design protocols have been studies in [CCD96, USD87, EG87, GM98, MGW98, KG08, JY09]. design protocol analysis methods have evolved into a compendium of techniques which have been succesfully used to study the conceptual design process.

We propose the study of design using a hybrid combination of protocol analysis and EEG signal monitoring to further and validate current understanding of the conceptual design process. The aim of this hybrid study is to provide scientific methods for the validation of design theories and design methodologies. To analyze EEG signals, we use a wide array of machine learning techniques (clustering, segmentation, P2ML algorithm [PMML95]) to extract features (spatio-temporal and frequency domain features) and their associated underlying concepts (effort, fatigue, concentration). Such questions we ask ourselves are as follows: How can effort, fatigue and concentration be measured on a subject solving design problems? How does effort impact the conceptual design process? How does fatigue relate to effort in the conceptual design process? What is the relationship between concentration and creativity or fixation? How does concentration manifests itself in the conceptual design process? Is the design process fundamentally iterative and recursive?

4.6.1 Quantitative Analysis of EEG signals of Design Protocols

A first step in the analysis of design protocols using EEG signals is to be able to associate EEG features and their associated patterns to the video sequences provided in the design protocol. In this thesis, to perform this analysis, we first compute a feature curve from the EEG data (spatio-temporal or frequency domain features). It is often the case that those feature curves are sampled at frequencies that are too high to provide human-readable information and insight. Following the computation of these feature curves, we either interpolate these curves (to cancel out the noise) or cluster the values into smaller numbers of segments. In the case of interpolation, once interpolation has been performed, we can perform operations such as correlation on the feature curves to see if the features relate to each other (we do this when analyzing fatigue). In the case of clustering, we can then segment the cluster classification of the feature curves into time segments and easily compare with the EEG video protocol for patterns (we do this when analyzing concentration). For example, if the EEG feature curve clusters to the following: 2, 2, 2, 3, 3, 5, 5, 5, 4, 4, 2, 2 (where the integer values are the cluster centroid index), we can determine that there are 5 segments in the feature curve: (2,2,2), (3,3), (5,5,5), (4,4), (2,2), each of which are associated with a time range in the original video. Clustering and interpolation allow for a form of dimensionality reduction which makes the original feature curve more tractable to analysis and processing.

Algorithm 4.1 describes a general process to compute a human-readable segmentation from feature curves (transient microstates and PSD). Larger values of w yield coarser segmentations and larger values of k yield finer grained segmentations.

The goal of this analysis is many-fold. We look to associate concepts (effort, fatigue, concentration) to EEG features (transient microstates, frequency ranges). Sometimes the association is already well-known from the medical and physiology literature. Also, we find relations between different EEG features and their associated concepts (related concepts

should correlate with each other). We find patterns between the underlying video design protocol (of subjects performing design tasks while having their EEG recorded) and the concepts and features we have extracted from the data as to provide insight in the conceptual design process. In some cases, the patterns we uncover by analysis of EEG signals may validate existing design theories or provide new insight on design phenomena. For example, in the case of concentration, we were able to validate the theories of design creativity discussed in [NZ12c].

From a design perspective, the usage of physiological signals to analyze the conceptual design processes can help validating theories of design and methodologies of design. It provides insight into design processes which are seen as human-centric phenomena.

4.6.1.1 Quantifying Effort

In [NNZ15a], it was determined that the transient microstate percentage correlated with subjective ratings of effort and problem hardness. This can be understood by seeing that, as scalp field maps change their configuration in a more transient manner (short lasting configuration changes), the brain is using more energy and this is more likely to correlate with mental effort. Since transient microstate percentages only correlate with subjective effort ratings, we must add that transient microstate percentages are not causative of subjective ratings of effort (as correlation is not causation) and only a metric for mental effort.

Transient microstate percentage curves by themselves are too high frequency to provide any valuable information on the design process. To address this, we have extracted from the transient microstate percentage curves cluster information using a conventional clustering algorithm (since the data is 1-dimensional, the performance of the clustering algorithm is not an issue). To do this, we have effectively clustered the transient microstate percentage curve into n clusters and from the cluster index information, we have extracted time segments. This process defines the transient microstate percentage segmentation. In practice, the parameter n we used was 5 and defines the granularity of the segmentation. Lower values of

n yield coarser segmentations while higher values of n yield finer grained segmentations.

Algorithm 4.1: General Segmentation Algorithm

```
Data: potential data V, number of centroids k and window size w
Result: segmentation S
i=0;
while i<⌊length(V)/w⌋ do
    F_i = compute features of V_{i*w,(i+1)*w−1};
    ++i;
C=Cluster F using k centroids;
i=0;
while i<length(C) do
    if C_{i+1} = C_i then
        ++i;
    else
        S_j=timestamp(C_i);
        ++i, j;
Return S;
```

4.6.1.2 Quantifying Fatigue

Fatigue is a well-studied concept in the related EEG medical and physiology literature. Table 4.5 lists a set of frequency based features that are commonly used in EEG analysis. Many of them relate to fatigue and it is a valid question to determine if all these fatigue metrics actually refer to the same underlying concept. To address this question, we can verify if all these fatigue metrics correlate with each other. If indeed they refer to the same concept of fatigue, it is safe to say that they should correlate with each other. If not, we can assume that these fatigue metrics do not refer to the same notion of fatigue and that fatigue may be a multidimensional concept from an EEG perspective. On the latter, [Hoc13] states that different types of fatigue (mental, drowsiness, physical) are often confused with each other in research.

To perform this analysis, we have computed the correlation between different EEG feature curves. More specifically, we have tried to determine if the transient microstate percentage curve (effort) correlated with different metrics of fatigue. An intuitive rule of

thumb in design studies would push us to believe that a negative correlation exists between effort and fatigue as when a subject is fatigued, he can no longer produce high levels of effort. Furthermore, we try to determine if fatigue is a single dimensional concept in EEG analysis (all fatigue metrics correlate with each other) or multidimensional (some fatigue metrics do not correlate with each other).

To compute the correlation between feature curves however, we need to take into account that such feature curves are often too noisy (high frequency) to be effectively correlated without yielding spurious results. We have therefore interpolated the feature curves prior to computing correlation. The interpolation method we used is radial basis function interpolation as it is known to handle nonlinear data well (EEG data is often seen as nonlinear with non integral fractal dimensions) This effectively provides the general trend of the feature curves and effectively cancels out noise.

Algorithm 4.2: Levels of Concentration Algorithm Using Binning

Data: time window size w and time offset s
Result: levels of concentration $\mathbf{C}$

```
S = compute beta segmentation using Algorithm 3;
i=0;
t=0;
while i<⌊ time_length(S/s ⌋) do
    C_i = # segments in S between times t and t + w;
    ++i;
    t = t + s;
Return C;
```

4.6.1.3 Quantifying Concentration

To measure segments with higher levels of concentration, we first computed the PSD curve on the beta range of the EEG of each design protocols. After analyzing the beta range PSD, we noticed from the protocols that segments where the subjects were visibly concentrating corresponded to segments where the beta range PSD was highly volatile. We computed this volatility by segmenting the beta PSD into time domain values (like for the previous

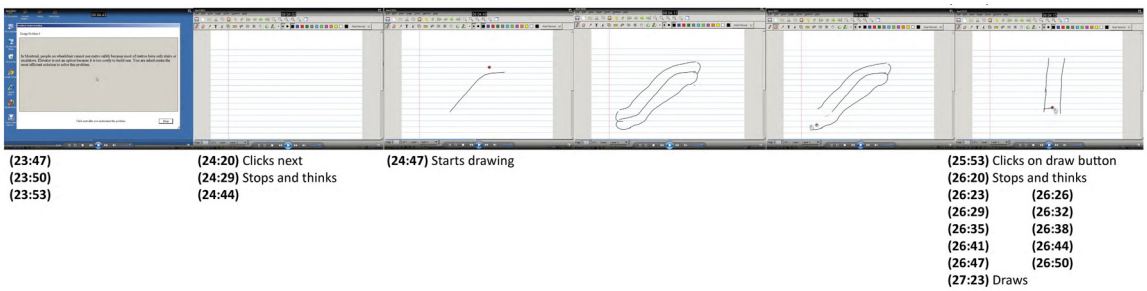

Figure 4.16: Excerpt from the design protocol data of a subject solving Problem 4. Below are timestamps generated by the segmentation algorithm. At screenshot 6, a large quantity of timestamps are generated. This indicates a modal shift in concentration. In this case, the modal shift occurs while the subject is erasing his previous design and redrawing from scratch a new one (tabula rasa event).

effort and fatigue features). This was done by clustering the beta range PSD into 5 clusters and identifying time domain values as time slots where the cluster values changed. The parameter 5 was determined by testing other values and looking for the best granularity segmentation. Following this, heightened concentration was determined to be lapses of time where the time segmentation generated many values. More specifically, we used a sliding window of length 1 minute and offset 5 seconds. For example, if the time segmentation (in minutes and seconds) was 2:30, 3:30, 4:20, 4.21, 4:30, 4:32, 4:40, 4:50, we determined that high levels of concentration were measurable between 4:20 and 4:40. Binning of the time segmentation based on a sliding window is displayed in Figure 4.17. Algorithm 4.2 shows how these bins were calculated.

Heightened concentration in a subject is not only measurable through high values in the beta frequency range, but also through higher variability in the beta range. We determined that higher concentration in a subject was detectable when the beta frequency range segmentation of the protocol produced a large number of segments clustered in a short time period. This means that subjects had a higher variability in their beta range rather than a sustained higher value of the range. From a design perspective, this would in turn hint at the fact that concentration may not be a continuous state of heightened beta values but rather an increased variability in those values.

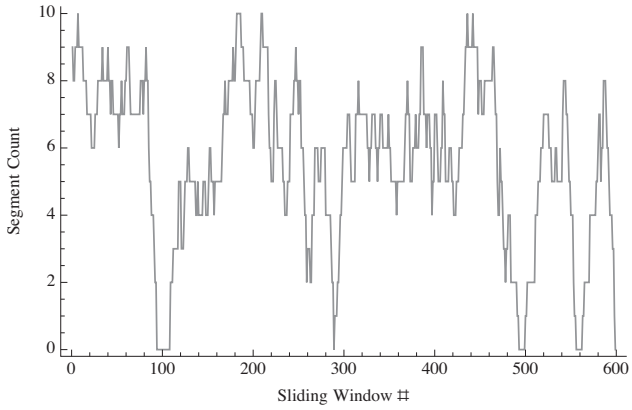

Figure 4.17: Plot of computed concentration levels for a given protocol: a sliding window of length 1 second and offset 5 seconds was used on the time segmentation of the Beta range curves. The number of segments that occurred within the range of the sliding window was counted (y-axis).

4.6.2 Analysis

In this section, we discuss how EEG metrics of effort, fatigue and concentration, monitored using the techniques discussed in the previous sections, may impact our understanding of the conceptual design process. We first discuss the impact of effort monitoring and then discuss how fatigue correlated with effort. We finish our analysis by discussing how concentration relates to creativity and fixation and how the design process can be shown to be iterative in nature from our study of concentration.

From our analysis on effort in the conceptual design process, we have found that low peaks in effort (Figure 4.14a shows an example of this) could be found at the beginning of the design process and the end of the process (while local smaller peaks also occurred during the process). We also found that high peaks of fatigue could be found at the beginning and at the end of the design process (Figure 4.14b shows an example of this). For the peak found at the beginning of the design process, we can safely infer the existence of an *ice-breaking* phenomenon. An *ice-breaking* phenomenon could be defined as a situation where the effort required by a designer to start the design process is high regardless of whether what he is performing is hard or easy. The existence of an *ice-breaking* phenomena

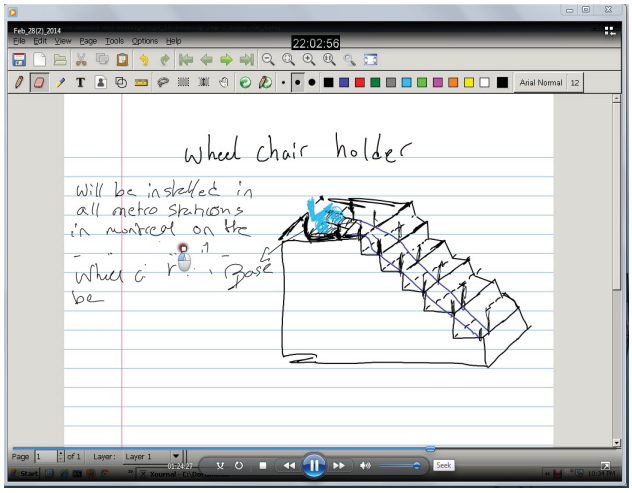

Figure 4.18: Screenshot from a video protocol (the question was to design an escalator for people in wheelchairs) where the subject is entering a *tabula rasa* sequence and erasing partially his design to replace it with a new design. Such sequences were found to have heightened measured concentration levels.

reinforces the need for warm-up problems in the conceptual design process as performance at start is low no matter what the nature of the problem is [WSJ13]. For the peak found at the end of the design process, we can infer that the impacting factor for effort in the design process is the overall length of the design process. We explained peaks at the end of the design process using the theory on continuous work and performance/fatigue described in [Ara12, KDKM12]. Surprisingly, effort incurred during the design process seems to be transient with only smaller local peaks occurring on harder tasks.

Furthermore, we found that effort and some measures of fatigue (i.e. the TYPE-2 (theta+alpha)/beta fatigue feature) were negatively correlated which would lead to the conclusion that there is a trade-off between effort and fatigue: as fatigue increases, there is less energy left to provide an effort. Figure 4.14 shows an example of this pattern that can be found in our data. Trended features curves (in red) of effort and fatigue (i.e. TYPE-2 fatigue) show a negative correlation. This pattern was found throughout our datasets and the average value of this negative correlation was found to be -0.847. This confirms the existence of a capacity model for effort and fatigue [Kah73]. We also found a negative

correlation between the theta band and effort, albeit a less convincing value of -0.604. The theta band usually measures the idleness and drowsiness dimensions of fatigue. There was also a negative correlation between the alpha band and effort (a value of -0.816): the alpha band measure relaxation states. We posit that TYPE-2 fatigue (i.e. the fatigue measure which correlated the most with effort) measured mental fatigue. Like for effort, peaks in fatigue occur at the beginning and the end of the design session although in the case of fatigue, they are high peaks. This confirms the existance of an *ice-breaking* phenomenon and an end-of-session phenomenon. This is in line with studies which show that to improve designer strategies, it is best to reduce the length of each design session rather than to decrease the difficulty of each individual design problems. It also stresses the importance of warm-up problems and the importance of not starting with the harder and more important problems [WSJ13]. This is a clear case where physiological studies of design can validate a design strategy.

During our analysis of concentration, we found that heightened levels of concentration were detected in segments where the subjects where in a *tabula rasa* sequence. *Tabula rasa* sequences were sequences where subjects were undergoing complete reevaluation of their design and were detected by noticing that the subjects were erasing completely or partially their previous design on the sketchpad. These sequences were also often accompanied by long pauses in the design protocol which would indicate thought and hence concentration. As stated in the previous section, concentration seemed to not be so much a constant state of heightened concentration but rather a higher variability in the concentration metrics used, which would lead to indicate that concentration is a state of higher turbulence rather than a constant state of mind.

In addition to high concentration sequences, we found that low concentration sequences were associated to automatic responses where the subjects went from problem analysis (reading the question) to solution draft immediately without much pauses in the video protocol. Automatic responses may be related to the problem of fixation in design problem

solving [NZ16a] where a first response may not be the good one (and conveys a bias that is sometimes hard to get rid of in the design process).

In terms of concentration, protocols can be seen as oscillating between sequences where the answer is easy and automatic and sequences where the subject doubt their answers and restart from scratch (which we term *tabula rasa* sequences).

This pattern found in concentration levels of various subjects validates a theory on design creativity brought forth by [NZ12c]. In the latter, it is postulated that design can be seen as the sequence of iterates $\{P_i,S_i\}$, $\{P_{i+1},S_{i+1}\}$, $\{P_{i+2},S_{i+2}\}$, ... where P, S are Problem-Solution pairs. This sequence of iterates being nonlinear can end up in a chaotic state. More specifically, it is said that design creativity is the proces of generating these iterates: P_{i+1} replaces P_i and S_{i+1} replaces S_i. This is exactly what occurs during design segments where subjects are solving a more complex problem. They effectively erase part or all of their previous solution to replace it with a new one and we can infer that since the solution changed, the problem domain might have changed as well.

4.7 Modal Shifts in Concentration Indicate Creativity

Modal shifts are said to indicate heightened creativity in the conceptual design process. These modal shifts are traditionally detected using concurrent verbal protocols. However, it is known that verbal protocols fail in some situations such as when dealing with creativity, insight, nonverbalizable and nonconscious processes. It is an open debate in the design literature on verbal protocols whether nonconscious (nonverbalizable) processing is significant or not. We used EEG signals recorded on subjects who were asked to solve design problems on a sketch pad to detect modal shifts in concentration. We found that modal shifts in concentration were often occurring when subjects were erasing completely their previous solution and restarting a new solution from scratch (i.e. tabula rasa event), indicating heightened creativity. From EEG segments where modal shifts in concentration were deemed

to be high, we performed source localization using the LORETA algorithm. Cross-checking with the physiology literature on the neurology of creativity, we found that regions of the brains associated with creativity (e.g. prefrontal lobe) were activated during modal shifts. Furthermore, we determined that the right prefrontal lobe, associated with insight (e.g. Aha! experience) solutions, was dominant in circa 25% of the samples in our modal shift excerpts. This leads us to believe that nonconscious (nonverbalizable and insight) processing is non negligible in the analysis of the conceptual design process.

Modal shifts [CCD94] were proposed as a model for detecting creativity bursts in the study of the conceptual design process. Modal shifts are episodes where "especially during creative periods of conceptual design, designers alternate rapidly in shifts of attention between different aspects of their task, or between different modes of activity", or different design strategies [Cro01]. Traditionally, these modal shifts are detected using verbal protocol [ES84]. A subject concurrently verbalizes his thoughts while solving a design problem. The recordings of these verbal protocols are then encoded and segmented. When a large number of segments related to ideation and solution generation occurs in a given short time period, modal shifts are said to occur. These modal shifts were found to indicate creativity [Cro01]. However, verbal protocols are known to have weaknesses. They are known to fail when faced with nonreportable processes [CS10] such as: creative tasks, insight (e.g. Aha! experience, gestalt), affective judgment, task parallelism or automated tasks (e.g. facial recognition, visual recognition tasks) [KP00].

While verbal protocols may fail in particular situations, electroencephalograms (EEG) excel at measuring states of mind (e.g. mental effort, concentration, fatigue). Used in conjunction with source localization techniques, regions of the brain that are activated at a given time can be approximately identified and cross-referenced with the physiology literature. For example, if creativity is said to occur, the prefrontal cortex is most likely to be activated and, if an insight solution [JBBH$^+$04] is said to occur, the right prefrontal cortex and the right anterior superior temporal gyrus are most likely to be activated. In [NNZ15b],

a method to segment design protocols based on mental effort (measured using EEG transient microstate percentages) was discussed. More specifically, variations in mental effort were used as a heuristic to segment a design protocol into time points. These segments could emulate basic segmentations performed by domain experts while providing insight into hidden cognitive structures that are not easily visible. Following this line of research, we segmented our design protocols using an EEG metric for concentration (i.e. beta band). Concentration "means a work state where cognitive resources are assigned to target work" [SOM+13]. In EEG analysis, concentration is associated to the beta band [BBGW08]. We found that periods of high concentration followed a modal shift model. More specifically, we found that periods of heightened concentration were associated with higher variability of the beta band segmentation of an EEG signal. That is, heightened concentration produced more short duration time segments indicating modal shifts in concentration. These periods of heightened concentration were associated with segments in the design protocols where subjects were rethinking completely their sketched solutions and erasing their previous solution to sketch a new solution (we term those sequences tabula rasa events).

Using these beta band segmentations, we isolated segments in the EEG signals where heightened concentration occurs. We then used Low Resolution Electromagnetic Tomography (LORETA) as a method to perform source localization on the associated scalp field data [PMML94b]. creativity is often associated to the prefrontal cortex. Based on the left/right hemisphere model of brain function, it is known that the right hemisphere is associated with insight (e.g. Aha! experience, not easily verbalizable solutions) while the left hemisphere is associated with logic and language (e.g. verbalizable solutions). Using source localization, we were then able to distinguish insight solutions from verbalizable solutions.

We have found evidence supporting the following:

- Modal shifts in concentration indicate creativity (they often happen when a tabula rasa event is under way).

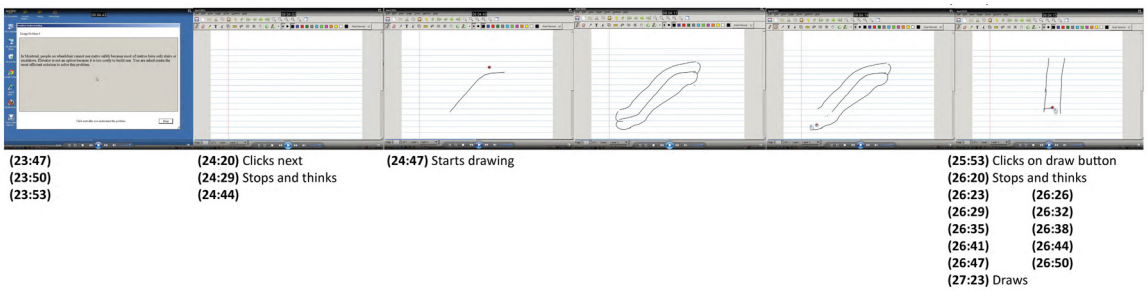

Figure 4.19: Excerpt from the design protocol data of a subject solving Problem 4. Below are timestamps generated by the segmentation algorithm. At screenshot 6, a large quantity of timestamps are generated. This indicates a modal shift in concentration. In this case, the modal shift occurs while the subject is erasing his previous design and redrawing from scratch a new one (tabula rasa event).

- During modal shifts in concentration, the left and right prefrontal lobes are activated with, as pattern, an alternation between insight (nonconscious, right obe) solutions and verbalizable (conscious, left lobe) solutions.

- During modal shifts in concentration, dominance of the left and right upper frontal area occured in circa 25

Evidence gathered through our experiments shows that the importance of nonconscious and nonverbalizable processing should not be ignored and that insight (nonreportable) solutions do effectively occur in the conceptual design process.

As a first step in our analysis, we extracted from the design protocol data available sequences where we determined that concentration was high. High concentration was determined to happen when modal shifts in the beta feature curves occurred. More specifically, we segmented the design protocols using the beta values and when, on short time lapses, many time segments were produced, we determined that a modal shift in concentration occurred. Figure 4.19 shows an EEG signal and its beta filtering for such a sequence where concentration was high. Interestingly, we found that such modal shifts in concentration often occurred when subjects were in a tabula rasa event.

We then performed source localization on the samples (scalp field maps) of these excerpts

where it was determined that concentration was high. The goal was to determine if these sequences were indicative of higher levels of creativity. If such was the case, modal shifts in concentration would then be indicative of creativity. To determine this, we crosschecked with the physiology literature where creativity is said occur when the prefrontal lobe is activated. Some work shows that creativity also occurs when the right posterior cingulate and the basal ganglia are activated. Furthermore, two types of creativity occur: insight creativity (e.g. Aha! experience and gestalt) and verbalizable creativity (e.g. logic and language). Insight creativity is said to occur when the right prefrontal lobe or the right anterior superior temporal gyrus (right upper temporal lobe) are activated. Verbalizable creativity is said to occur when the left prefrontal lobe is activated. Table 4.7 shows that activation regions were found to be the left and right prefrontal and frontal lobes, the right temporal lobe and other regions associated with creativity. Activation of the left and right frontal lobe (motor cortex) was most likely due to voluntary movement control (subjects were sketching on a sketchpad). During the segment of the design protocol we analyzed, we found that there was an alternation between left prefrontal lobe activation and right prefrontal lobe activation indicating alternation between insight and logical solution finding.

Figure 4.20 shows a sequence of samples that were source localized and Table 4.7 summarizes the activation patterns of each source localized sample. While in a tabula rasa event, a subjects mind effectively alternates between insight (nonconscious) solutions and verbalizable (conscious) solutions.

While in a *tabula rasa* event, a subject's mind effectively alternates between insight (nonconscious) solutions and verbalizable (conscious) solutions. To compare activation patterns in the left-frontal-upper and the right-frontal-upper quadrants of our brain model, we determined the number of times the average magnitude per voxel in any of the 8 quadrants of our 3D model was a maximum value. Following this analysis, we determined that the left-frontal-upper quadrant (which contains the left frontal and prefrontal lobes) dominated in 23.68% of samples whereas the right-frontal-upper quadrant (which contains the right frontal

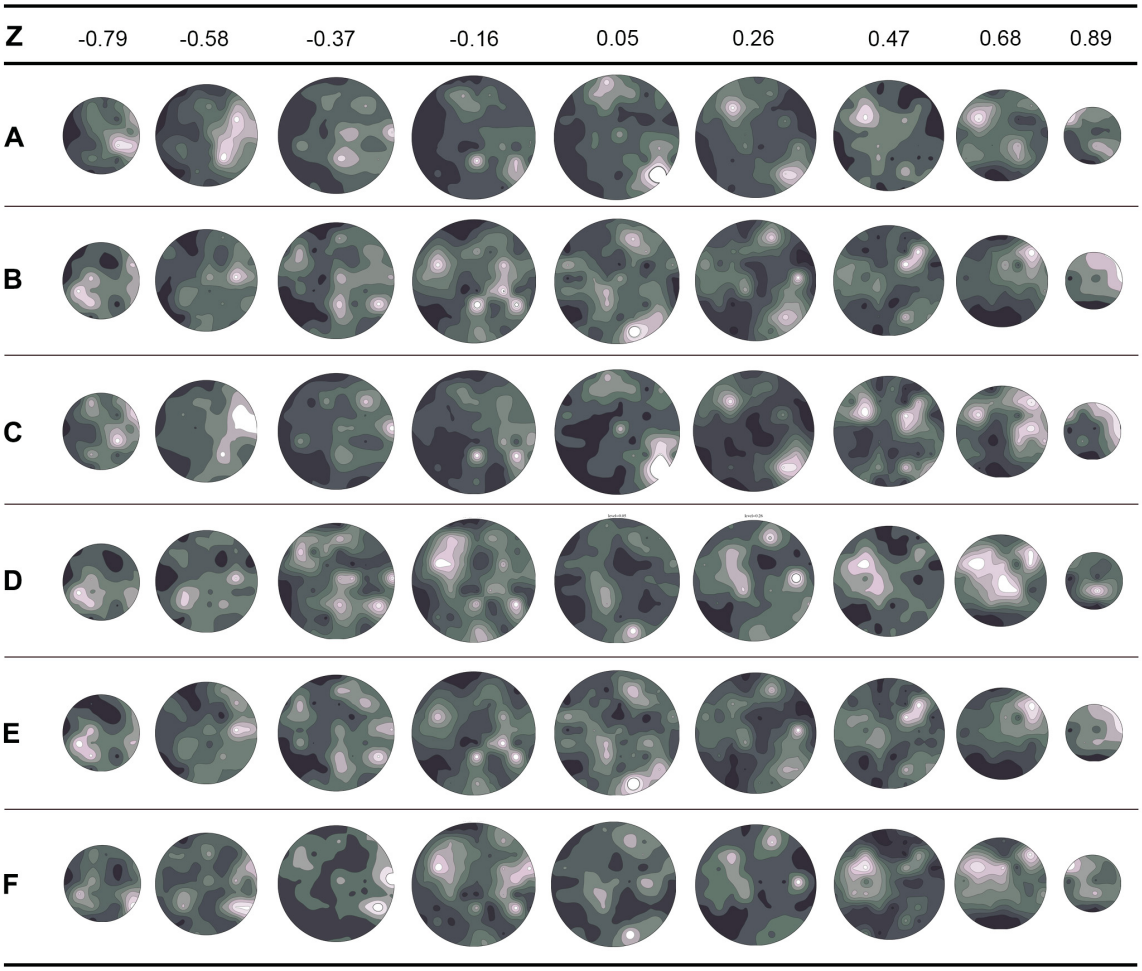

Figure 4.20: Slices of the spherical 3D model of the brain we used at different z values (-0.79, -0.58, - 0.37, -0.16, 0.05, 0.26, 0.47, 0.68, 0.89) which also corresponded to the location of the voxel slices. White denotes high density magnitudes while black denotes low density magnitudes.

and prefrontal lobes) dominated in 26.66% of samples. Although both values are similar, indicating that insight and intuitive solutions were at par with logical and verbalizable solutions, insight solutions can be seen to have a slight edge in the design protocol excerpt we used, emphasizing the importance of nonconscious processing.

Although LORETA is only an approximation of source localization (as the underlying matrix equations are underdetermined), we saw a clear activation pattern in the alternation of right and left frontal and prefrontal lobe activation during the design segment where we found modal shifts in concentration. Furthermore, other structures often associated with

Table 4.7: Approximate regions of the brain activated related to creativity. Timestamps are relative to the beginning of the sequence (with high levels of concentration) excerpted from a design episode. The sequence occurs while a subject is solving Problem 4 and is in a tabula rasa event.

Segment	Timestamp	Activation
A	1 sec.	left frontal and prefrontal lobe, right temporal lobe
B	3 sec.	right frontal and prefrontal lobe, basal ganglia
C	28 sec.	right frontal and prefrontal lobe, left prefrontal lobe, right temporal lobe
D	36 sec.	left frontal and prefrontal lobe, left superior temporal gyrus
E	52 sec.	right frontal and prefrontal lobe
F	58 sec.	left frontal and prefrontal lobe, right superior temporal gyrus

creativity, such as the superior temporal lobes, were at moment activated. These activation patterns where stable for subsecond periods and quickly shifted to another stable subsecond pattern.

Modal shifts seem to be indicative of designer creativity. "The apparent importance of frequent shifts of attention or activity mode in influencing either the creativity or overall quality of the design concepts produced" is discussed in [Cro01, CCD94]. [NZ12c] describes creativity as a sequence of iterates that can fall into a chaotic state. More specifically, the iterates $\{P_i, K_i, S_i\}, \{P_{i+1}, K_{i+1}, S_{i+1}\}, \{P_{i+2}, K_{i+2,S_{i+2}}\}$, where P, K, S are Problem-Knowledge-Solution triplets are considered. In our research, we found that concentration (beta band) was better understood using the concept of modal shifts as segments of the protocol data where subjects were experiencing tabula rasa events (erasing their prior design and replacing it with a new one) were associated with high levels of short duration segments in the beta feature segmentation. In contrast, segments where the beta features were simply elevated did not describe as completely the subject's state of mind as did modal shifts in beta features. These theories (the theory of modal shifts [Cro01] and the non-linear dynamic theory of creativity [NZ12c]) fit well with the empirical evidence we have found using EEG frequency domain analysis and source localization (LORETA). Although LORETA is only

an approximation, we were still able to find a pattern in the activation loci of the EEG signals we gathered while subjects were performing design tasks, which were in agreement with underlying theories on the neurology of creativity.

4.8 A Real-Time Algorithm for Transient Microstate Percentages

4.8.1 Real-Time Approximation of Transient Microstates

Given a set of N measurements at time $t = 0, \ldots, N-1$ and n electrode locations, a scalp field map is a sequence of n electrode potential values $\mathbf{V}_t$ at a given time t. More specifically, if an epoch consists of a matrix $\mathbf{V}_{x,t}$ measured at $x = 0, \ldots, n-1$ and $t = 0, \ldots, N-1$, a scalp field map is a $1 \times n$ vector given by $\mathbf{V}_t$ for some value $t \in [0, N-1]$.

The transient microstate percentage is then given by:

$$T.M.\% = \frac{\#\ of\ transient\ microstates}{N} \tag{4.4}$$

Using the P2ML algorithm, the number of transient microstates is given by the difference between the number of segments found using the P2ML algorithm and the number of segments found using the regularized P2ML algorithm which penalizes short duration microstates. The computation of the P2ML algorithm is expensive computationally as datasets grow larger. Our approximation technique measures the norm of the rate of change between two adjacent scalp fields. More specifically, we have the following filter:

$$F_1(\mathbf{x}, \mathbf{y}) = \begin{cases} 1, & \|\mathbf{x} - \mathbf{y}\|_2 \geq \epsilon \\ 0, & otherwise \end{cases} \tag{4.5}$$

for some sensitivity parameter ϵ and some contiguous scalp fields given by $\mathbf{x} = \mathbf{V}_{\kappa t}$ and $\mathbf{y} = \mathbf{V}_{\kappa(t+1)}$, each of length n. In particular, we are first taking the pairwise difference of contiguous scalp fields and then taking the Euclidean norm of the resulting vector. This filter marks segments where the rate of change between two scalp fields is high using a

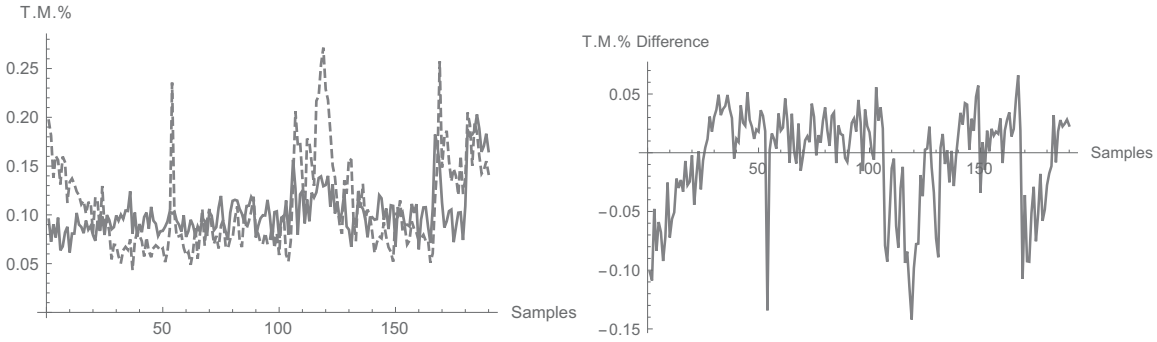

(a) Transient microstate percentages computed using P2ML (solid) and our method (dashed)

(b) Computed error between both computations

Figure 4.21: Computation of the transient microstate percentages using P2ML and our method comparisons. F_1 and F_2 parameters were $\epsilon = 15$, $\kappa = 1$ and $\omega = 2$. The average number of transient microstates found using P2Ml was 513.116 and 537.858 using our method, or less than half a percent difference.

compact bitstream. To approximate the number of microstates, we then sum the values obtained by the filter:

$$\sum_{t=0}^{\lfloor (N-1)/\kappa \rfloor} F_1\left(\mathbf{V}_{\kappa t}, \mathbf{V}_{\kappa(t+1)}\right) \tag{4.6}$$

for some parameter κ used to compensate for data bandwidths (e.g. $\kappa = 1$). To approximate the number of transient microstates, we introduce another filter which counts samples that incur successive changes:

$$F_2(\mathbf{x}) = \begin{cases} 1, \ \sum_{i=j}^{j+\omega} \mathbf{x}_i = \omega + 1 \\ 0, \ otherwise \end{cases}, \ \forall \mathbf{x}_j = 1 \tag{4.7}$$

for some sensitivity window length ω (e.g. $\omega = 2$). F_1 effectively approximates the number of microstates using an algorithm such as the P2ML algorithm while F_2 filters the number of transient microstates. The number of transient microstates is then approximated by:

$$\sum F_2 \circ \bigcup_{t=0}^{\lfloor (N-1)/\kappa \rfloor} F_1\left(\mathbf{V}_{\kappa t}, \mathbf{V}_{\kappa(t+1)}\right) \tag{4.8}$$

where the union operator generates an F_1-bitmap. Both filters can be computed in $O(N)$ yielding a linear overall computational complexity and can be implemented as a streaming algorithm with low memory footprint.

Table 4.8: Performance benchmarks

Problem Size	P2ML Performance	Filter Method Performance
$1,000 \times 63$	4.50843 secs	0.0936 secs
$5,000 \times 63$	36.5166 secs	0.998406 secs
$10,000 \times 63$	78.8741 secs	4.05603 secs
$50,000 \times 63$	115.628 secs	10.8265 secs
$\vdots$	$\vdots$	$\vdots$
$900,000 \times 63$	441.072 mins	6.41997 mins

4.8.2 Experiments and Validation

We experimented with our method using an EEG signal of $900,000$ samples measured at a sample rate of 500 samples/sec using P2ML as a baseline of comparison. Figure 4.21(a) shows the transient microstate percentage of an EEG epoch divided into disjoint windows using P2ML and our method and Figure 4.21(b) shows the error computed between the results of both methods. The error experimentally camps within a range of $\pm 10\%$ and $\pm 0.5\%$ on average. While the transient microstate percentage computed using our method showed peaks with respect to the transient micostate percentage computed using the P2ML algorithms, it can be noted that accuracy can be improved by repeating the computation over different samples and averaging the results. To show this, we computed the transient microstate percentages of the EEG signal containing $900,000$ samples using a window of $5,000$ samples. The average number of transient microstates computed using the P2ML algorithms was 513.116 while the average number of transient microstates computed using our method was 537.858. This gives a transient microstate percentage of 10.2623% using P2ML and 10.7572% using our method.

4.8.3 Discussion

The biggest gain of using our method with respect to other algorithms is the computational performance and the low memory footprint of the algorithm. Filters F_1 and F_2 can be implemented using a streaming algorithm which alleviates the usage of main memory during

computation. Table 4.8 compares the runtime performance of both approaches using a basic Mathematica implementation (that could be converted to C for further optimization) and a 64GB RAM 16 core machine. On the larger dataset (900,000 samples), the memory footprint ranged from 10GB to 20GB for the P2ML approach and was negligeable using our method. The memory footprint of our method scales linearly with the output which is itself linear in the input. Since the bit vectors of F_1 and F_2 are sparse, the memory footprint can furthermore be compressed using sparse matrix representations or low-level bit codes. A low memory footprint makes our method suitable for integration in realtime subsystems.

In terms of precision, a 10% maximum deviation was found using this approximation while the average deviation was 0.5%. Our method performed better when averaging was used to aggregate results from different runs of the algorithm. In the later case, a transient microstate percentage of 10.7572% was computed with respect to a 10.2623% using P2ML. Since the algorithm scales linearly in the input, repeating the algorithm a constant number of times also incurs a linear complexity.

For many applications such as medical diagnosis, only the transient microstate percentage is necessary and the full EEG segmentation into microstates can be ignored.

Chapter 5

Conclusion

Physiological methods used to analyze the conceptual design process form a compendium of new and exciting methods to understand design. Currently, the most popular techniques remain concurrent verbal protocols but physiological methods such as EEG are emerging and promising. In this thesis, we have addressed the following 7 hypotheses using quantitative EEG analysis on design protocol data to study the conceptual design process:

Hypothesis 1. *Design protocol segmentation using EEG is a feasible method.*

We addressed this hypothesis in Section 4.3 where we described a new algorithm to segment design protocols using transient microstate percentages as a surrogate for mental effort. We showed that microstate segmentation can emulate basic manual segmentation. In Section 4.4, we validated our method by comparing different EEG features (spatio-temporal and frequency domain) used to segment the design protocols and manual segmentation by domain experts. The average deviation of the best performing algorithm was 2 seconds while manual segmentations deviated by 1.5 second when compared to each other.

Hypothesis 2. *Mental effort can be measured using transient microstates.*

We addressed this hypothesis in Section 4.2 by showing that transient microstates somewhat correlated with mental effort measured using subjective rating scales. We then

posited the use of transient microstate percentages to measure the evoked mental effort of a subject performing tasks based on the heuristic that when a subject performs a bigger effort, the spatio-temporal patterns of his EEG changed more rapidly. Transient microstate percetages were then shown to camp between 2-3% (for a subject at rest) to 15-20% (for a subject performing a task needed large effort).

Hypothesis 3. *Effort (and by extension fatigue) is subject to an ice-breaking and end of task phenomena during the conceptual design process.*

We addressed this hypothesis in Sections 4.5 and 4.6 by showing that the feature curves for TYPE-2 Fatigue (i.e. (theta+alpha)/beta) spiked at the beginning and at the end of the design episodes. We interpreted this as an ice-breaking phenomena and an end-of-task phenomena (where fatigue accumulates by executing short repetitive tasks).

Hypothesis 4. *Fatigue and effort follow a capacity model.*

We addressed this hypothesis in Section 4.6 by showing that the TYPE-2 Fatigue curve correlated negatively with the transient microstate percentage curve. We then deduced that a capacity model, where low levels of fatigue generated more capacity for mental effort and highe levels of fatigue generated lower capacity for mental effort, could explain this negative correlation.

Hypothesis 5. *Fatigue is multidimensional.*

We addressed this hypothesis in Section 4.5 where we showed that some metrics for fatigue did not correlate with each other. This hypothesis is in line with the physiology literature which reports that fatigue is a multidimensional concept.

Hypothesis 6. *Concentration follows a modal shift model during the conceptual design process.*

We addressed this hypothesis in Section 4.6 by showing that when concentration (measured through beta features) was highly variable the associated video protocols seemed to

indicate that the subject was actively thinking or being creative. We then posited that it was not enough to determine segments where concentration was high and segments where concentration levels where highly variable provided better results.

Hypothesis 7. *Modal shifts in concentration indicate creativity.*

We addressed this hypothesis in Sections 4.6 and 4.7 by showing that segments where modal shifts in concentration occurred often happened when subjects were erasing completely their previous designs and restarting a new design from scratch (which indicates heightened creativity). We termed these segments *tabula rasa* events. We furthermore performed source localization on these segments and determined that these *tabula rasa* events seemed to be using high levels of insight and intuition, contradicting the mainstream opinion that the level of nonconscious processing is negligible. Regions of the brain indicating insight (e.g. left prefrontal lobe) dominated in around 25% of samples while logic and language regions (e.g. right prefrontal lobe) dominated in around 20% of samples in the *tabula rasa* segments we analyzed.

Through these 7 hypotheses, we have outlined methods and algorithms that can be used to understand and describe quantitatively the conceptual design process.

Bibliography

[Aki09] Ö. Akin. Variants and invariants of design cognition. In *About: Designing - Analysing Design Meetings*, pages 119–133. CRC Press / Balkema, 2009.

[ALCJ14] M. Ahn, M. Lee, J. Choi, and S.C. Jun. A review of brain-computer interface games and an opinion survey from researchers, developers and users. *Sensors*, 14:14601–14633, 2014.

[Alt84] G.S. Altshuller. *Creativity as an exact science: The theory of the solutions of inventive problems*. Gordon and Breach Science Publishers, 1984.

[Ara12] T. Arai. *Mental fatigue*. Teachers College, Columbia University, 1912.

[ASL08] S. Adólfsdóttir, L. Sørensen, and A. J. Lundervold. The attention network test: A characteristic pattern of deficits in children with adhd. *Behavioral and Brain Functions*, 4(1):9, 2008.

[AZJG09] K. Alexiou, T. Zamenopoulos, J.H. Johnson, and S.J. Gilbert. Exploring the neurological basis of design cognition using brain imaging: some preliminary results. *Design Studies*, 30(6), 2009.

[BBGW08] J. Baumeister, T. Barthel, K. R. Geiss, and M. Weiss. Influence of phosphatidylserine on cognitive performance and cortical activity after induced stress. *Nutritional Neuroscience*, 11(3):103–110, 2008.

[BC09] L.J. Ball and B.T. Christensen. Analogical reasoning and mental simulation in design: Two strategies linked to uncertainty resolution. In *About: Designing - Analysing Design Meetings*, pages 137–152. CRC Press / Balkema, 2009.

[BDRE13] R. Bhat, A. Deshpande, R. Rai, and E.T. Esfahani. Bci-touch based system: A multimodal cad interface for object manipulation. *ASME 2013 International Mechanical Engineering Congress and Exposition, San Diego, California, USA*, 12, November 15-21, 2013.

[Ber37] H. Berger. Über das elektrenkephalogramm des menschen. *Archiv für Psychiatrie und Nervenkrankheiten*, 106(1):577–584, 1937.

[BLC+04] C. Berka, D. J. Levendowski, M. M. Cvetinovic, M. M. Petrovic, G Davis, M. N. Lumicao, V. T. Zivkovic, M. V. Popovic, and R. Olmstead. Real-time analysis of eeg indexes of alertness, cognition, and memory acquired with a wireless eeg headset. *International Journal of Human-Computer Interaction*, 17(2):151–170, 2004.

[BM98] D. Braha and O. Maimon. *A Mathematical Theory of Design: Foundations, Algorithms, and Applications*. Springer, 1998.

[BMM11] D. Brunet, M.M. Murray, and C.M. Michel. Spatiotemporal analysis of multichannel EEG: Cartool. *Computational Intelligence and Neuroscience*, 2011, 2011.

[BR03] D. Braha and Y. Reich. Topological structures for modeling engineering design processes. *Research in Engineering Design*, 14(4):185–199, 2003.

[BRSU09] D. Bratzke, B. Rolke, M. B. Steinborn, and R. Ulrich. The effect of 40 h constant wakefulness on task-switching efficiency. *Journal of Sleep Research*, 18(2):167–172, 2009.

[BS01] L.A. Baccalá and K. Sameshima. Partial directed coherence: a new concept in neural structure determination. *Biol. Cybern.*, 84:463–474, 2001.

[BS15] Stephanie Balters and Martin Steinert. Capturing emotion reactivity through physiology measurement as a foundation for affective engineering in engineering design science and engineering practices. *Journal of Intelligent Manufacturing*, pages 1–23, 2015.

[BTV+10] B. Blankertz, M. Tangermann, C. Vidaurre, T. Dickhaus, C. Sannelli, F. Popescu, S. Fazli, M. Danczy, G. Curio, and K.R. Müller. Detecting mental states by machine learning techniques: The berlin braincomputer interface. In *Brain-Computer Interfaces: Revolutionizing Human-Computer interaction*, pages 113–136. Springer, 2010.

[CCD94] N. Cross, H. Christiaans, and K. Dorst. Design expertise amongst student designers. *Journal of Art and Design Education*, 13(1):39–56, 1994.

[CCD96] N. Cross, H. Christiaans, and K. Dorst. Introduction: Th deflt protocols workshop. In *Analysing Design Activity*, pages 1–14. Wiley, 1996.

[CGT+12] R. Carabalona, F. Grossi, A. Tessadri, P. Castiglioni, A. Caracciolo, and I. de Munari. Light on! real world evaluation of a p300-based braincomputer interface (bci) for environment control in a smart home. *Ergonomics*, 55(5):552–563, 2012.

[Cha13] E. Charney. Can tasks be inherently boring? *Behav Brain Sci*, 36(6):684, 2013.

[Cho59] N. Chomsky. Verbal behavior by b.f. skinner. *Language*, 35:26–58, 1959.

[CN14] D. Carneiro and P. Novais. *Conflict Resolution and its Context: From the Analysis of Behavioural Patterns to Efficient Decision-Making*. Springer, 2014.

[Cro01] N. Cross. *Design Cognition: Results From Protocol And Other Empirical Studies Of Design Activity*, pages 79–103. Elsevier, 2001.

[CS10] I. Chiu and L. H. Shu. Potential limitations of verbal protocols in design experiments. *Proceedings of ASME International Design Engineering Technical Conferences and Computers and Information in Engineering Conference (DTM)*, 2010.

[Csi96] M. Csikszentmihalyi. *Creativity: Flow and the psychology of discovery and invention*. Harper Collins, 1996.

[CZLC13] W. Cai, C. Zhu, V.C.M. Leung, and M. Chen. A cognitive platform for mobile cloud gaming. *IEEE International Conference on Cloud Computing Technology and Science*, 2013.

[Dam99] A. Damasio. *The Feeling of What Happens*. Harcourt Brace & Co., 1999.

[Dav16] C. P. Davis. Fatigue diagnosis. http://www.emedicinehealth.com/fatigue/page5_em.htm#Exams%20and%20Tests/, 2016. [Online; accessed 6-July-2016].

[DCMG01] C. Davisa, A. Castlesa, K. McAnallya, and J. Graya. Lapses of concentration and dyslexic performance on the ternus task. *Cognition*, 81(2):B21B31, 2001.

[DD09] C. Le Dantec and E.Y.L. Do. The mechanisms of value transfer in design meetings. In *About: Designing - Analysing Design Meetings*, pages 101–118. CRC Press / Balkema, 2009.

[DDVS+09] M. Desseilles, T. T. Dang-Vu, S. Schwartz, P. Peigneux, and P. Maquet. *Neuroimaging in sleep and sleep disorders*, pages 198–217. Saunders Elsevier, 2009.

[De 05] J. De Luca. *Fatigue as a window to the brain*. The MIT Press, 2005.

[Des12] P. A. Desmond. *Handbook of operator fatigue*. CRC Press, 2012.

[dGT+14] L.C. de Souza, H.C. Guimarães, A.L. Teixeira, P. Caramelli, R. Levy, B. Dubois, and E. Volle. Frontal lobe neurology and the creative mind. *Front Psychol.*, 5:761, 2014.

[Die04] A. Dietrich. The cognitive neuroscience of creativity. *Psychon Bull Rev.*, 11:1011–1026, 2004.

[DJJ+97] T. Dierks, V. Jelic, P. Julin, K. Maurer, L.O. Wahlund, O. Almkvsit, W.K. Strik, and B. Winblad. EEG-microstates in mild memory impairment and Alzheimer's disease: possible association with disturbed information processing. *J. Neural Transm.*, pages 483–495, 1997.

[DKV09] A. Dong, M. Kleinsmann, and R. Valkenburg. Affect-in-cognition through the language of appraisal. In *About: Designing - Analysing Design Meetings*, pages 119–133. CRC Press / Balkema, 2009.

[DM08] K. E. DeLeeuw and R. E. Mayer. A comparison of three measures of cognitive load: Evidence for separable measures of intrinsic, extraneous, and germane load. *Journal of Educational Psychology*, 100(1):223–234, 2008.

[DP09] D.P. Dubhashi and A. Panconesi. *Concentration of Measure for the Analysis of Randomized Algorithms*. Cambridge University Press, 2009.

[DT11] V.B. Deepa and P. Thangaraj. Classification of EEG data using FHT and SVM based bayesian network. *IJCSI International Journal of Computer Science Issues*, 8(5):239–243, 2011.

[DVDP+07] T. T. Dang-Vu, M. Desseilles, D. Petit, S. Mazza, J. Montplaisir, and P. Maquet. Neuroimaging in sleep medicine. *Sleep Med*, 8:349–372, 2007.

[EG87] C.W. Enis and S.W. Gyeszly. Protocol analysis of the engineering systems design process. *Research in Engineering Design*, 3(1):15–22, 1987.

[ES84] K. A. Ericsson and H. A. Simon. *Protocol analysis: Verbal reports as data*. MIT Press, 1984.

[ES07] J. Euzanat and P. Shvaiko. *Ontology Matching*. Springer, 2007.

[Fai01] S. H. Fairclough. *Mental effort regulation and the functional impairment of the driver*. Erlbaum, 2001.

[FCH+05] T. K. Fredericks, S. D. Choi, J. Hart, S. E. Butt, and A. Mital. An investigation of myocardial aerobic capacity as a measure of both physical and cognitive workloads. *International Journal of Industrial Ergonomics*, 35(12):1097–1107, 2005.

[FH04] S. H. Fairclough and K. Houston. A metabolic measure of mental effort. *Biological Psychology*, 66(2):177–190, 2004.

[Fre03] J. Freudiger. Brain states analysis for direct brain-computer communication. *Swiss Federal Institute of Technology*, 2003.

[FS93] M. Fallshore and J. W. Schooler. Verbal vulnerability of perceptual expertise. *J Exp Psychol Learn Mem Cogn.*, 21(6):1608–1623, 1993.

[FWV07] D. Francois, V. Wertz, and M. Verleysen. The concentration of fractional distances. *IEEE Trans. on Knowledge and Data Engineering*, 2007.

[GAP10] B. Graimann, B. Allison, and G. Pfurtscheller, editors. *Brain-Computer Interfaces: Revolutionizing Human-Computer interaction*. Springer, 2010.

[GASD96] E. Granholm, R. F. Asarnow, A. J. Sarkin, and K. L. Dykes. Pupillary responses index cognitive resource limitations. *Psychophysiology*, 33(4):457–461, 1996.

[Gaz67] M. Gazzaniga. The split brain in man. *Scientific American*, 217(2):24–29, 1967.

[GEGS15] V. Goel, I. Eimontaite, A. Goel, and I. Schindler. Differential modulation of performance in insight and divergent thinking tasks with tdcs. *Journal of Problem Solving*, 8(1), 2015.

[Ger90] J. Gero. Design prototypes: a knowledge representation schema for design. *AI Magazine*, 11(4):26–36, 1990.

[Ger00] J. Gero, editor. *Artificial Intelligence in Design00*. Kluwer Academic, 2000.

[GHN04] P. Gu, M. Hashemian, and A.Y.C. Nee. Adaptable design. *CIRP Annals - Manufacturing Technology*, 53(2):539–557, 2004.

[GM98] J.S. Gero and T. McNeill. An approach to the analysis of design protocols. *Design Studies*, 19(1):21–61, 1998.

[Go7] M.H. Goöker. The effects of experience during design problem solving. *Design Studies*, 18(4), 1997.

[Goe10] V. Goel. Neural basis of thinking: Lab problems vs. real-world problems. *Cognitive Science*, 1(4), 2010.

[Goe14] V. Goel. Creative brains: Designing in the real world. *Frontiers in Human Neuroscience*, 8, 2014.

[Gol90] G. Goldschmidt. Linkography: assessing design productivity. In *Cybernetics and Systems*. World Scientific, 1990.

[Gor92] S. E. Gordon. *Implications of Cognitive Theory for Knowledge Acquisition*. Springer Verlag, 1992.

[GRSA13] P. Ghorbanian, S. Ramakrishnan, A.J. Simon, and H. Ashrafiuon. Stochastic dynamic modeling of the human brain EEG signal. *ASME 2013 Dynamic Systems and Control Conference*, 2, October 21-23, 2013.

[GVWH12] A.K. Goel, S. Vattam, B. Wiltgen, and M. Helms. Cognitive, collaborative, conceptual and creative - four characteristics of the next generation of knowledge-based cad systems: a study in biologically inspired design. *Computer-Aided Design*, 44(10):879–900, 2012.

[GWW88] G.Pahl, W.Beitz, and K. Wallace. *Engineering design: A systematic approach.* Springer-Verlag, 1988.

[GYdL+13] G. Gonen-Yaacovi, L.C. de Souza, R. Levy, M. Urbanski, G. Josse, and E. Volle. Rostral and caudal prefrontal contribution to creativity: a meta-analysis of functional imaging data. *Front Hum Neurosci.*, 7:465, 2013.

[GZD+79] A. S. Gevins, G. M. Zeitlin, J. C. Doyle, R. E. Schaffer, and E. Callaway. EEG patterns during cognitive tasks. ii. analysis of controlled task. *Electroencephalography and Clinical Neurophysiology*, 47(6):704–710, 1979.

[Hac03] P. Hacker. *Philosophical Foundations of Neuroscience.* Blackwell, 2003.

[Haz96] G. A Hazelrigg. *Systems engineering: An approach to information-based design.* Prentice Hall, 1996.

[HBJ10] Y. Heussen, F. Binkofski, and J. Jolij. The semantics of the lying face - an EEG study. *International Journal of Psychophysiology*, 77(3), 2010.

[HDVDS10] K. Hoedlmoser, T. T. Dang-Vu, M. Desseilles, and M. Schabus. *Non-pharmacological alternatives for the treatment of insomnia - Instrumental EEG conditioning, a new alternative?* Nova Publishers, 2010.

[HE88] V. Hubka and W. Eder. *Theory of technical systems: A total concept theory for engineering design*. Springer-Verlag, 1988.

[Hee86] M. L. Heemstra. n efficiency model of information processing. *Energetics and human information processing*, 1986.

[HNB03] K.M. Heilman, S.E. Nadeau, and D.O. Beversdorf. Creative innovation: Possible brain mechanisms. *Neurocase*, 9:369–379, 2003.

[Hoc13] R. Hockey. *The Psychology of Fatigue: Work, Effort and Control*. Cambridge University Press, 2013.

[HRC+15] F. A. Haji, D. Rojas, R. Childs, S. de Ribaupierre, and A. Dubrowski. Measuring cognitive load: performance, mental effort and simulation task complexity. *Med Educ.*, 49(8):815–827, 2015.

[HW03] A. Hatchuel and B. Weil. A new approach of innovative design: An introduction to C-K theory. *International Conference On Engineering Design ICED03*, 2003.

[HW09] A. Hatchuel and B. Weil. CK design theory: an advanced formulation. *Research in Engineering Design*, 19(4):181–192, 2009.

[JBBH+04] M. Jung-Beeman, E.M. Bowden, J. Haberman, J.L. Frymiare, S. Arambel-Liu, R. Greenblatt, P.J. Reber, and J. Kounios. Neural activity when people solve verbal problems with insight. *PLoS Biol.*, 2:E97, 2004.

[JFR+15] S. Jaarsveld, A. Fink, M. Rinner, D. Schwab, M. Benedek, and T. Lachmann. Intelligence in creative processes: An EEG study. *Intelligence*, 49:171–178, 2015.

[JHL+08] T.P. Jung, C. Humphries, T.W. Lee, S. Makeig, M.J. McKeown, V. Iragui, and T.J. Sejnowski. Removing electroencephalographic artifacts: Comparison

between ICA and PCA. *Advances in Neural Information Processing Systems*, 10, 2008.

[JLFB09] Budi Thomas Jap, Sara Lal, Peter Fischer, and Evangelos Bekiaris. Using EEG spectral components to assess algorithms for detecting fatigue. *Expert Syst. Appl.*, 36(2):2352–2359, March 2009.

[JNKFB14] M.A. Jatoia, A. S. Malika N. Kamela, I. Fayeb, and T. Begumc. A survey of methods used for source localization using eeg signals. *Biomedical Signal Processing and Control*, 11:42–52, 2014.

[Jon63] J.C. Jones. *A Method of Systematic Design*. Conference on Design Methods. Pergamon, 1963.

[JSB+10] R.E. Jung, J.M. Segall, H.J. Bockholt, R.A. Flores, S.M. Smith, R.S. Chavez, and J.R. Haier. Neuroanatomy of creativity. *Hum Brain Mapp.*, 31(3):398–409, 2010.

[JY09] H. Jiang and C.C. Yen. Protocol analysis in design research: a review. *International Association of Societies of Design Research*, 2009.

[Kah73] D. Kahneman. *Attention and Effort*. Prentice Hall, 1973.

[Kap03] S. Kapur. Psychosis as a state of aberrant salience: a framework linking biology, phenomenology, and pharmacology in schizophrenia. *American Journal of Psychiatry*, 160:13–23, 2003.

[KASR13] M. Kaur, P. Ahmed, A.K. Soni, and M.Q. Rafiq. Wavelet transform use for p300 signal clustering by self-organizing map. *International Journal of Scientific and Engineering Research*, 4(11):1631–1638, 2013.

[KB91] M.J. Kaminski and K.J. Blinowska. A new method of the description of the information flow in the brain structures. *Biol. Cybern.*, 65:203–210, 1991.

[KB04] D. Kahneman and J. Beatty. Pupil diameter and load on memory. *Science*, 154(3756):1583–1585, 2004.

[KDKM12] R. Kurzban, A. Duckworth, J. W. Kable, and J. Myers. An opportunity cost model of subjective effort and task performance. *Behavioral and Brain Sciences*, 2012.

[KG08] J.W.T. Kan and J.S. Gero. Acquiring information from linkography in protocol studies of designing. *Design Studies*, 29(4):315–337, 2008.

[KG09] J. Kan and J. Gero. Using fbs ontology to capture semantic design information in design protocol studies. In *About: Designing - Analysing Design Meetings*, pages 213–229. CRC Press / Balkema, 2009.

[KLM+99] T. Koenig, D. Lehmann, M.C.G. Merlo, K. Kochi, D. Hell, and M. Koukkou. A deviant EEG brain microstate in acute neuroleptic-naive schizophrenics at rest. *Eur. Arch. Psychiatry Clin. Neuroscience*, 249:205–211, 1999.

[Kol02] J.F. Kolen. Reducing the time complexity of the fuzzy c-means algorithm. *IEEE Transactions on Fuzzy Systems*, 10(2):263–267, 2002.

[KP00] H. Kuusela and P. Paul. A comparison of concurrent and retrospective verbal protocol analysis. *American Journal of Psychology*, 113(3):387404, 2000.

[KPL+02] T. Koenig, L. Prischep, D. Lehmann, P.V. Sosa, E. Braeker, H. Kleinlogel, R. Isenhart, and E.R. John. Millisecond by millisecond, year by year: Normative EEG microstates and developmental stages. *NeuroImage*, 16:41–48, 2002.

[Kre15] M. Krell. Evaluating an instrument to measure mental load and mental effort using item response theory. *Science Education Review Letters*, pages 1–6, 2015.

[LC11] Christopher Liapis and Samir Chatterjee. *Service-Oriented Perspectives in Design Science Research: 6th International Conference, DESRIST 2011, Milwaukee, WI, USA, May 5-6, 2011. Proceedings*, chapter On a NeuroIS Design Science Model, pages 440–451. Springer Berlin Heidelberg, Berlin, Heidelberg, 2011.

[LCX+04] S. Liu, H.M. Chow, Y. Xu, M.G. Erkkinen, K.E. Swett, M.W. Eagle, D.A. Rizik-Baer, and A.R. Braun. Neural activity when people solve verbal problems with insight. *PLoS Biol.*, 2:E97, 2004.

[Leh71] D. Lehmann. Multichannel topography of human alpha EEG fields. *Electroencephalography and Clinical Neurophysiology*, 31(5):439–449, 1971.

[Leh90] D. Lehmann. Brain electric microstates and cognition: The atoms of thought. In *Machinery of the Mind*, pages 209–224. Birkhaüser, 1990.

[LHW15] P. Le Masson, A. Hatchuel, and B. Weil. Design theory at bauhaus: teaching splitting knowledge. *Research in Engineering Design*, pages 1–25, 2015.

[LMPM+97] G. Lantz, C.M. Michel, R.D. Pascual-Marqui, L. Spinelli, M. Seeck, S. Seri, T. Landis, and I. Rosen. Extracranial localization of intracranial interictal epileptiform activity using LORETA (low resolution electromagnetic tomography). *Electroencephalography and Clinical Neurophysiology*, 102:414–422, 1997.

[LNZH16] L. Liu, T.A. Nguyen, Y. Zeng, and B. Hamza. Identification of relationships between electroencephalography (EEG) bands and design activities. *ASME 2016 International Design Engineering Technical Conferences and Computers and Information in Engineering Conference*, 2016.

[LOP87] D. Lehmann, H. Ozaki, and I. Pal. EEG alpha map series: brain micro-states by space-oriented adaptive segmentation. *Electroencephalography and Clinical Neurophysiology*, 67:271–288, 1987.

[LWC11] C.T. Lin, Y.K. Wang, and S.A. Chen. An EEG-based brain-computer interface for dual task driving detection. *Neural Information Processing*, 7062:701–708, 2011.

[Mat09] B. Matthews. Intersections of brainstorming rules and social order. In *About: Designing - Analysing Design Meetings*, pages 137–152. CRC Press / Balkema, 2009.

[MES+09] A. Mabogunje, O. Eris, N. Sonalkar, M. Jung, and L. Leifer. Spider webbing: A paradigm for engineering design conversations during concept generation. In *About: Designing - Analysing Design Meetings*, pages 137–152. CRC Press / Balkema, 2009.

[Met86] J. Metcalfe. Premonitions of insight predict impending error. *Journal of Experimental Psychology: Learning, Memory, and Cognition*, 12:623–634, 1986.

[MGW98] T. McNeill, J.S. Gero, and J. Warren. Understanding conceptual electronic design using protocol analysis. *Research in Engineering Design*, 10(3):129–140, 1998.

[MHM+14] E. Mohedano, G. Healy, K. McGuiness, X. Gir'o i Nieto, N.E. O'Connor, and A.F. Smeaton. Object segmentation in images using EEG signals. *Proceedings of the ACM International Conference on Multimedia*, pages 417–426, 2014.

[MKB+09] C.M. Michel, T. Koenig, D. Brandeis, L.R.R. Gianotti, and J. Wackermann. *Electrical Neuroimaging*. Medecine. Cambridge University Press, 2009.

[ML09] J. McDonnell and P. Lloyd. *About: Designing - Analysing Design Meetings*. CRC / Balkema, 2009.

[MOK+92] A. Moriguchi, A. Otsuka, K. Kohara, H. Mikami, K. Katahira, and et al. T Tsunetoshi. Spectral changes in heart rate variability in response to mental arithmetic before and after beta-adrenoceptor blocker. *Clinical Autonomic Research*, 2(4):267–270, 1992.

[Mor12] A. Moran. *Attention theory*. Oxford University Press, 2012.

[Nag74] T. Nagel. What is it like to be a bat? *Philosophical Review*, 83:435–456, 1974.

[Ngu16] T. A. Nguyen. *Understanding Conceptual Design Activities: Extended Axiomatic Theory of Design Modeling and Physiological Experimentation*. Ph.D. dissertation, Concordia Unviersity, 2016.

[NNZ15a] P. Nguyen, T. A. Nguyen, and Y. Zeng. Measuring the evoked hardness of design problems using transient microstates. *Proceedings of the ASME 2015 International Design Engineering Technical Conferences and Computers and Information in Engineering Conference*, 2015.

[NNZ15b] P. Nguyen, T. A. Nguyen, and Y. Zeng. Physiologically based segmentation of design protocol. *International Conference on Engineering Design (ICED)*, 2015.

[NNZ16] P. Nguyen, T. A. Nguyen, and Y. Zeng. Quantitative analysis of the effort-fatigue tradeoff in the conceptual design process: A multistate EEG approach. *Proceedings of the ASME 2016 International Design Engineering Technical Conferences and Computers and Information in Engineering Conference*, 2016.

[NNZ17a] P. Nguyen, T.A. Nguyen, and Y. Zeng. Empirical approaches to quantifying effort, fatigue and concentration in the conceptual design process. *submitted*, 2017.

[NNZ17b] P. Nguyen, T.A. Nguyen, and Y. Zeng. Modal shifts in concentration indicate creativity. *International Conference on Engineering Design (ICED), submitted*, 2017.

[NNZ17c] P. Nguyen, T.A. Nguyen, and Y. Zeng. Segmentation of design protocols using EEG. *submitted*, 2017.

[NXZ13] T.A. Nguyen, X. Xu, and Y. Zeng. Distribution of mental stresses during conceptual design activities. *International Conference on Engineering Design (ICED)*, 2013.

[NZ10a] T. A. Nguyen and Y. Zeng. Analysis of design activities using EEG signals. *Proceedings of the ASME 2010 International Design Engineering Technical Conferences & Computers and Information in Engineering Conference, Montreal, August 15-18 2010*, 2010.

[NZ10b] T. A. Nguyen and Y. Zeng. Analysis of design activities using EEG signals. *ASME Conference Proceedings*, pages 277–286, 2010.

[NZ12a] T. A. Nguyen and Y. Zeng. Clustering designer's mental activities based on EEG power. *Tools and methods of competitive engineering, Karlsruhe, Germany*, 2012.

[NZ12b] T. A. Nguyen and Y. Zeng. Clustering designers mental activities based on EEG power. *Proceedings of Tools and Methods of Competitive Engineering (TMCE) 2012, May 711, 2012, Karlsruhe, Germany*, 2012.

[NZ12c] T. A. Nguyen and Y. Zeng. A theoretical model of design creativity: Nonlinear design dynamics and mental stress-creativity relation. *Journal of Integrated Design and Process Science*, 16(3):37–60, 2012.

[NZ14a] T. A. Nguyen and Y. Zeng. A physiological study of relations between designers mental effort and mental stress during conceptual design. *Computer Aided Design*, 54:3–18, 2014.

[NZ14b] T. A. Nguyen and Y. Zeng. A physiological study of the relationship between designer's mental effort and mental stress during conceptual design. *Computer-Aided Design*, 54:3–18, 2014.

[NZ14c] T. A. Nguyen and Y. Zeng. An entropy based approach to grouping design problems in terms of difficulty level using designer's physiological responses, working paper. *Design Lab, Concordia Institute for Information Systems Engineering, Concordia University, Montreal, Canada*, October 28, 2014.

[NZ15] T. A. Nguyen and Y. Zeng. Subjective workload rating and physiological measures of cognitive state in design tasks. *submitted to J. Intell. Manuf.*, 2015.

[NZ16a] T. A. Nguyen and Y. Zeng. A theory of design fixation. *International Journal of Design Creativity and Innovation*, 2016.

[NZ16b] T.A. Nguyen and Y. Zeng. Effects of stress and effort on self-rated reports in experimental study of design activities. *Journal of Intelligent Manufacturing*, pages 1–14, 2016.

[ÖBrW05] G. Östlund, K. Borg, and Å. Wahlin. Cognitive functioning in post-polio patients with and withour general fatigue. *J Rehabil Med*, 37:147–151, 2005.

[Orn77] R.E. Ornstein. *Psychology of Consciousness*. Harcourt Brace Jovanovich, 1977.

[OZG93] T. Otto, F. R. H. Zijlstra, and R. Goebel. *Efficiency in Work Behavior: A Design Approach for Modern Tools*. Delft University Press, 1993.

[PBFG07] G. Pahl, W. Beitz, J. Feldhusen, and K.H. Grote. *Engineering Design: A Systematic Approach*. Springer, 2007.

[PDG12] V. Presutti, F. Draicchio, and A. Gangemi. Knowledge extraction based on discourse representation theory and linguistic frames. *Knowledge Engineering and Knowledge Management*, 7603:114–129, 2012.

[PDY+09] H. Petkar, S. Dande, R. Yadav, Y. Zeng, and T.A. Nguyen. A pilot study to assess designers mental stress using eye gaze system and electroencephalogram. *ASME 2009 International Design Engineering Technical Conferences and Computers and Information in Engineering Conference*, 2009.

[Pes11] V. Pestov. Indexability, concentration, and vc theory. *Journal of Discrete Algorithms*, 2011.

[PL08] B. Pang and L. Lee. Opinion mining and sentiment analysis. *Foundations and Trends in Information Retrieval*, 2(1-2), 2008.

[PM07] R.D. Pascual-Marqui. Discrete, 3d distributed, linear imaging methods of electric neuronal activity. part 1: exact, zero error localization. http://arxiv.org/pdf/0710.3341/, 2007. [Online; accessed 27-August-2016].

[PMML94a] R.D. Pascual-Marqui, C.M. Michel, and D. Lehmann. Low resolution electromagnetic tomography: a new method for localization electrical activity in the brain. *Journal of Psychophysiology*, 18:49–65, 1994.

[PMML94b] R.D. Pascual-Marqui, C.M. Michel, and D. Lehmann. Low-resolution electromagnetic tomography: a new method for localizing electrical activity in the brain. *Journal of Psychophysiology*, 18:49–65, 1994.

[PMML95] R.D. Pascual-Marqui, C. M. Michel, and D. Lehmann. Segmentation of brain electrical activity into microstates: Model estimation and validation. *IEEE Transactions on Biomedical Engineering*, 42(7):658–665, 1995.

[Pow13] D. Powell. Toy helicopter guided by power of thought. *Nature: International Weekly Journal of Science*, June 5, 2013.

[PRCS00] W. D. Penny, S. J. Roberts, E. A. Curran, and M. J. Stokes. EEG-based communication: A pattern recognition approach. *IEEE Transactions on Rehabilitation Engineering*, 8(2):214–215, 2000.

[Pug91] S. Pugh. *Total design: Integrated methods for successful product engineering*. Prentice Hall, 1991.

[PV93] F. G. W. C. Paas and J. J. G. Van Merriënboer. The efficiency of instructional conditions: An approach to combine mental effort and performance measures. *Human Factors: the Journal of the Human Factors and Ergonomics Society*, 35(4):737–743, 1993.

[Rei95] Yoram Reich. A critical review of general design theory. *Research in Engineering Design*, 7(1):1–18, 1995.

[RJ91] J. Rasmussen and A. Jensen. Mental procedures in real life tasks. a case study in electronics trouble shooting. *Ergonomics*, 17:293–330, 1991.

[RL11] J. Vom Brocke BR. Riedl and P.M. Léger. Neuroscience in design-oriented research: Exploring new potentials. *Proceedings of the 6th International Conference on Design Science Research in Information Systems and Technology*, pages 427–439, 2011.

[RL13] J. Vom Brocke BR. Riedl and P.M. Léger. Application strategies for neuroscience in information systems design science research. *Journal of Computer Information Systems*, 53(3):1–13, 2013.

[RL16] R. Riedl and P.M Léger, editors. *Fundamentals of NeuroIS: Information Systems and the Brain*. Springer, 2016.

[SB10] C. Saavedra and L. Bougrain. Wavelet denoising for p300 single-trial detection. *Neurocomp. Proccedings of the 5th french conference on computational neuroscience - Neurocomp10, Lyon, France*, pages 227–231, 2010.

[SB15] M. K. Sharma and M. M. Bundele. Design & analysis of k-means algorithm for cognitive fatigue detection in vehicular driver using respiration signal. *IEEE International Conference on Electrical, Computer and Communication Technologies (ICECCT)*, pages 1–6, 2015.

[SCG11] B. Sylcott, J. Cagan, and G.Tabibnia. Understanding of emotions and reasoning during consumer tradeoff between function and æsthetics in product design. *Proceedings of the ASME 2011 International Design Engineering Technical Conferences and Computers and Information in Engineering Conference*, 2011.

[SE93] J. W. Schooler and T. Y. Engstler-Schooler. Verbal overshadowing of visual memories: Some things are better left unsaid. *Cognitive Psychology*, 17:31–71, 1993.

[Sea92] J. R. Searle. *The Rediscovery of the Mind*. The MIT Press, 1992.

[SEE09] M. Stacey, C. Eckert, and C. Earl. From ronchamp by sledge: On the pragmatics of object references. In *About: Designing - Analysing Design Meetings*, pages 361–380. CRC Press / Balkema, 2009.

[SGD+14] J. Sandry, H. M. Genova, E. Dobryakova, J. De Luca, and G. Wylie. Subjective cognitive fatigue in ms depends on task length. *Front Neurol.*, 5(214), 2014.

[SHHM+14] P. Seitamaa-Hakkarainen, M. Huotilainen, M. Mkela?, C. Groth, and K. Hakkarainen. The promise of cognitive neuroscience in design studies. *Design Research Society Conference*, 2014.

[SJ13] M. Steinert and K. Jablokow. Triangulating front end engineering design activities with physiology data and psychological preferences. *Proceedings of the 19th International Conference on Engineering Design (ICED13)*, 2013.

[SLF+12] F. Schlegel, D. Lehamnn, P.L. Faber, P. Milz, and L.R.R. Gianotti. EEG microstates during resting represent personality differences. *Brain Topogr*, 25:20–26, 2012.

[Sma89] P. Smagorinsky. The reliability and validity of protocol analysis. *Written Communication*, 6(4):463–447, 1989.

[SOKB93] J. W. Schooler, S. Ohlsson, and K. K. Brooks. Thoughts beyond words: When language overshadows insight. *Journal of Experimental psychology: General*, 122:166–183, 1993.

[SOM+13] Hiroshi Shimoda, Kotaro Oishi, Kazune Miyagi, Kosuke Uchiyama, Hirotake Ishii, Fumiaki Obayashi, and Mikio Iwakawa. *An Intellectual Productivity Evaluation Tool Based on Work Concentration*, pages 364–372. Springer Berlin Heidelberg, Berlin, Heidelberg, 2013.

[SR04] O. Shai and Y. Reich. Infused design: I theory. *Research in Engineering Design*, 15(2):93–107, 2004.

[SR14] S. S. Shankar and R. Rai. Human factors study on the usage of bci headset for 3d cad modeling. *Computer Aided Design*, 54:51–55, 2014.

[SRMB07] N. Stevenson, L. Rankine, M. Mesbah, and B. Boashash. Modelling newborn EEG background using a time-varying fractional brownian process. *15th european Signal Processing Conference (EUSIPCO 2007)*, 2007.

[SRQ00] R.M. Stern, W. Ray, and K.S. Quigley. *Psychophysiological Recording*. 2000.

[SRR91] J. W. Schooler, R. Ryan, and L. M. Reder. Better the second time around: Representation reverses verbalization's impairment of face recognition. *International Conference on Memory*, 1991.

[Sta04] M. A. Staal. Stress, cognition, and human performance: A literature review and conceptual framework. *NASA/TM*, 212824, 2004.

[Suh90] N. Suh. *The principles of design*. Oxford University Press, 1990.

[SVR13] S. Shankar, A. Verma, and R. Rai. Creating by imagining: Use of natural and intuitive bci in 3d cad modeling. *ASME 2013 International Design Engineering Technical Conferences and Computers and Information in Engineering Conference, Portland, Oregon, USA*, 2A, August 47, 2013.

[Swe88] J. Sweller. Cognitive load during problem solving: Effects on learning. *Cognitive Science*, 12(2):257–285, 1988.

[TJD+04] N. Tchen, H. G. Juffs, F. P. Downie, Q. L. Yi, H. Hu H, I. Chemerynsky, M. Clemons, M. Crump, P. E. Goss, D. Warr, M. E. Tweedale, and I. F. Tannock. Cognitive function, fatigue, and menopausal symptoms in women receiving adjuvant chemotherapy for breast cancer. *Journal of Clinical Oncology*, pages 4175–4183, 2004.

[Tor04] E.P. Torrance. Un résumé historique du développement des tests de pensée crative de Torrance. *Rev. Eur. Psychol. Appl.*, 54:57–63, 2004.

[TZ09] Y. Tang and Y. Zeng. Quantifying designer's mental stress in the conceptual design process using kinesics study. *Proceedings of the 17th international conference on engineering design*, 2009.

[USD87] D.G. Ullman, L.A. Stauffer, and T.G. Dietterich. Preliminary results of and experimental study of the mechanical design process. *Proceedings of the NSF Workshop on Design Theory and Methodology*, 1987.

[VBM10] D. Van De Ville, J. Britz, and C.M. Michel. EEG microstate sequences in healthy humans at rest reveal scale-free dynamics. *Proceedings of the National Academy of Sciences of the United States of America*, 107(42):18179–18184, 2010.

[VC02] S. Vorobyov and A. Cichocki. Blind noise reduction for multisensory signals using ICA and subspace filtering, with application to EEG analysis. *Biol. Cybern.*, 86:293–303, 2002.

[Vis09] W. Visser. The function of gesture in architectural design meetings. In *About: Designing - Analysing Design Meetings*, pages 269–284. CRC Press / Balkema, 2009.

[VMMD73] H. P. A. Van Dongen, G. Maislin, J. M. Mullington, and D. F. Dinges. Quantification of sleepiness: a new approach. *Psychophysiology*, 10(4):431–436, 1973.

[VP09] I. Volnyansky and V. Pestov. Curse of dimensionality in pivot-based indexes. *2009 Second International Workshop on Similarity Search and Applications*, pages 39–46, 2009.

[Wai11] M. Waibel. Braindriver: A mind controlled car. *IEEE Spectrum*, February 17, 2011.

[Wec44] D. Wechsler. *The measurement of adult intelligence*. The Williams & Wilkins Company, 1944.

[WFG+15] D. Wobrock, J. Frey, D. Graeff, J. B. De La Riviere, J. Castet, and F. Lotte. Continuous mental effort evaluation during 3d object manipulation tasks based on brain and physiological signals. *Human-Computer Interaction*, pages 472–487, 2015.

[Wil84] T. D. Wilson. The proper protocol: Validity and completeness of verbal reports. *Psychological Science*, 5:249–252, 1984.

[Wit54] L. Wittgenstein. *Philosophical Investigations*. Macmillan, 1954.

[WLB12] W. Wong, W. Lieu, and M. Bennamoun. Ontology learning from text: A look back and into the future. *ACM Computing Surveys*, 44(4):20–36, 2012.

[WLS+13] T. D. Wilson, D. J. Lisle, J. W. Schooler, S. D. Hodges, K. J. Klaaren, and S. J. Lafleur. *Introspecting about reasons can reduce post-choice satisfaction*, pages 471–486. Cambridge University Press, 2013.

[WS91] T. D. Wilson and J. W. Schooler. Thinking too much: Introspection can reduce the quality of preferences and decisions? *Journal of Personality and Social Psychology*, 60:181–192, 1991.

[WSJ13] Emily Worinkeng, Joshua D. Summers, and Shraddha Joshi. *Can a Pre-sketching Activity Improve Idea Generation?*, pages 583–592. Springer Berlin Heidelberg, Berlin, Heidelberg, 2013.

[WZCE13] M. Wang, Y. Zeng, L. Chen, and A. Eberlein. An algorithm for transforming design text rom diagram into fbs model. *Computers in Industry*, pages 499–513, 2013.

[XNZ14] X. Xu, T. A. Nguyen, and Y. Zeng. Galvanic skin response as index of mental workload in design. *Proceedings of TMCE 2014, May 19-23, Budapest, Hungary*, 2014.

[YN04] G. B. Yeo and A. I. Neal. A multilevel analysis of effort, practice and performance: Effects of ability, conscientiousness and goal orientation. *Journal of Applied Psychology*, 89(2):231–247, 2004.

[Yos81] H. Yoshikawa. General design theory and a cad system. In *Man-Machine Communication in CAD/CAM*. North-Hlland Publishing Company, 1981.

[ZC91] Y. Zeng and G.D. Cheng. On the logic of design. *Design Studies*, 12(3):137–141, 1991.

[Zen02] Y. Zeng. Axiomatic theory of design modeling. *Transaction of SDPS: Journal of Integrated Design and Process Science*, 6(3):1–28, 2002.

[Zen04] Y. Zeng. Environment-based design formulation of design problems. *Journal of Integrated Design and Process Science*, 8(4):45–63, 2004.

[Zen08] Y. Zeng. Recursive object model (ROM)-modelling of linguistic information in engineering design. *Computers in Industry*, 59(6):612–625, 2008.

[Zen11] Y. Zeng. Environment-based design (EBD). *ASME Conference Proceedings*, pages 237–250, 2011.

[ZG99a] Y. Zeng and P. Gu. A science-based approach to product design theory part i: Formulation and formalization of design process. *Robotics and Computer Integrated Manufacturing*, 15:331–339, 1999.

[ZG99b] Y. Zeng and P. Gu. A science-based approach to product design theory part ii: Formulation of design requirements and products. *Robotics and Computer Integrated Manufacturing*, 15:331–339, 1999.

[ZPR+12] S. Zugal, J. Pinggera, H. Reijers, M. Reichert, and B. Weber. Making the case for measuring mental effort. *EESSMod '12 Proceedings of the Second Edition of the International Workshop on Experiences and Empirical Studies in Software Modelling*, 2012.

[ZYZ07] S. Zhu, S. Yao, and Y. Zeng. A novel approach to quantifying designers mental stress in the conceptual design process. *ASME International Design Engineering Technical Conferences and Computers and Information in Engineering Conference*, 2:593–600, 2007.

Appendix A: A Mathematica Implementation of P2ML and Transient Microstates Calculation

The code in Listing 1 is a *Mathematica* implementation of the P2ML algorithm. It requires as input a data matrix of dimensions $N \times M$, where N is the number of samples and M is the number of electrodes, a number of clusters (*e.g.* 4) and a convergence parameter ϵ (*e.g.* 0.0001). Additionally, it accepts the following options: *MaxIterations* (the maximum number of iterations allowed), *Verbose* (print execution details) and *Microstates* (provide as output parameters the microstates in addition to the segmentation).

The original P2ML algorithm is sensible to data lengths as it expects all clusters defined in the input parameter to be represented in the data. This occurs with higher probability on longer epochs. Experimentally, an epoch length of $2,500$ samples at a data rate of 500 samples per second is usually enough. Future work could handle this error case.

Listing 1: P2ML Algorithm Implementation

```
MicrostateSegmentation[data0_,numclusters0_,epsilon0_,opts:OptionsPattern[]]:=
Module[{data=data0,numclusters=numclusters0,epsilon=epsilon0},
ARGMAX[vector_,clusters_]:=Flatten[Position[(clusters.vector)^2,Max[(clusters.vector)
    ^2]]][[1]];
centroids=RandomReal[{Min[Min[data]],Max[Max[data]]},{numclusters,63}];
centroids=centroids/Map[Norm,centroids];
sigma0=ConstantArray[0,numclusters];
```

```
iter=If[Values@FilterRules[{opts},"MaxIterations"]=={},Infinity,Values@FilterRules[{opts},"
    MaxIterations"][[1]]];
For[i=1,i<=iter,++i,
lk=Map[(ARGMAX[#,centroids])&,data];
sk=Map[Function[var,Total[Map[Transpose[{#}].{#}&,data[[Flatten[Position[lk,var]]]],1]],
    Range[numclusters]];
centroids=Map[(Eigensystem[sk[[#]]][[2,1]])&,Range[numclusters]];
sigma1=Map[Total,Outer[(data[[#2]].data[[#2]]-(centroids[[#1]].data[[#2]])^2)&,Range[
    numclusters],Range[Dimensions[data][[1]]]]]/(Dimensions[data][[1]]*(Dimensions[data
    ][[2]]-1));
If[Values@FilterRules[{opts},"Verbose"]=={True},
Print["Iteration:"<>ToString[i]];
Print["Data_Variance:"<>ToString[Abs[sigma0-sigma1]]];
Print["Target_Variance:"<>ToString[epsilon*sigma1]];,
];
Which[Total[Boole@Map[((Abs[sigma0-sigma1])[[#]]<=(epsilon*sigma1)[[#]])&,Range[numclusters
    ]]]!=numclusters,sigma0=sigma1,Total[Boole@Map[((Abs[sigma0-sigma1])[[#]]<=(epsilon*
    sigma1)[[#]])&,Range[numclusters]]]==numclusters,Break[];];
];
If[Values@FilterRules[{opts},"Microstates"]=={True},{lk,centroids},lk]
];
```

The code in Listing 2 is a *Mathematica* implementation of the P2ML regularized smoothing algorithm. It requires a data matrix of the same dimensions as above, a number of clusters (*e.g.* 4), a convergence parameter ϵ (*e.g.* 0.0001), a smoothness penalty parameter λ (*e.g.* 5) and a window size parameter w (*e.g.* 3).

Listing 2: Regularized P2ML Algorithm Implementation

```
MicrostateRegularizedSmoothing[data0_,centroids0_,numclusters0_,epsilon0_,lambda0_,beta0_,
    opts:OptionsPattern[]]:=
Module[{data=data0,centroids=centroids0,numclusters=numclusters0,epsilon=epsilon0,lambda=
    lambda0,beta=beta0},
ARGMAX[vector_,clusters_]:=Flatten[Position[(clusters.vector)^2,Max[(clusters.vector)
    ^2]]][[1]];
DELTA[x_,y_]:=If[x==y,1,0];
sigma0=ConstantArray[0,numclusters];
iter=If[Values@FilterRules[{opts},"MaxIterations"]=={},Infinity,Values@FilterRules[{opts},"
    MaxIterations"][[1]]];
lk=Map[(ARGMAX[#,centroids])&,data];
error=Map[Total,Outer[(data[[#2]].data[[#2]]-(centroids[[#1]].data[[#2]])^2)&,Range[
    numclusters],Range[Dimensions[data][[1]]]]]/(Dimensions[data][[1]]*(Dimensions[data
    ][[2]]-1));
For[i=1,i<=iter,++i,
delta=Map[Function[var,Developer`PartitionMap[Total,Transpose[Outer[DELTA[#1,#2]&,lk,Range[
    numclusters]]][[var]],2*beta,1]],Range[numclusters]];
```

```
regfactor=Map[PadRight[delta[[#]],Dimensions[data][[1]],Last[delta[[#]]]]&,Range[numclusters
    ]];
lk=Flatten[Map[(Position[#,Min[#]])&,Transpose[Outer[(data[[#2]].data[[#2]]-(centroids[[#1]].
    data[[#2]])^2)&,Range[numclusters],Range[Dimensions[data][[1]]]]/(2*error*(Dimensions[
    data][[2]]-1))-(lambda*regfactor)]]];
sigma1=Map[Total,Outer[(data[[#2]].data[[#2]]-(centroids[[#1]].data[[#2]])^2)&,Range[
    numclusters],Range[Dimensions[data][[1]]]]]/(Dimensions[data][[1]]*(Dimensions[data
    ][[2]]-1));
If[Values@FilterRules[{opts},"Verbose"]=={True},
Print["Iteration:"<>ToString[i]];
Print["Data_Variance:"<>ToString[Abs[sigma0-sigma1]]];
Print["Target_Variance:"<>ToString[epsilon*sigma1]];,
];
Which[
Total[Boole@Map[((Abs[sigma0-sigma1])[[#]]<=(epsilon*sigma1)[[#]])&,Range[numclusters]]]!=
    numclusters,sigma0=sigma1,Total[Boole@Map[((Abs[sigma0-sigma1])[[#]]<=(epsilon*sigma1)
    [[#]])&,Range[numclusters]]]==numclusters,Break[];];
];
lk
];
```

A sample usage to compute the transient microstate percentage is in Listing 3. It includes the package we developed for the P2ML and regularized P2ML algorithms.

Listing 3: Transient Microstate Computation

```
In[1]:=Needs["EEGSegmentationTools`"]
In[2]:=DATA=Import["feb_05(1)_2014-filter_eyeclosed.csv"];
In[3]:=segments=MicrostateSegmentation[DATA, 4,0.0001,"Microstates->True,"MaxIterations
    ->100,"Verbose->True];
In[4]:=smoothsegments=MicrostateRegularizedSmoothing[DATA,segments[[2]],4,0.0001,5,3,"
    MaxIterations->100,"Verbose->True];
In[5]:=numsegments=Length[segments[[1]]]-Count[Differences[segments[[1]]],0];
In[6]:=numsmoothsegments=Length[smoothsegments]-Count[Differences[smoothsegments],0];
In[7]:=informationloss=numsegments-numsmoothsegments;
In[8]:=transient=informationloss/Length[DATA];
```

Appendix B: A Mathematica Implementation of LORETA

Listing 4 shows the computation of a brain model using 104 scalp field map points and 452 voxel locations with parameter $d = 0.21$ interpolated on a unit sphere.

Listing 4: Computation of the Brain Model

```
In[1]:=scalp=Transpose[{Transpose[DeleteCases[Tuples[Flatten[{Range[-1, 1, 0.17]}], 2]*Map[If
    [#[[1]]^2 + #[[2]]^2 < 1, 1, Infinity] &,Tuples[Flatten[{Range[-1, 1, 0.17]}],2]], {∞,
    ∞} | {∞,−∞} | {−∞, ∞} | {−∞, −∞}]][[1]],Transpose[DeleteCases[Tuples[Flatten[{
    Range[-1, 1, 0.17]}], 2]*Map[If[#[[1]]^2 + #[[2]]^2 < 1, 1, Infinity] &,Tuples[Flatten[{
    Range[-1, 1, 0.17]}],2]], {∞, ∞} | {∞,−∞} | {−∞, ∞} | {−∞, −∞}]][[2]],Sqrt[1 -
    #1^2 - #2^2] & @@Transpose[DeleteCases[Tuples[Flatten[{Range[-1, 1, 0.17]}], 2]*Map[If
    [#[[1]]^2 + #[[2]]^2 < 1, 1, Infinity] &,Tuples[Flatten[{Range[-1, 1, 0.17]}],2]],{∞, ∞
    } | {∞,−∞} | {−∞, ∞} | {−∞, −∞}]]}];
In[2]:=d=0.21;
In[3]:=voxels=DeleteCases[Tuples[Flatten[{Range[-1, 1, d]}], 3]*Map[If[#[[1]]^2 + #[[2]]^2 +
    #[[3]]^2 <= 1, 1, Infinity] &,Tuples[Flatten[{Range[-1, 1, d]}],3]], {∞, ∞, ∞} | {∞,
    ∞, −∞} | {∞, −∞, ∞} | {∞, −∞, −∞} | {−∞, ∞, ∞} | {−∞, ∞, −∞} | {-∞, −∞,
    ∞} | {−∞, −∞, −∞}];
```

Listing 5 shows how to compute the resolution matrix T with conductivity $\sigma = 0.185$.

Listing 5: Computation of the LORETA Resolution Matrix

```
In[1]:=Sigma=0.185;
In[2]:=K=Partition[Flatten[Transpose[Table[(1/4 Pi Sigma)*(2*(scalp[[i]] - voxels[[j]])/Norm[
    scalp[[i]] - voxels[[j]]]^3 +1/(Norm[scalp[[i]]]*Norm[scalp[[i]] - voxels[[j]]]*(Norm[
    scalp[[i]]]*Norm[scalp[[i]] - voxels[[j]]] + scalp[[i]].(scalp[[i]] - voxels[[j]])))*(
    scalp[[i]]*Norm[scalp[[i]] - voxels[[j]]] + (scalp[[i]] -voxels[[j]])*Norm[scalp[[i]]])),
     {i, 1, Length[scalp]}, {j, 1, Length[voxels]}]]], 3*Length[voxels]];
```

```
In[3]:=B=(6/d^2) (KroneckerProduct[0.5 (IdentityMatrix[Length[voxels]] + Inverse[
    DiagonalMatrix[Table[If[Norm[voxels[[i]] - voxels[[j]]] == d, 1/6, 0], {i, 1, Length[
    voxels]}, {j, 1, Length[voxels]}].ConstantArray[1, Length[voxels]]]]).Table[If[Norm[
    voxels[[i]] - voxels[[j]]] == d, 1/6, 0], {i, 1,Length[voxels]}, {j, 1, Length[voxels]}],
    IdentityMatrix[3]] - IdentityMatrix[3*Length[voxels]]);
In[4]:=Ktemp=Map[(1/4 Pi Sigma)*(2*(scalp[[#[[1]]]] - voxels[[#[[2]]]])/Norm[scalp[[#[[1]]]]
    - voxels[[#[[2]]]]]^3 + 1/(Norm[scalp[[#[[1]]]]]*Norm[scalp[[#[[1]]]] - voxels
    [[#[[2]]]]]*(Norm[scalp[[#[[1]]]]]*Norm[scalp[[#[[1]]]] - voxels[[#[[2]]]]] + scalp
    [[#[[1]]]].(scalp[[#[[1]]]] - voxels[[#[[2]]]]]))*(scalp[[#[[1]]]]*Norm[scalp[[#[[1]]]] -
     voxels[[#[[2]]]]] + (scalp[[#[[1]]]] - voxels[[#[[2]]]])*Norm[scalp[[#[[1]]]]])) &,Outer
    [List, Range[Length[scalp]], Range[Length[voxels]]] // Flatten[#, 1] &];
In[5]:=Omega=DiagonalMatrix[ParallelTable[Sqrt[Total[Map[Ktemp[[#*i]].Ktemp[[#*i]] &, Range[
    Length[scalp]]]]], {i, 1, Length[voxels]}]];
In[6]:=W=(KroneckerProduct[Omega, IdentityMatrix[3]]).Transpose[B].B.(KroneckerProduct[Omega,
     IdentityMatrix[3]]);
In[7]:=T=Inverse[W].Transpose[K].(PseudoInverse[K.Inverse[W].Transpose[K]]);
```

Listing 6 shows how to compute the LORETA densities from a scalp field map. We interpolate the 2D scalp field values that we have to a 3D scalp field map model of 107 points using radial basis interpolation.

Listing 6: Computation of the LORETA Densities

```
In[1]:=dataz=Import["april_2(1)_excerpt_tabularasa.csv"];
In[2]:=datagridpolar={{-18, 0.5111}, {0, 0.2556}, {-39, 0.33333}, {-54, 0.51111}, {-72,
    0.63889}, {-69, 0.39444}, {-45, 0.17778}, {-90, 0.25556}, {-90, 0.51111}, {-108,
    0.63889}, {-111, 0.39444}, {-135, 0.17778}, {180, 0.25556}, {-141, 0.33333}, {-126,
    0.51111}, {-162, 0.51111}, {180, 0.51111}, {162, 0.51111}, {141, 0.33333}, {126,
    0.51111}, {108, 0.63889}, {111, 0.39444}, {135, 0.17778}, {90, 0.25556}, {90, 0.51111},
    {72, 0.63889}, {69, 0.39444}, {45, 0.17778}, {39, 0.33333}, {54, 0.51111}, {18, 0.51111},
     {-38, 0.51111}, {-23, 0.41111}, {0, 0.38333}, {-22, 0.27778}, {-49, 0.41667}, {-72,
    0.51111}, {-62, 0.27778}, {0, 0.12778}, {-90, 0.12778}, {-90, 0.383333}, {-108, 0.51111},
     {-118, 0.27778}, {-158, 0.27778}, {-131, 0.41667}, {-144, 0.51111}, {-157, 0.41111},
    {180, 0.38333}, {157, 0.41111}, {144, 0.51111}, {131, 0.41667}, {158, 0.27778}, {180,
    0.12778}, {118, 0.27778}, {108, 0.51111}, {90, 0.38333}, {90, 0.12778}, {62, 0.27778},
    {72, 0.51111}, {49, 0.41667}, {22, 0.27778}, {23, 0.41111}, {38, 0.51111}};
In[3]:=datagrid=Map[{x[[2]]*Cos[x[[1]]*Pi/180], x[[2]]*Sin[x[[1]]*Pi/180]}&, datagridpolar];
In[4]:=datarow=dataz[[1]];
In[5]:=data3d=Table[{datagridratio[[i]], datarow[[i]]}, {i, Length[datarow]}];
In[6]:=fun=Interpolation[data3d, Method -> "RBF", RadialBasisFunction -> "Gaussian",
    DistanceFunction -> EuclideanDistance];
In[7]:=interpolatedV=Map[fun[#[[1]], #[[2]]] &, grid]
In[8]:=J=T.interpolatedV;
In[9]:=Jdensity=Partition[J, 3];
In[10]:=Jmagnitude=Map[Norm[#] &, Jdensity];
```

Index

Adaptable Design, 13, 15

Analysis, Synthesis and Evaluation Model (ASE), 12, 13

anterior superior temporal gyrus, 24

Artificial intelligence-Based Design, 13, 15

Axiomatic Design, 12, 13

Axiomatic Theory of Design Modeling, 13, 14

basal ganglia, 24

Brain-Computer Interfaces (BCI), 32, 38

C-K Theory, 13–15

capacity model, 5, 19, 20, 22, 113

CARTOOL, 50

clustering, 3, 18, 31, 37, 39, 47, 49, 71, 92–94, 97

cognitive structures, 77

concentration, 92, 96, 101, 103

concentration of measure, 61, 62

conceptual design process, 2, 5, 17, 20, 33, 37, 92–94, 98, 101, 102, 104, 113

Concordia Design Lab, 7

content based non-textual design protocols, 31

corpus callosi, 23

Coupled Design Process, 13, 14

creativity, 1, 5, 10, 17, 18, 22–24, 32, 34, 93, 94, 98, 101–105, 107, 108

Decision-Based Design Theory, 13, 14

Delft protocols, 26, 28

design cognition, 2, 28, 85

design moves, 28

design protocol analysis, 2, 3, 17, 24, 26, 27, 29, 30, 33, 92

directional derivative, 44

EEG, 18, 36, 37, 39–41, 43, 50, 64–67, 72, 74, 85, 87, 91–94, 101, 103, 108

EEG analysis, 36, 61

EEG filtering, 37

EEG interpolation, 41

electrocardiograms (ECG), 7

Environment Based Design (EBD), 13, 15

eye-tracking, 7

fatigue, 84, 85, 92, 95

FBS ontology, 27, 28

Formal Design Theory, 14
Fourier transform, 55
fractional Brownian motion (fBm), 61
frequency-domain features, 55
Function-Behavior-Structure (FBS) Model, 13, 14
fuzzy c-means clustering, 47, 49

Galvanic Skin Response (GSR), 7
General Design Theory, 12, 13
generative methods, 14
global field power, 47
gradient fields, 42

hardness of problem, 64
Heart-Rate Variability (HRV), 7
Hurst indices, 40

ice-breaking phenomenon, 88
Infused Design, 13, 15
insight, 102, 105

k-means clustering, 47, 49

lingual gyrus, 24
linkographs, 28
LORETA, 9, 56, 58, 102, 107, 118

machine learning, 58
mental effort, 69, 92, 94
microstate segmentation, 65, 68, 70, 75
microstates, 8, 39, 47, 50, 108
modal shifts, 101, 104, 107
multistate analysis, 84, 86, 87

nonconscious processing, 106
nonlinear theory of creativity, 101
nonverbalizable processing, 34, 101

P2ML algorithm, 47, 48, 50, 66, 68, 115
P2ML objective function, 50
P2ML regularized objective function, 52
physiological methods, 32, 92
Power Spectral Density (PSD), 55, 75, 96
prefrontal lobe, 24, 105
Principal Component Analysis (PCA), 8

radial basis function, 41, 42
right posterior cingulate, 24
ROM diagram, 15

scalp field maps, 36, 38, 39, 41, 42, 44, 47, 48, 50, 58, 94, 105
segmentation, 68, 70, 74–77, 80–82, 95, 97, 103
skin conductivity, 7
source localization, 56, 105
spider web, 27
split brain theory, 23

splitting function, 15

stochastic differential equation, 39

superior temporal gyrus, 105

Systematic Design Theory, 12, 13

tabula rasa, 100, 105

textual design protocols, 29

Theory of Inventive Problem Solving (TRIZ), 11, 13

Theory of Technical Systems, 12, 13

Total Design, 13, 14

transient microstates, 55, 66–68, 70, 72, 75, 89, 91, 94, 108

types of fatigue, 90, 95

verbalization, 33, 34

video design protocols, 31

weaknesses of verbal protocols, 33

Wechsler Intelligence Scale, 24